Deformation-strength characteristics of unsaturated granular subbase course material under monotonic and cyclic loading

単調および繰返し載荷を受ける不飽和粒状路盤材の変形－強度特性に関する研究

By

Yuan ZHANG

A thesis submitted in partial fulfilment of the requirements for the degree of Doctor of Philosophy in Engineering

Professor Tatsuya ISHIKAWA

Supervisor

English Engineering Program (e^3)

Laboratory of Analytical Geomechanics

Division of Field Engineering for the Environment

Graduate School of Engineering

Hokkaido University

Sapporo, Japan

ABSTRACT

Throughout a year, climatic changes highly influence the degree of saturation of subbase course layer inside pavement structures in cold snowy regions, such as Hokkaido, Japan. Besides, pavements have to transfer traffic loads from the asphalt-mixture layer to the subbase course layer. Accordingly, it is necessary to understand the mechanical behaviors of the subbase course layer effected by seasonal variations of degree of saturation and traffic loads. In this study, a series of monotonic and cyclic triaxial compression tests was performed to measure the deformation-strength characteristics of the unsaturated granular subbase course material (called C-40) using the newly developed medium-size triaxial apparatus. The suction-controlled laboratory element test method for unsaturated soils in this study is based on the axis translation technique using the triaxial apparatus with special deign on cap and pedestal, which can control pore water pressure and pore air pressure separately, thereby reducing the total testing time. To begin with, the soil-water characteristic test was carried out on C-40 specimen to obtain the relationship between the matric suction and the degree of saturation. The water-air-particle system in unsaturated soils are introduced to describe the transition of pore water and pore air inside soils. Second, the influences of degree of saturation and strain rate on strength characteristics of unsaturated specimens were evaluated through monotonic triaxial compression tests. The experimental results implied that the degradation in shear strength of C-40 specimen, with the increment in degree of saturation and decrement in strain rate, was found under monotonic loads. The effects of degree of saturation and strain rate on the total internal friction angle appear to be negligible, while the total cohesion can be affected by the degree of saturation and the strain rate. More specifically, the failure surface drawn through the failure envelope with respect to the matric suction is curved surface. Finally, to examine the effect of degree of saturation on resilient modulus (M_r) for C-40, the cyclic triaxial compression tests, i.e., the modulus resilient tests (MR tests), were performed on C-40 specimens with different degrees of saturation pursuant to AASHTO T307-99 (2003). The test results indicated that the degree of saturation of the specimen and the applied stress level have a considerable influence on the resilient

deformation characteristics of C-40 in MR test. The testing results obtained from monotonic and cyclic triaxial compression tests indicate that the degree of saturation and the strain rate influence the deformation-strength characteristics of the unsaturated granular subbase course material C-40 strongly. Therefore, to rationalize a design method for pavement structures better suited to the climatic conditions in cold snowy regions, the laboratory element tests under monotonic and cyclic loading, which take the influences of above-mentioned two factors into account, should be employed.

ACKNOWLEDGEMENT

My deepest gratitude goes first and foremost to my supervisor, Prof. Tatsuya Ishikawa for his guidance and invaluable advices throughout the course of this study.

Thanks are also due to all members of doctoral committee, Prof. Hiroyuki Tanaka and Prof. Yoshiaki Fujii For their comments and help.

I am sincerely grateful to Prof. Seiichi Miura for his support and assistance during the past three years.

I want to express my sincere thanks Associate Prof. Koichi Isobe and Assistant Prof. Shoji Yokohama for their big support and advices. I am also greatly indebted to Dr. Inam Aasim and Dr. Satoshi Matsumura who were always forward to help me during experiments. I grateful acknowledge to the students of Laboratory of Analytical Geomechniacs for their help during these three years.

I would like to thank Dr. Tetsuya Tokoro, who taught me technique and useful trick in unsaturated tests. I grateful acknowledge Prof. Tomoyoshi Nishimura and Associate Prof. Satoshi Nishimura for their advices for my research.

This research was made possible through the financial support of the China Scholarship Council.

Finally, my special thanks are extended to my beloved parents. Without their encouragement and confidence in me all through these years, it would not be possible for me to complete this thesis.

TABLE OF CONTENTS

ABSTRACT I
ACKNOWLEDGEMENT III
1 INTRODUTION 1
1.1 BACKGROUND 1
1.2 LITERATURE REVIEW 3
1.2.1 Unsaturated soils 3
1.2.2 Triaxial compression tests on unsaturated soils 4
1.2.3 Suction-controlled test method 6
1.3 THESIS OBJECTIVES 7
1.4 RESEARCH APPROACH 7
2 TEST MATERIAL AND APPARATUS 10
2.1 TEST MATERIAL 10
2.2 TEST APPARATUS 13
3 TEST METHODS AND EXPERIMENTAL CONDITIONS 19
3.1 TEST METHODS 19
3.1.1 Preparation of filters 19
3.1.2 Preparation of test specimens 20
3.1.3 Soil-water characteristic test 21
3.1.4 Triaxial compression tests 22
3.2 EXPERIMENTAL CONDITIONS 29
3.2.1 Experimental conditions for monotonic triaxial compression test 29
3.2.2 Experimental conditions for resilient modulus test 35
4 TEST RESULTS OF SOIL-WATER CHARACTERISTIC TEST 36
4.1 SOIL-WATER CHARACTERISTIC CURVE 36
4.2 WATER-AIR-PARTICLE SYSTEM 39
5 TEST RESULTS OF MONOTONIC TRIAXIAL COMPRESSION TESTS 41
5.1 EVALUATION OF MEASUREMENT PRECISION 41

5.1.1 System compliance and bedding errors 41
5.1.2 Measuring accuracy of volumetric strain 45
5.2 EFFECT OF DEGREE OF SATURATION 49
5.3 EFFECT OF STRAIN RATE 57
5.4 STRENGTH PARAMETERS 73
5.4.1 The total cohesion and total internal friction angle 73
5.4.2 The shear parameters for unsaturated soils 74
6 TEST RESULTS OF RESILIENT MODULUS TESTS 81
6.1 REPRODUCTION OF LOADING CONDITIONS FOR MR TEST 81
6.2 INFLUENCES OF DEGREE OF SATUTION ON RESILIENT MODULUS 82
7 CONCLUSIONS AND SUGGESTIONS 90
7.1 CONCLUSIONS 90
7.2 SUGGESTIONS 92
REFERENCES 93
NOTATIONS 99

1 INTRODUTION

1.1 BACKGROUND

Water can penetrate into pavement structures through many methods, such as rainfall and ground water (Dempsey and Elzeftawy, 1976), thereby causing change in degree of saturation inside pavement structures. In a cold snowy region, such as Hokkaido, Japan, enormous amounts of thaw water occurring due to the snow melt in springtime can infiltrate pavement structures besides the rainfall and the ground water, with the result that the degree of saturation in pavement structures was increasing. Therefore, it can be considered that climatic changes highly influence the degree of saturation of the subbase course layer at pavement structures in Hokkadio, Japan. Ishikawa et al. (2012a) pointed out that the increase in degree of saturation triggered by the water inflow led to temporal deterioration in bearing capacity of pavement structures. In addition, Oloo et al. (1997) revealed that the matric suction associated with water content has a significant effect on the bearing capacity of pavement structures. Thus, to provide rational designs for transportation infrastructures better suited to climatic conditions in cold snowy regions, it is of great importance to understand mechanical behaviors of subbase course materials constituting pavement structures under different unsaturated conditions.

On the other hand, to evaluate the mechanical stability of pavement structures towards traffic loads, the influence of the strain rate on shear behaviors of subbase course materials should be considered. According to Yamamuro and Lade (1993), it was revealed that monotonic shear behaviors of a granular soil was susceptible to the strain rate, and the shear strength under drained condition increased with the increase of the strain rate. Moreover, Aqil et al. (2005) performed drained triaxial compression tests at different constant strain rates on a crushed concrete aggregate as a backfill material, and detected that the mechanical behaviors were similar to the above-mentioned results with regard to the strain rate. However, Tatsuoka et al. (2008) performed drained traxial compression tests on Hime gravel material at largely different constant strain rates and found that the strength of the gravel material decreased with an increase in strain rate. Accordingly, it seems to be no uniform tendency regarding the effect of strain rate on the characteristics of granular materials. Especially, there is limited available information in existing literatures about mechanical behaviors of unsaturated subbase course materials with maximum particle size of almost 40 mm subjected to different strain rates.

In addition, the resilient modulus (M_r) of the subbase course material is an important stiffness parameter for analysing fatigue cracking in the subbase course layer of pavement structures, which mathematically is defined as the ratio of the cyclic deviator stress and the resilient (recoverable) axial strain when the applied stress is removed from the specimen. The "Determining the Resilient Modulus of Soils and Aggregate Material (AASHTO T307-99 2003)" has been introduced as the testing methods for subgrade soils used in design calculations of pavement structures. These testing methods were generally designed to examine the resilient modulus (M_r) parameter under optimum water content, but not to evaluate the effects of degree of saturation on the mechanical behaviors of subbase course materials. However, as discussed above, the subbase course layer of pavement structures is often under unsaturated conditions due to seasonal variations of degree of saturation. Changes in degree of saturation associated with the increases in the pore water pressure caused the reductions in the bearing capacity and the resilient modulus of soils. Accordingly, the results of resilient modulus tests (MR tests) for the unsaturated subbase course material have not yet been sufficiently clarified by laboratory element tests. Therefore, it is of great importance to evaluate the effect of degree of saturation on resilient properties for the subbase course material used at pavement structures in Japan.

Besides, it is well known that unsaturated soil tests are time-consuming, especially for the specimen with large particles. Therefore, experimental studies on the mechanical behaviors of a gravelly soil such as the subbase course material under unsaturated conditions are very limited. Nishimura et al. (2012) and Ishikawa et al. (2010) have performed some laboratory element tests for unsaturated soils by means of the pressure membrane method. In their studies, the validity of the pressure membrane method was confirmed by comparing the test results with those of the pressure plate method, which has been widely adopted for the unsaturated tests in the past. The methodology of the pressure membrane method was proved to successfully shorten the testing time to a significant extent. Ishikawa et al. (2014), in addition, developed a medium-size triaxial apparatus applicable for unsaturated gravelly soils, and the usefulness of the apparatus was confirmed based on the test results of a subbase course material and the Toyoura sand.

1.2 LITERATURE REVIEW

1.2.1 Unsaturated soils

Fredlund et al. (2012) proposed that the zone between the ground surface and the water table is referred to as the unsaturated soil zone as shown in Figure 1-1, and the ground surface climate is an important factor that controls the depth to the groundwater table and therefore the thickness of the unsaturated zone. The zone subjected to negative pore water pressures has become widely referred as the unsaturated soil zone in geotechnical engineering. Any soil near the ground surface, present in an environment where the water table is below the ground surface, will be subjected to negative pore water pressures and possible reduction in degree of saturation. Therefore, it is necessary to investigate the difference of mechanical properties between the saturated soil and the unsaturated soil.

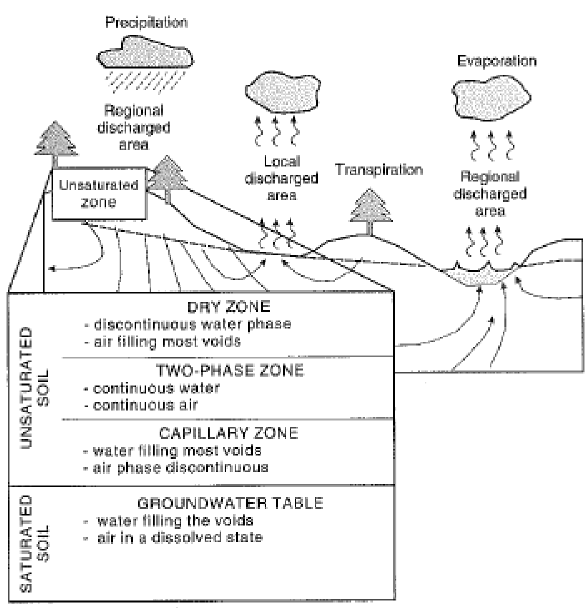

Figure 1-1 Subdivisions of unsaturated soil zone on local and regional basis (Fredlund et al. 2012)

The saturated soil and the air-dried soil have only two phases, i.e., soil structure and other fluid in the voids (e.g., water or air) pursuant to the principles and concepts of classical soil mechanics. However, the unsaturated soil has commonly been considered to have more than two phases, i.e., soil structure, water, and air. It is recently realized that the air-water interface (i.e., the contractile skin) plays an important role as an additional phase in unsaturated soils. Fredlund et al. (2012) suggested that when the air phase is continuous, the contractile skin interacts with the soil particles and provides an influence on the mechanical behavior of the soil. Figure 1-2 shows an element of unsaturated soil with a continuous air phase.

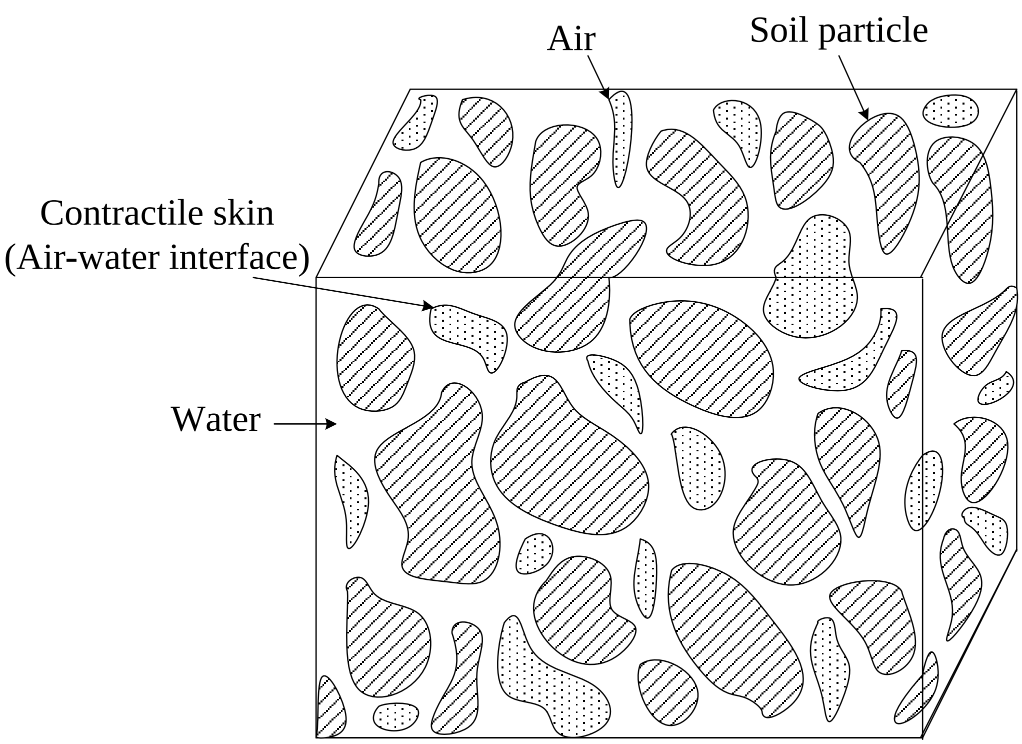

Figure 1-2 An element of unsaturated soil with a continuous air phase (Fredlund et al., 2012)

1.2.2 Triaxial compression tests on unsaturated soils

In the past decades, unsaturated soil mechanics has been developed considerably from theoretical analyses to experimental investigation. Unsaturated soil mechanics concerning shear strength, permeability and compaction etc. have been studied and established by many researchers (e.g., Bishop and Donald, 1961; Fredlund et al., 1978; Rahardjo et al., 2004; Zhan and Ng, 2006; Vanapalli and Lacasse, 2010; Oka et al., 2010). For example, Rahardjo et al. (2004) conducted consolidated drained and constant water content tests on the unsaturated sand to investigate the shear strength characteristics of sand associated with rainfall-induced slope failures. Zhan and Ng (2006) studied the shear strength characteristics of an expansive clay, and discussed the contribution of the matric suction to the shear strength. Oka et al. (2010) found that the initial matric suction strongly influenced the stress-strain behavior of the unsaturated silt. Thus, previous studies tended to focus on the unsaturated soil mechanics of sand, silt and clay, which have relatively small constituting particles. It is well known that unsaturated soil tests are time-consuming, especially for the specimen with large particles. Therefore, experimental studies on the mechanical behaviors of a gravelly soil such as a subbase course material under unsaturated conditions are very limited.

On the other hand, the stiffness of the granular subbase course material is an important factor for structural design and performance of pavement structures. The resilient modulus (M_r) obtained from cyclic triaxial compression tests can be used to evaluate the stiffness of pavement material under stress states produced by traffic loads. The pavement materials employed in in-situ construction are usually compacted at the optimum water content and maximum dry density. However, in-situ pavements are often under unsaturated conditions and the degree of saturation of pavement structures varies due to the seasonal variation and environmental changes. Therefore, it is important to consider the effects of matric suction on the resilient modulus for pavement materials. Ng et al. (2013) performed the cyclic triaxial compression tests on a subgrade soil to investigate the resilient modulus (M_r) values under various stress and matric suction conditions. The results showed that the matric suction played an important role on resilient modulus of the subgrade material, and the resilient modulus was highly dependent on the stress states. Ekblad and Isacsson (2008) present the experimental results from cyclic triaxial testing at various water contents using constant confining pressure on two different continuously graded granular materials, and proposed that increased water contents cause a reduction in resilient modulus and an increase in strain ratio. Therefore, it is necessary to evaluate effects of degree of saturation on resilient modulus

(M_r) for the granular subbase course material employed in the subbase course layer of pavement structures in Hokkaido, Japan.

1.2.3 Suction-controlled test method

Progress in unsaturated soil testing technology enables the control and the measurement of the matric suction in a variety of laboratory element tests for unsaturated soils (Fredlund, 2006). As a laboratory element test on unsaturated base course materials, which has a maximum particle size over 20 mm, various testing methods have been proposed in accordance with the research objectives and the experimental conditions to evaluate the deformation-strength characteristics and the water retention-permeability characteristics (e.g., Kolisoja et al., 2002; Coronado et al., 2005; Ekblad and Isacsson, 2008; Zhang et al., 2009; Yano et al., 2011; Craciun and Lo, 2010). For example, as a water retentivity tests for subbase course materials, which have a maximum particle size of almost 40 mm, Yano et al. (2011) employed the suction method (water-head type), while Ishigaki and Nemoto (2005) employed the soil column method. Moreover, Yano et al. (2011) conducted permeability tests on unsaturated subbase course material using a steady-state method (flux-control type). Those tests have revealed that the resilient modulus of unsaturated base course materials decreases with the increase in degree of saturation (Coronado et al., 2005; Ekblad and Isacsson, 2008). However, the mechanical behaviors of unsaturated subbase course materials have not yet been sufficiently cleared in Japan by laboratory element tests, although shear tests on unsaturated granular subbase course materials have been conducted overseas by measuring the matric suction. This is because laboratory element tests on unsaturated soils with large size particles are quite time-consuming due to the ceramic disk with very low permeability that is usually used in the test apparatus for unsaturated soils. For a detailed examination of the deformation-strength characteristics of unsaturated subbase course materials, therefore, it is indispensable that a new medium-size triaxial apparatus to be developed for these unsaturated soils, which can reduce the testing time as well as examine the deformation-strength characteristics of granular subbase course materials under various degrees of compaction and degree of saturation with high precision under sufficiently controlled experimental conditions.

1.3 THESIS OBJECTIVES

This thesis focused on evaluating the deformation-strength characteristics of the unsaturated subbase course material subject to monotonic and cyclic loadings. Keeping in mind the above discussion, the objectives in this study are shown as follows.

(1) To examine the effect of degree of saturation on strength characteristics of the unsaturated subbase course material.

(2) To evaluate the effect of strain rate on strength properties of the unsaturated subbase course material.

(3) To discuss the total internal friction angle and the total cohesion attributed to the matric suction and the strain rate.

(4) To examine the effect of degree of saturation on the resilient modulus (M_r) properties of the unsaturated subbase course material subject to cyclic loading.

In order to finish the objectives, a series of monotonic triaxial compression tests was carried out under desired unsaturated and strain rate conditions using the medium-size triaxial apparatus developed by Ishikawa et al. (2014). A new experimental method was designed and conducted to determine the resilient modulus (M_r) properties of the unsaturated subbase course material based on the standard method of test for "Determining the Resilient Modulus of Soils and Aggregate Material (AASHTO T307-99, 2003)".

1.4 RESEARCH APPROACH

This thesis introduces effects of degree of saturation and strain rate on the strength characteristics of the unsaturated subbase course material, along with resilient properties influenced by degree of saturation. The layout of the research approach is described in Figure 1-3.

The thesis is divided into seven chapters. A brief summary of the chapters is as follows. Chapter 1 presents the research background, literature review related to the behavior of unsaturated soils and objectives of this thesis. Chapter 2 is devoted to describing the test material and the newly developed triaxial compression apparatus that was used to control the matric suction by special design on the cap and pedestal. Chapter 3 introduces test methods and experimental conditions for monotonic triaxial compression tests and resilient modulus tests. The results of soil-water characteristic test is briefly presented in Chapter 4. Chapter 5 presents the test results of monotonic triaxial compression tests, while Chapter 6 discusses the effect of degree of saturation on resilient modulus properties of the subbase course material obtained by cyclic triaxial compression tests. Finally, Chapter 7 summarizes all of the findings in this study and provides suggestions for the future work.

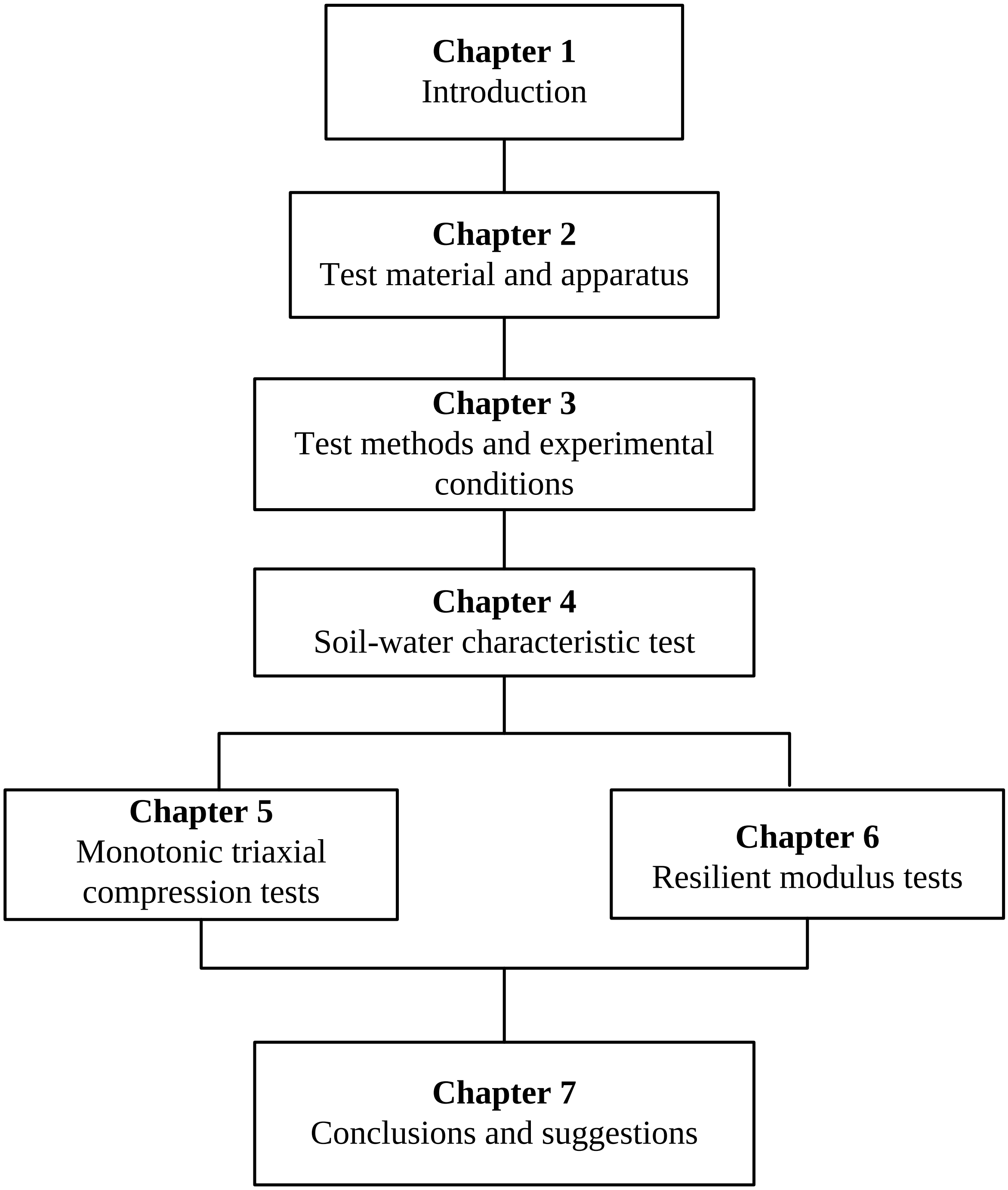

Figure 1-3 Layout of research approach.

2 TEST MATERIAL AND APPARATUS

2.1 TEST MATERIAL

The experimental pavement was constructed at the Tomakomai test road in Hokkaido (a cold and snowy island in northern Japan), which was used for long-term field measurement and in-situ tests. We conducted long-time field measurements of ground temperature, soil water content and settlement by layer inside the pavement structures. The pavement structures contain four layers, i.e., the asphalt-mixture layer, the subbase course layer, the anti-frost layer and the subgrade layer as shown in Figure 2-1 (Ishikawa, et al., 2012a). The base course layer of the pavement is composed of two layers (i.e., the subbase course layer and the anti-frost layer). The subbase course layer is constituted of natural andesite crusher-run with a maximum particle size of 40 mm, therefore it is called C-40. The test material in this study is the subbase course material C-40, which is a natural crusher-run made from angular, crush, hard andesite stone commonly used in the subbase course layer of pavements in Japan.

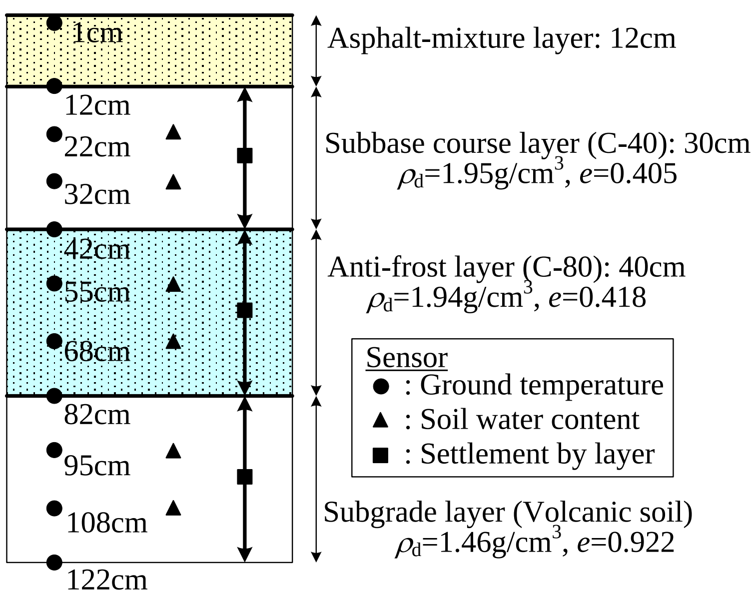

Figure 2-1 In-situ pavement for long-term field measurements (Ishikawa, et al., 2012a).

Figure 2-2 shows the photo of the subbase course material C-40. Though the maximum grain size of C-40 is 40 mm, test specimens were prepared by screening out particles larger than 38.1 mm from the original material pursuant to “Method of Test for Resilient Modulus of Unbound Granular Base Material and Subgrade Soils (E016)” (Japan Road Association 2007). The finer particle with grain size less than 0.075 mm was about 2 %. Physical properties and grain size distribution curve for test specimens are shown in Table 2-1 and Figure 2-3, respectively. The compaction curve for C-40 material was determined by the E-b method of Japanese industrial standard (2009). The water content-dry density curve for C-40 material with the w_{opt} of 8.2 % and the maximum dry density ρ_{dmax} of 2.070 g/cm^3 is shown in Figure 2-4.

Figure 2-2 Photo of the granular subbase course material C-40.

Table 2-1 Physical properties of C-40.

ρ_{dmax} *1 (g/cm^3)	w_{opt} *1 (%)	F_c (%)	PI	ρ_{dmax} *2 (g/cm^3)	ρ_{dmin} *2 (g/cm^3)
2.070	8.2	2.00	NP	2.270	1.680

Note: *1 ρ_{dmax} is w_{opt} obtained from compaction E-b method (JIS A 1210, 2009).

*2 ρ_{dmax} and ρ_{dmin} are obtained from test method for minimum and maximum densities of gravels (JGS 0162, 2009a).

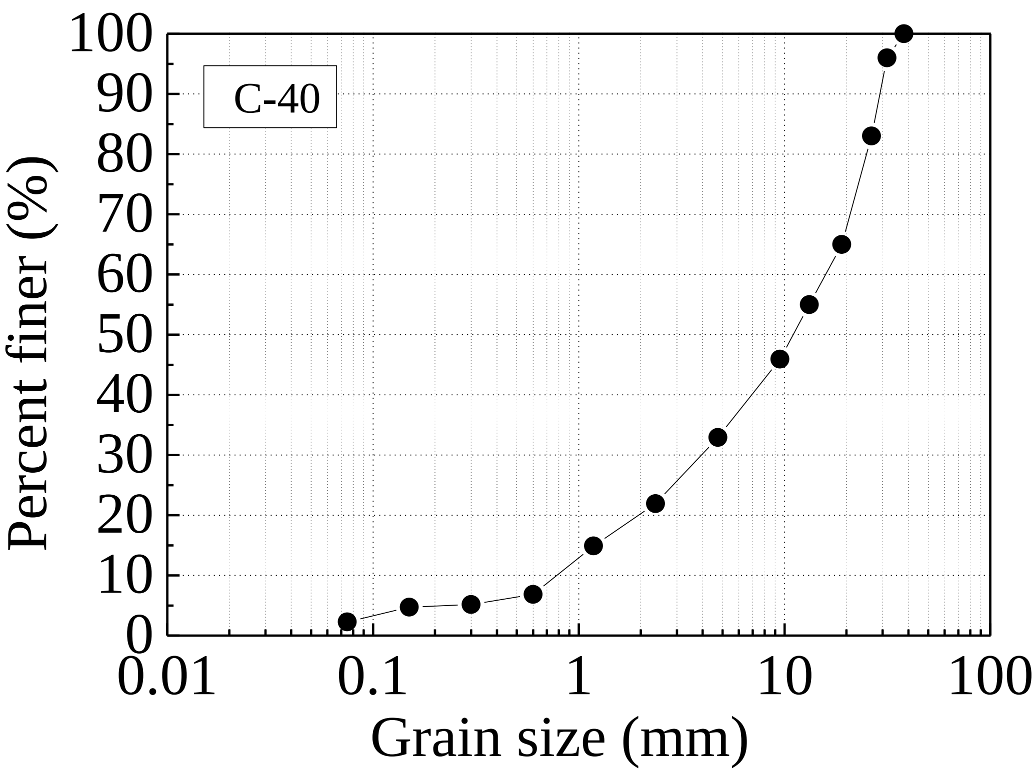

Figure 2-3 Grain size distributions of C-40 material.

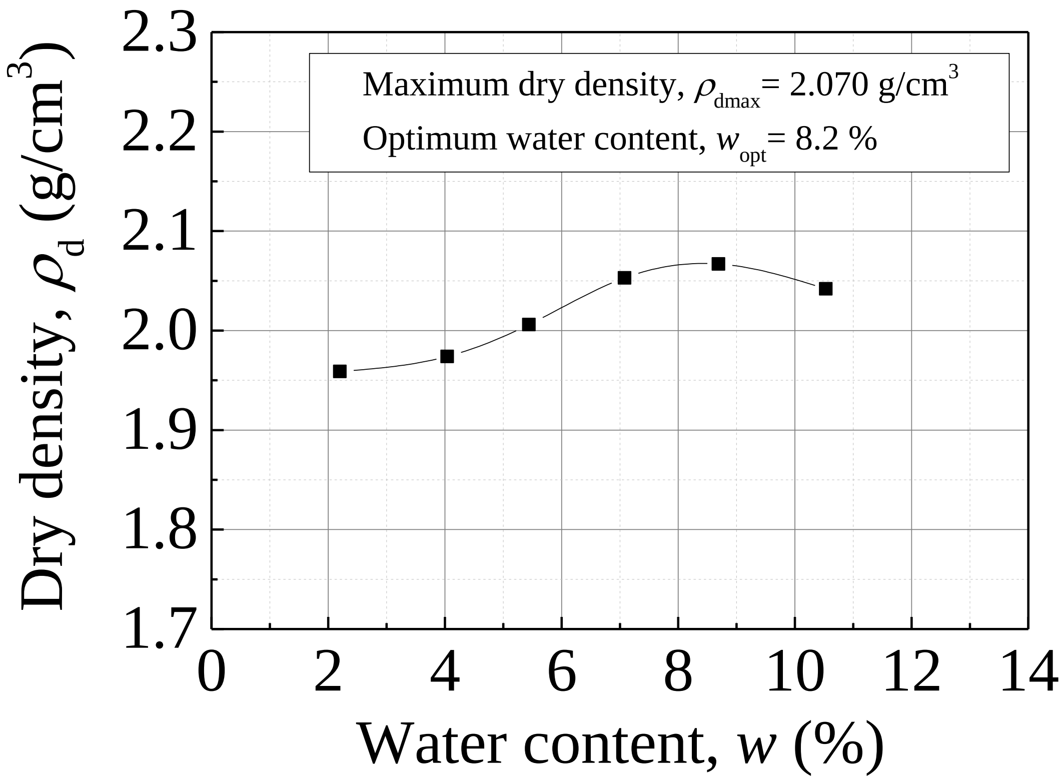

Figure 2-4 Water content-dry density curve.

2.2 TEST APPARATUS

A schematic diagram of the medium-size triaxial apparatus for the unsaturated granular subbase course materials is shown in Figure 2-5. The monotonic and cyclic triaxial compression tests were performed using this medium-size triaxial apparatus by the suction-controlled method along with pressure membrane method.

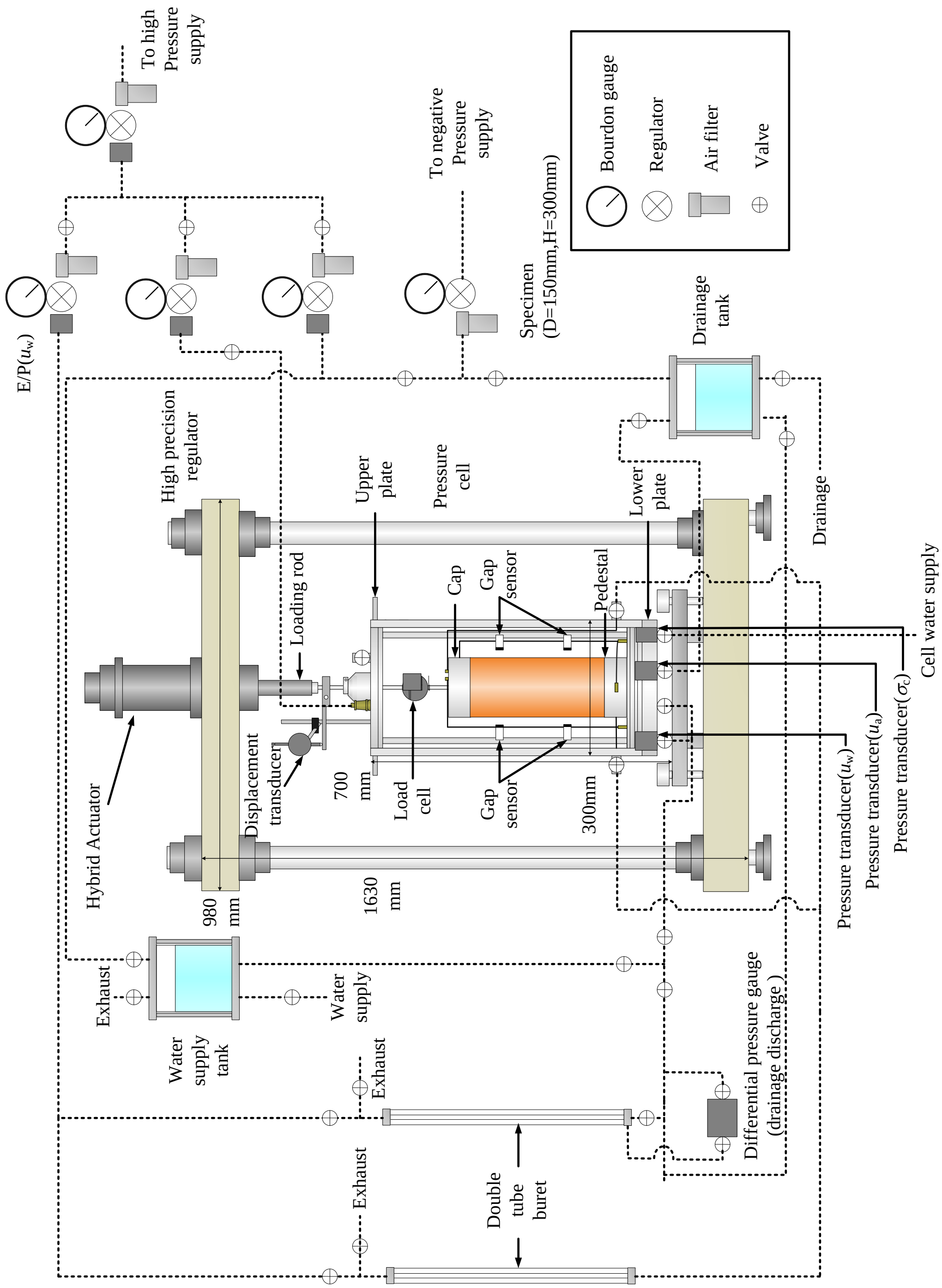

Figure 2-5. Medium-size triaxial compression apparatus for unsaturated granular subbase course materials.

One key feature of the apparatus is the structural design on the cap and the pedestal as shown on Figure 2-6. The designs for the cap and the pedestal are the same, which can control the pore water pressure and the pore air pressure independently. Therefore, the apparatus can apply the matric suction from both top and bottom ends of the specimen.

In the cap and the pedestal, the pore water pressure is applied to the specimen through a versapor membrane filter attached to the water plumbing path, while the pore air pressure is applied through a hydrophobic polyflon filter attached to the air supply path as shown in Figure 2-7. The photos of the versapor membrane filter and the hydrophobic polyflon filter are presented in Figure 2-8, respectively. Here, the versapor membrane filter is a kind of microporous membrane filters made from a hydrophilic acryic copolymer. Physical properties of the filters are shown in Table 2-2. The use of the cap and the pedestal to control matric suction may cause a problem of non-homogeneity of water content for two ends of the specimen. However, the effect of non-homogeneity of water content on the top and the base of the specimen could be ignored by evaluating bedding errors (BE) simultaneously, as will be described in the Chapter 5.

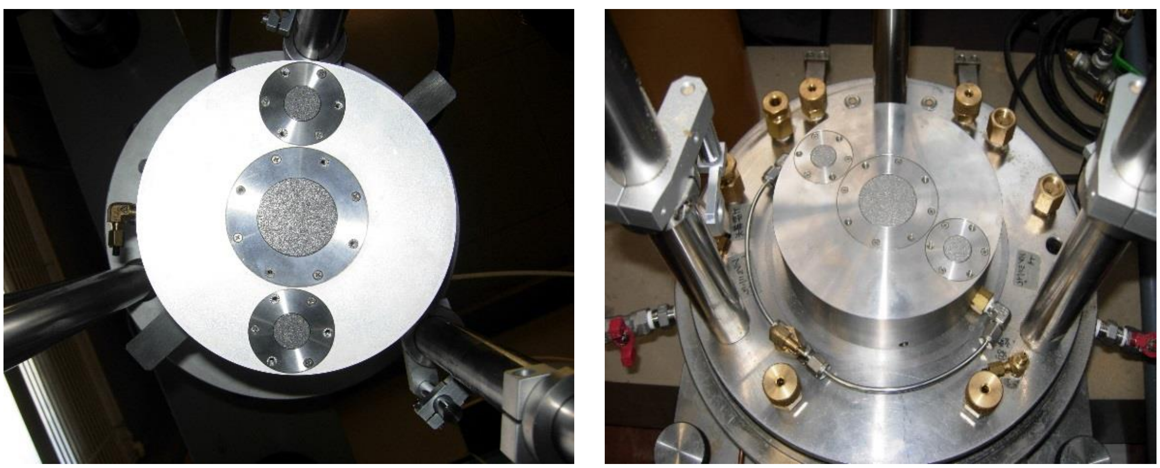

(a) The cap (b) The pedestal

Figure 2-6. Photos of cap and pedestal of medium-size triaxial compression apparatus.

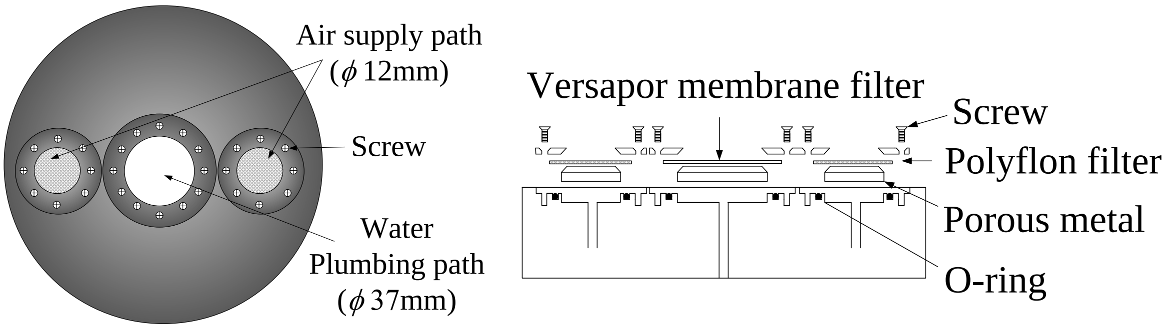

Figure 2-7. The diagrammatic sketch for membrane filters on pedestal and cap.

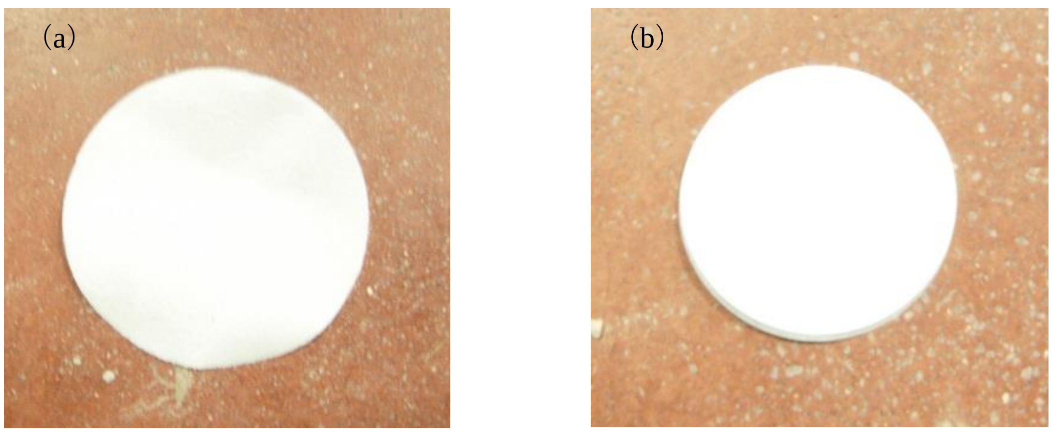

Figure 2-8. The photos of (a) versapor membrane filter and (b) hydrophobic polyflon filter.

Table 2-2 Physical properties of filters.

Name	Thickness (μm)	Pore size (μm)	AEV/WEV*1 (kPa)	Water flow*2 (ml/min/cm^2)
Versapor membrane filter	94.0	0.8	60.0	142
Hydrophobic polyflon filter	540.0	-	14.9	-

Note: *1 AEV is the air entry value of the versapor membrane filter, while WEV is the water entry value of hydrophobic polyflon filter.

*2 Water flow is the maximum water flow of the versapor membrane filter under the differential pressure of 70 kPa.

Other key features of the apparatus are as follows:

- Since the apparatus can use a medium-size cylindrical specimen with initially 300 mm in height (*H*) and 150 mm in diameter (*D*), a triaxial compression test can be performed in accordance with the "Standard Method of Test for Determining the Resilient Modulus of Soils and Aggregate Materials (AASHTO Designation: T307-99, 2003)" or the "Method of Test for Resilient Modulus of Unbound Granular Base Material and Subgrade Soils (E016)" (Japan Road Association 2007).
- The apparatus can apply the matric suction from both ends of the specimen (Figure 2-6). Besides, pore water is allowed to drain from both cap and pedestal. Accordingly, the apparatus can reduce the testing time by shortening the length of drainage path to half of the specimen height, in addition to the effect of the versapor membrane filter (Ishikawa et al., 2012b).
- The apparatus can apply axial load to a specimen with high accuracy by both the strain control method and the stress control method with only one hybrid actuator. Moreover, the apparatus can perform both monotonic loading tests with very slow strain rate and cyclic loading tests in which the maximum frequency of cyclic loading is up to about 10 Hz.

The measurements of stress and strain in a specimen for monotonic and cyclic triaxial compression tests are performed as follows. Axial stress (σ_a) of both tests was measured by a load cell installed inside the triaxial cell. Volumetric strain (ε_v) was mainly calculated by the lateral displacements of the specimen, namely the change in the specimen diameter, measured by two sets of two proximity transducers (gap sensors) attached at the points of 1/4 and 3/4 of the specimen height diagonally opposite to each other around the specimen diameter, respectively. For the saturated specimen, the volume of water drainage during test was also measured with a double tube burette.

The different measurements of axial strain (ε_a) for monotonic triaxial compression test and cyclic triaxial compression tests are discussed as follows.

(1) For monotonic triaxial compression tests, axial strain (ε_a) was mainly obtained by measuring the displacement of the loading piston with an external displacement transducer and two linear variable differential transducers (LVDTs), as shown in

Figure 2-9. Note that the influence of bedding errors (BE) was evaluated by using other two local linear variable differential transducers (called LLVDTs) attached at the center of the specimen shown in Figure 2-9. The effects of bedding error (BE) will be discussed in tests results in Chapter 5.

(2) For cyclic triaxial compression test, axial strain (ε_a) was obtained by measuring the displacement of the loading piston with an external displacement transducer, two linear variable differential transducers (LVDTs) and two LVDTs attached at the center of the specimen, in parallel with two side lines located at the diagonal position pursuant to AASHTTO T274-82 (AASHTO, 1986), as shown in Figure 2-9.

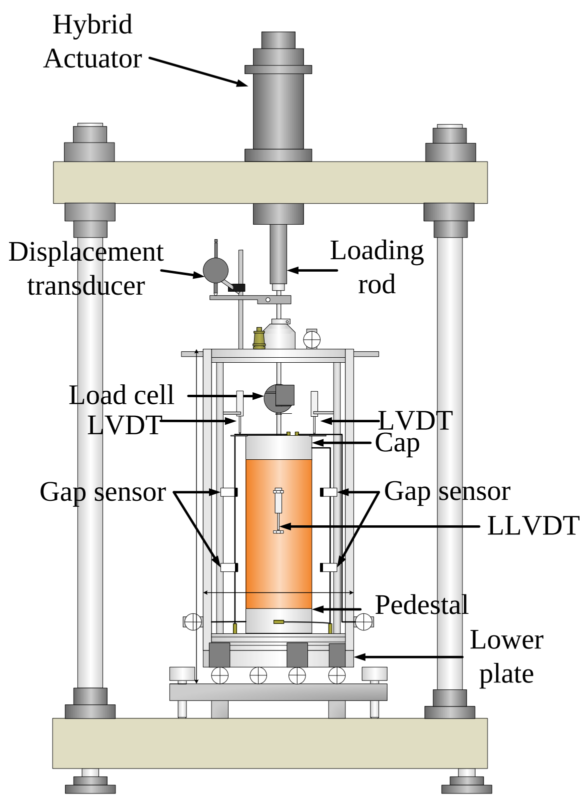

Figure 2-9. The setting of displacement measurement devices for the monotonic and cyclic triaxial compression.

3 TEST METHODS AND EXPERIMENTAL CONDITIONS

3.1 TEST METHODS

3.1.1 Preparation of filters

In this study, the versapor membrane filter was used to control and measure the matric suction for unsaturated specimens substitute for the ceramic disk. The pressure membrane method is classified as an "indirect method" of measuring soil suction, which is based on the assumption the filter will come to equilibrium with a soil having a specific suction (Fredlund and Rahardjo, 1993). The preparation of the versapor membrane filter is as follow. Firstly, the de-aired water was prepared, which was used for saturation of vasapor membrane filters, along with saturation of specimens under the saturated condition. The pure water was stored in a sealed tank with pumping vacuum pressure for 24 hours in order to remove any air bubbles. Secondly, the versapor membrane filter was saturated by de-air water in a container for one day as shown in Figure 3-1a. After that, the versapor membrane served in the container was put into a sealed tank and pumped by vacuum pressure with 90 kPa for 24 hours (*see* Figure 3-1b). These processes ensured the versapor membrane filter to be fully saturated with de-aired water.

(a) Saturation of the filters (b) Vacuum pressure for the filters

Figure 3-1. Preparation for the versapor membrane filter.

3.1.2 Preparation of test specimens

A cylindrical specimen with initially 300 mm in height and 150 mm in diameter as shown in Figure 3-2 was prepared with air-dried C-40 material (w=1.2%) in five layers by tamping with a woody rammer and compacting with a vibrator (*see*. Figure 3-3). Air-dried specimen was placed into a cylindrical mold in steps and spread into each layer of 60 mm in thickness. Subsequently, each layer was compacted by the vibrator in 3 minutes with constant compaction energy so as to attain the degree of compaction (D_c) of 95 %.

Note that fine particles which have grain size under 2 mm were spread on both ends of the specimen with the thickness of 5 mm so as not to degrade the function of filters installed on both the cap and the pedestal due to the direct contact of coarse particles. However, the use of the finer particle for cap and pedestal may cause a problem of bedding error (BE) for two ends of the specimen. The bedding error (BE) is evaluated simultaneously, as will be described in the Chapter 5.

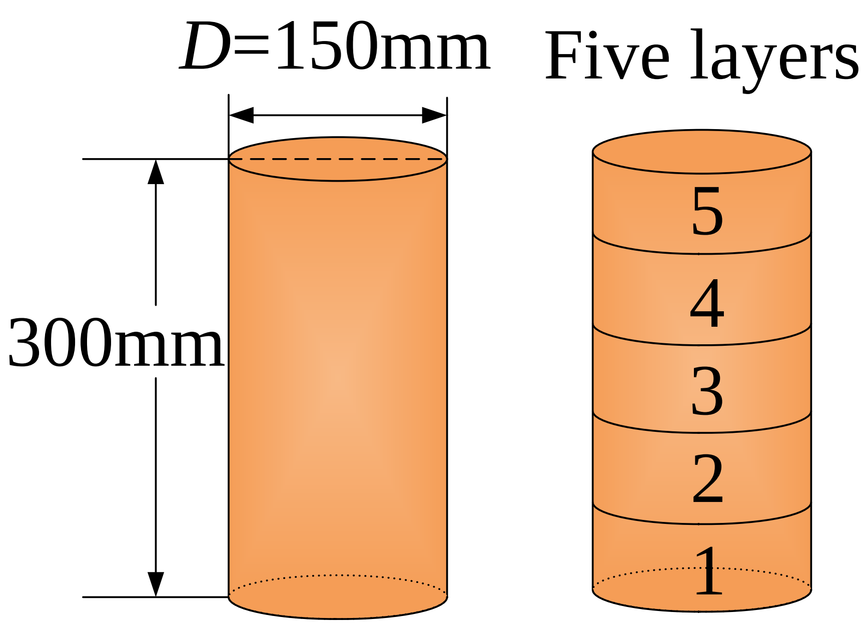

Figure 3-2. Preparation of test specimens.

Figure 3-3 Photo of the vibrator.

3.1.3 Soil-water characteristic test

A soil-water characteristic (SWCC) test was conducted based on the test method for water retentivity of soils of the Japanese Geotechnical Society (2009b). After setting the air-dried specimen in the triaxial cell, the specimen was permeated from the bottom end by de-aired water until the degree of saturation reached approximately 95 % or more. Note that based on the measurement of the water absorption into crushed stone particles during soil-water characteristic test pursuant to “Method of test for density and water absorption of coarse aggregates” (JIS A 1110), there is no water absorption or drainage to or from the soil particles after consolidation. Subsequently, the specimen was isotropically consolidated under a prescribed net normal stress (σ_{net}) of 49 kPa for 24 hours by applying confining pressure (σ_{c}) of 249 kPa, pore air pressure (u_a) of 200 kPa and pore water pressure (u_w) of 200 kPa. Here, the σ_{net} is defined as $\sigma_{\mathrm{net}}=\sigma_{\mathrm{c}} - u_a$. Note here that the axis-translation technique was used in the SWCC test in order to prevent pore water pressure less than zero based on Fredlund and Rahardjo (1993). The pore air pressure (u_a) here becomes equal to the externally applied air pressure. The pore water pressure can then be a positive pressure as pore air pressure. As a result, the pore water pressure undergoes the same pressure change as the change of applied air pressure. Therefore, the matric suction of the specimen remained 0 kPa regardless of the translation of both pore air pressure and pore water pressure.

After the consolidation process, the soil-water characteristic test was commenced at a condition near saturation, and it proceeded through a drying process in accordance with the following procedure. A starting point on the drying curve was established by decreasing u_w while keeping both σ_c and u_a constant, in other words by applying a low matric suction (s) to the soil specimen. Here, the s is defined as $s= u_a - u_w$. An increase in matric suction (s) causes the drainage of pore water from the specimen. Upon attaining an equilibrium condition, the water content corresponding to the applied matric suction was computed by reading the change in water volume between two successive applied matric suctions with a double tube burette. The above-described procedure was then repeated for higher values of matric suction by decreasing the applied pore water pressures in steps. Note that the volumetric change of the specimen could hardly be discerned during soil-water characteristic test.

3.1.4 Triaxial compression tests

In this study, two types of triaxial compression tests were performed on C-40 specimens, that is, monotonic triaxial compression tests and cyclic triaxial compression tests. Monotonic triaxial compression tests were carried out under four kinds of degrees of saturation with two different strain rates, in conformance with the standards of the Japanese Geotechnical Society (JGS 0524 2000a and JGS 0527 2000b). Cyclic triaxial compression tests, i.e., resilient modulus tests (MR tests) were conducted under three kinds of degrees of saturation pursuant to AASHTO T307-99 (2003).

Note that the mechanical properties of unsaturated coarse-grained specimens have often been investigated by compacting soil materials under various water contents, which causes the difference on the particle skeleton structure of the specimen. It is most important to realize in this study that the specimens were compacted at the same initial water content (w=1.2%) and with the same compacted effort. Then the specimens with different degree of saturation were obtained by adopting the suction-controlled method in accordance with soil-water characteristic curve (SWCC). Therefore, the C-40 specimens can be tested under unsaturated conditions and then the degree of saturations of unsaturated specimens were similar to the degree of saturation of the subbase course layer material encountered in the in-situ pavement structure.

3.1.4.1 Monotonic triaxial compression test

Monotonic triaxial compression tests under the consolidated drained condition (CD test) were performed under two different strain rates with four kinds of degrees of saturation, namely "air-dried"(S_r=8.2%, w=1.2%), "unsaturated"(about S_r=35%, w=7.69%) and (about S_r=57.2%, w=8.2%), as well as "saturated"(S_r=100%, w=12.20%).

The consolidations for specimens under air-dried, saturated, and unsaturated conditions were carried out as follows.

(1) For the air-dried specimen (S_r=8.2%), the specimen after setting up was isotropically consolidated under a prescribed effective confining pressure (σ_c') of 34.5 kPa, 49 kPa, or 68.9 kPa for 24 hours by applying the same cell pressures (σ_c) while the air supply path is opened to the atmosphere.

(2) For the saturated specimen (S_r=100%), the carbon dioxide gas was added from the bottom end of the air-dried specimen for about 3 hours, and subsequently specimen was permeated with de-aired water into the voids. In this case, "the double vacuuming method" (Ampadu and Tatsuoka, 1993) was used by suctioning pore air from the specimen with high negative pressure. Besides, a back pressure of 200 kPa was applied to ensure the saturation of the specimen. The pore water pressure coefficient B-value of saturated specimen was insured as 0.96 or more. Following the saturation, the specimen was isotropically consolidated under the above-mentioned effective confining pressures (σ_c') for 24 hours by applying a designated cell pressure (σ_c) of 234.5, 249, or 268.9 kPa and pore water pressure (u_w) of 200 kPa.

(3) For unsaturated specimen (S_r=35%) or (S_r=57.2%), the specimen was isotropically consolidated under a prescribed net normal stress (σ_{net}) for 24 hours by applying cell pressure (σ_c) of 234.5 kPa, 249 kPa, or 268.9 kPa, while keeping pore air pressure (u_a) of 200 kPa and pore water pressure (u_w) of 200 kPa. Here, the σ_{net} is defined as $\sigma_{\mathrm{net}}=\sigma_c - u_a$, which is numerically the same value of effective confining pressure (σ_c').

Subsequently, an unsaturated specimen under intended matric suction ($s=u_a-u_w$) of 10.0 kPa or 0.5 kPa was produced by decreasing pore water pressure (u_w) while keeping both cell pressure (σ_c) and pore air pressure (u_a) constant. For unsaturated specimen with degree of saturation of 35 % or 57.2 %, the matric suction ($s=u_a-u_w$) of 10 kPa or 0.5 kPa was set up based on the SWCC curve, as described in late section.

Upon attaining an equilibrium condition in the consolidation process, the specimen was continuously sheared by applying an axial deviator stress ($q=\sigma_a-\sigma_c$) at a designated axial strain rate ($\dot{\varepsilon}_a$) of 0.05 %/min or 0.5 %/min under consolidated drained condition (CD test) regardless of the water content, while all other testing parameters were held constant. Here, σ_a is the axial stress. Note that for the unsaturated condition both the pore air and the pore water are allowed to drain.

After finishing all the tests under unsaturated conditions, the air entry value (AEV) of the versapor membrane filter would be evaluated by applying matric suction increasingly until air passed through the filter. Figure 3-4 shows relationships of matric suction, volume of water drainage, along with time. As we can see from Figure 3-4, the matric suction was applied on the versapor membrane filter with 10 kPa step by step. At the beginning stage with matric suction of 0 kPa to 20 kPa, the water covering at surface of the versapor membrane filter passed through the filter quickly. At the range of the matric suction from 60 kPa to 80 kPa, the volume drainage of water became increasing gradually. The breaking point showed at matric suction of 80 kPa, because air passed through filter sharply. The measurements showed that the air entry value of versapor membrane filters after tests was nearly equal to that before tests (60 kPa). This indicated that the versapor membrane filters after tests suffered little degradation from the wear and tear during monotonic triaxial compression tests on the granular subbase course material.

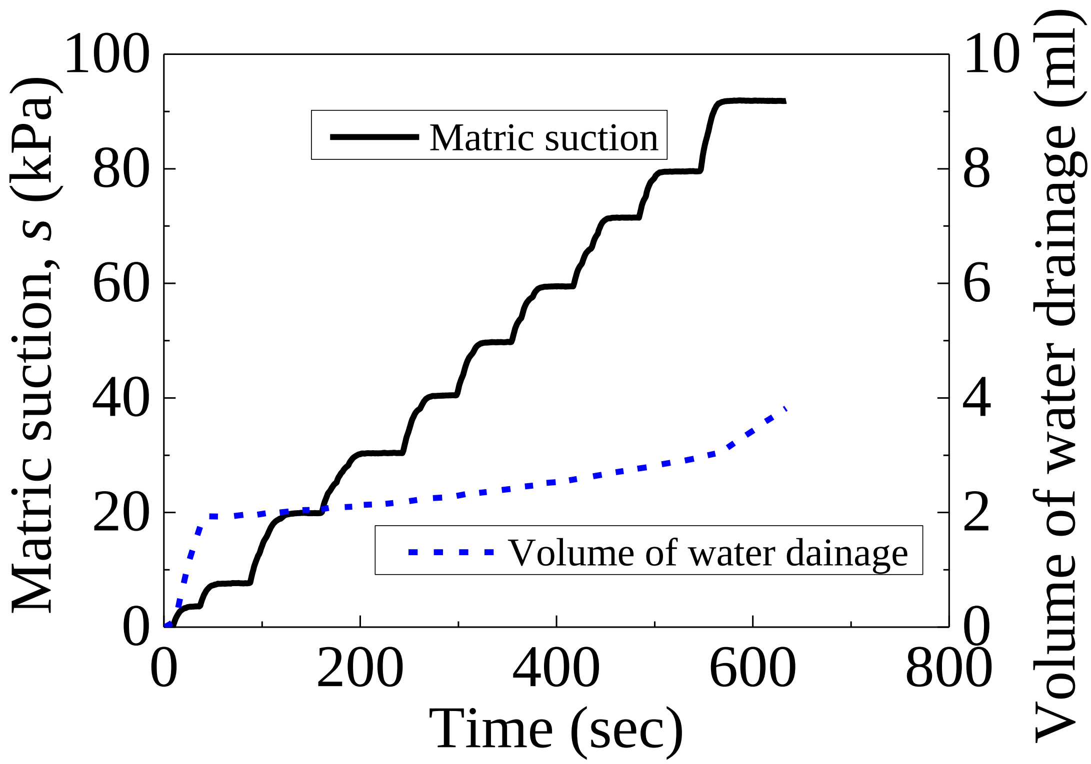

Figure 3-4. The AEV value of versapor membrane filter after unsaturated test.

3.1.4.2 Resilient modulus test (MR test)

A resilient modulus test (MR test) using the triaxial compression test with cyclic loading pursuant to the AASHTO T307-99 (2003) is designed to evaluate the resilient deformation characteristics of C-40 specimen by simulating the traffic wheel loading on in-situ pavement structure. The resilient modulus (M_r) values can be used with structural response analysis to calculate the pavement structural response to wheel loads, and with design procedures of pavement structure. In this study, the loading conditions standardized by AASHTO T307-99 (2003) for the subbase materials were employed (*see* Table 3-1).

Table 3-1 Loading conditions of MR tests.

Name	σ'_c (kPa)	q_{cont} (kPa)	q_{cyclic} (kPa)	q_{max} (kPa)	N_c (cycle)
Conditioning process	103.4	10.3	93.1	103.4	1000
Testing process MR-1	20.7	2.1	18.6	20.7	100
Testing process MR-2	20.7	4.1	37.3	41.4	100
Testing process MR-3	20.7	6.2	55.9	62.1	100
Testing process MR-4	34.5	3.5	31.0	34.5	100
Testing process MR-5	34.5	6.9	62.0	68.9	100
Testing process MR-6	34.5	10.3	93.1	103.4	100
Testing process MR-7	68.9	6.9	62.0	68.9	100
Testing process MR-8	68.9	13.8	124.1	137.9	100
Testing process MR-9	68.9	20.7	186.1	206.8	100
Testing process MR-10	103.4	6.9	62.0	68.9	100
Testing process MR-11	103.4	10.3	93.1	103.4	100
Testing process MR-12	103.4	20.7	186.1	206.8	100
Testing process MR-13	137.9	10.3	93.1	103.4	100
Testing process MR-14	137.9	13.8	124.1	137.9	100
Testing process MR-15	137.9	27.6	248.2	275.8	100

The maximum deviator stress (q_{max}) in Table 3-1 is composes of the cyclic deviator stress (q_{cyclic}) and the contact stress (q_{cont}). The MR stress sequence in Table 3-1 contains conditioning process, which eliminates the effects of the interval between compaction and loading and eliminates the initial loading and reloading. This conditioning process also aids in minimizing the effects of initially imperfect contact between the cap and the specimen (AASHTO T307-99, 2003). A haversine-shaped load pulse with a load duration of 0.1 second followed by a rest period of 0.9 second, i.e., a loading frequency of 10 Hz, was applied as the traffic wheel loading on the subbase course material as shown in Figure 3-5. The resilient modulus (M_r) was used to describe the response of the specimen, which can be given as Equation 3-1.

$$M_r = \frac{q_{max} - q_{cont}}{\varepsilon_r} = \frac{q_{cyclic}}{\varepsilon_r} \tag{3-1}$$

here, ε_r: is the resilient (recovered) axial strain due to cyclic deviator stress. q_{max}: the total deviator stress applied to the specimen, including the contact and cyclic (resilient) deviator stress. q_{cont}: vertical stress placed on the specimen to maintain a positive contact between the specimen cap and the specimen, $q_{cont} = 0.1q_{max}$. q_{cyclic}: the difference between the total deviator and vertical stress, $q_{cyclic} = q_{max} - q_{cont}$.

In addition, based on Table 3-1, the test procedure for MR tests requires both a conditioning process with 1000 loading cycles (N_c) and an actual testing process with 100 loading cycles under 15 successive paths with varying combinations of effective confining pressure (σ'_c) and deviator stress (q). The applied stress path for MR tests is shown on Figure 3-6. Hence, from a single test on a soil specimen under a specified degree of saturation, fifteen resilient moduli at different combinations of confining pressure and deviator stress were obtained. The resilient modulus (M_r) value was determined by averaging the resilient deformation of the last five cycles at each confining pressure.

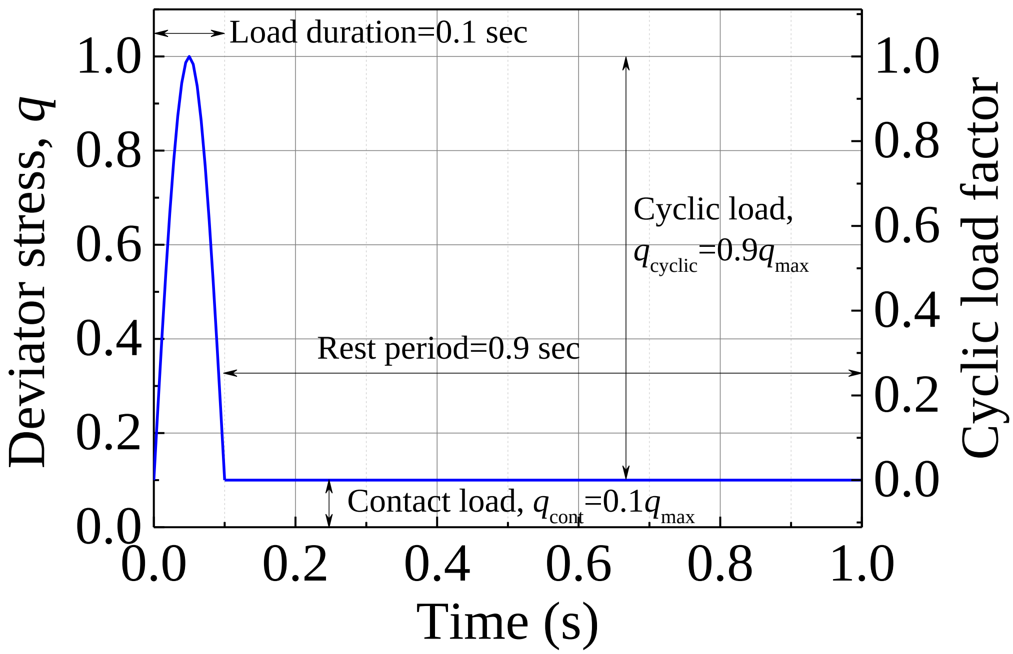

Figure 3-5. Loading wave of MR tests.

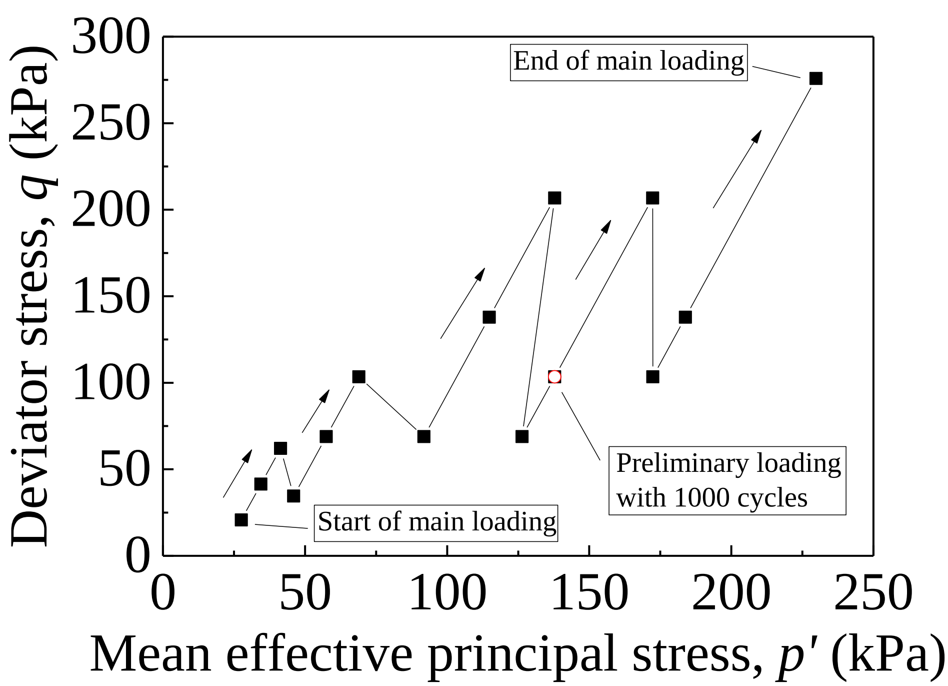

Figure 3-6. Applied stress path of MR tests.

Now, the test method for resilient modulus (MR) test will be introduced. After preparing the soil specimens under saturated (S_r=100%), unsaturated (S_r=36.7%), and air-dried (8.2%) conditions, in the same way as for the monotonic traxial compression tests mentioned above, MR tests on C-40 specimens were also performed under drained condition (CD test) as follows.

For air-dried and saturated specimens, conventional MR tests were conducted in accordance with AASHTO T307-99 (2003). Here, in the air-dried condition, the designated effective confining pressure (σ'_c) as shown on Table 3-1, was applied by providing a specified positive cell pressure (σ_c), while keeping the same pore air pressure (u_a) as atmospheric pressure and closing the pore water pressure path. In the saturated condition, it was applied by providing a specified σ_c, maintaining the pore water pressure (u_w) of 200 kPa, and closing the pore air pressure path. For the unsaturated specimen, suction-controlled MR tests were carried out on the specimen under a certain cell pressure (σ_c), while maintaining constant values for pore air pressure (u_a) and pore water pressure (u_w) of 200 kPa and 190 kPa, respectively, and keeping both pore pressure paths open. Note here that the effective confining pressure (σ'_c) for unsaturated specimen was equal to the difference between cell pressure (σ_c) and pore air pressure (u_a).

3.2 EXPERIMENTAL CONDITIONS

3.2.1 Experimental conditions for monotonic triaxial compression test

In this study, four kinds of degrees of saturation are selected for specimens, that is 100 %, 57.2 %, 35 % and 8.2 %. The effective confining pressures are 34.5 kPa, 49 kPa and 68.9 kPa, respectively. The strain rates are 0.5 %/min and 0.05 %/min. All experimental conditions for monotonic triaxial compression tests on C-40 specimens are summarized in Table 3-2.

Table 3-2 Experimental conditions for monotonic triaxial compression tests.

(a) Air-dried conditions

No.	A-1	A-2	A-3	A-4	A-5	A-6
σ_c' (kPa)	34.5	34.5	49.0	49.0	68.9	68.9
$\dot{\varepsilon}_a$ (%/min)	0.05	0.5	0.05	0.5	0.05	0.5
D_c (%)	95.2	95.7	96.2	96.0	94.9	96.0
ρ_{d0} (g/cm^3)	1.97	1.98	1.99	1.99	1.96	1.99

(b) Unsaturated conditions

	Simulated condition						Optimum condition					
No.	U-1	U-2	U-3	U-4	U-5	U-6	O-1	O-2	O-3	O-4	O-5	O-6
s (kPa)	10.0	10.0	10.0	10.0	10.0	10.0	0.5	0.5	0.5	0.5	0.5	0.5
σ_c (kPa)	234.5	234.5	249.0	249.0	268.9	268.9	234.5	234.5	249.0	249.0	268.9	268.9
u_w (kPa)	190.0	190.0	190.0	190.0	190.0	190.0	199.5	199.5	199.5	199.5	199.5	199.5
u_a (kPa)	200.0	200.0	200.0	200.0	200.0	200.0	200.0	200.0	200.0	200.0	200.0	200.0
σ_c' (kPa)	34.5	34.5	49.0	49.0	68.9	68.9	34.5	34.5	49.0	49.0	68.9	68.9
$\dot{\varepsilon}_a$ (%/min)	0.05	0.5	0.05	0.5	0.05	0.5	0.05	0.5	0.05	0.5	0.05	0.5
D_c (%)	94.4	96.5	95.3	96.0	95.4	95.4	95.8	95.6	95.3	95.4	95.0	96.1
ρ_{d0} (g/cm^3)	1.95	1.99	1.97	1.99	1.97	1.97	1.95	1.98	1.97	1.97	1.97	1.99

(c) Saturated conditions

No.	S-1	S-2	S-3	S-4	S-5	S-6
σ_c (kPa)	234.5	234.5	249.0	249.0	268.9	268.9
u_w (kPa)	200.0	200.0	200.0	200.0	200.0	200.0
σ_c' (kPa)	34.5	34.5	49.0	49.0	68.9	68.9
$\dot{\varepsilon}_a$ (%/min)	0.05	0.5	0.05	0.5	0.05	0.5
D_c (%)	95.8	96.0	96.2	96.2	95.8	96.0
ρ_{d0} (g/cm^3)	1.98	1.99	1.99	1.99	1.98	1.99

Firstly, the degree of saturation of 100 % is the saturated condition, while degree of saturation of 8.2 % is the air-dried condition. The degree of saturation of 35 % was selected in order to simulate the regular unsaturated condition of in-situ pavement. Figure 3-7 shows the temporal transitions in daily mean degree of saturation during the long-term field measurement in the subbase course layer of the experimental pavement in Tomakomai, Sapporo, Japan (Ishikawa et al., 2012a). From Figure 3-7, it is evident that the degree of saturation (S_r) for the subbase course layer is nearly stable at around 35 % during the regular seasons except for the freezing and thawing season. The degree of saturation of 57.2 % is the corresponding optimum water content of C-40 material. For simplicity, S_r=35 % and S_r=57.2 % were called "simulated" and "optimum" conditions hereafter, respectively.

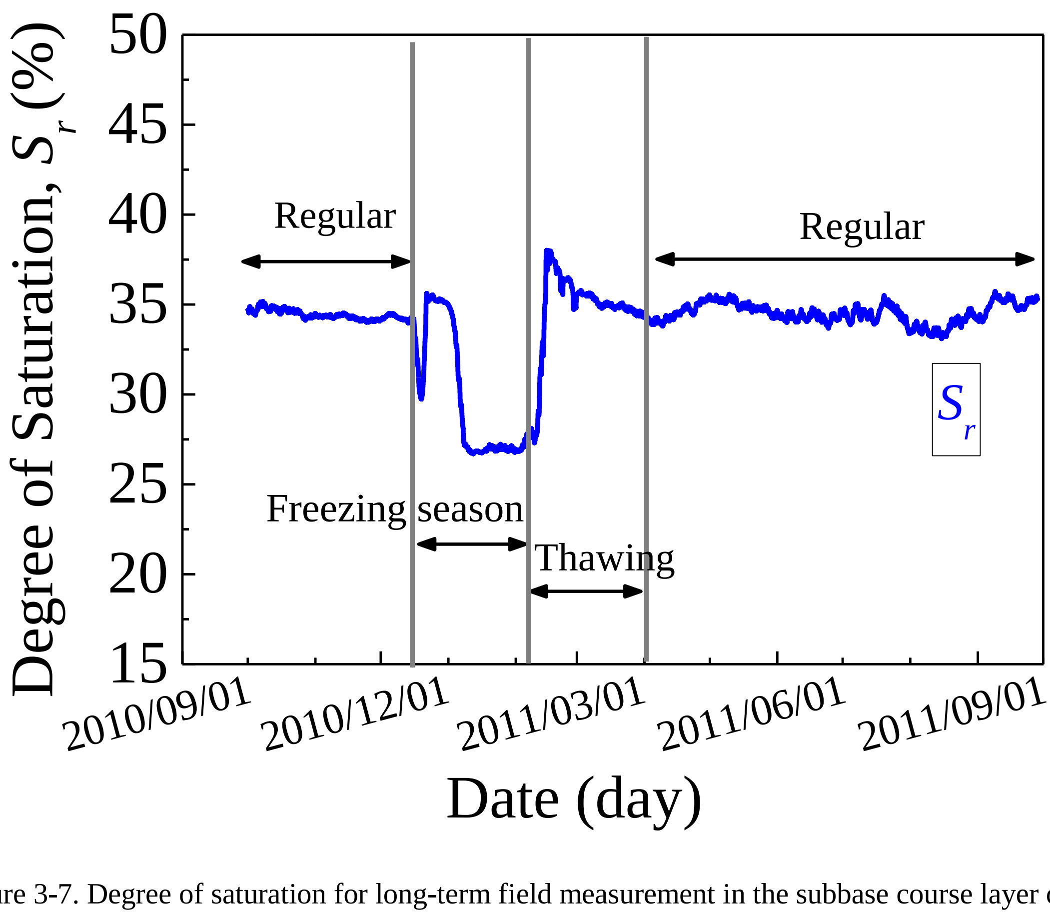

Figure 3-7. Degree of saturation for long-term field measurement in the subbase course layer of the in-situ pavement.

Secondly, the effective confining pressures (σ_c') of 34.5 kPa, 49 kPa, and 68.9 kPa were determined based on stress analysis of Japanese paved road model by GAMES (General Analysis Multi-layered Elastic Systems, Maina and Matsui, 2004). Figure 3-8 shows one kind of Japanese paved road model under standard design wheel loads, which was redrawn from Ishikawa et al. (2008). The standard design wheel load is 49 kN, which is divided equally on each wheel (i.e., 24.5 kN) and the wheel diameter and the distance between wheels as shown in Figure 3-8 are indicated in the pavement design manual for Japanese paved roads issued by the Japan Road Association (2006). The pavement structure shown in Figure 3-8 is one type of pavement in Japan, which includes three layers with different thickness, i.e., asphalt mixture layer, the subbase course layer, and subgrade layer. There are four types of pavement structures used for stress analysis by GAMES as shown in Table 3-3, and each layer of pavement structures has different elastic modulus (E) and the poison's ratio (v). Due to the different elastic modulus (E) for the first and second layers, the pavement type 1 and pavement type 2 can be subdivided into 12 types, while pavement type 3 and pavement type 4 can be subdivided into 21 types and 24 types, respectively.

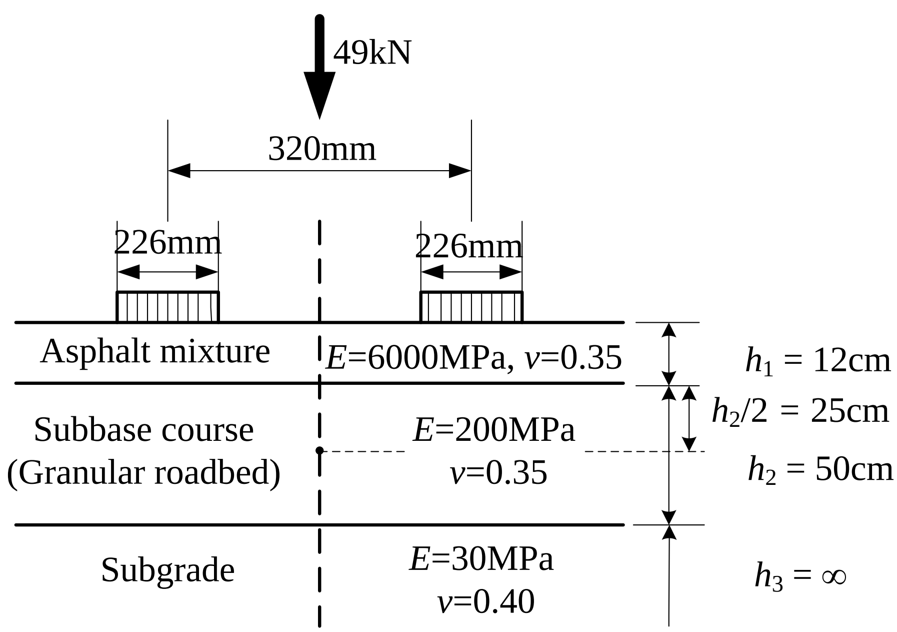

Figure 3-8. The cross section of double wheel loads on pavement.

Table 3-3 Summary of pavement types.

Pavement type 1

Layer	h (cm)	v	E (MPa)
1	12	0.35	2000/6000
2	40/50	0.35	50/200/500
3	-	0.40	30/200

Pavement type 2

Layer	h (cm)	v	E (MPa)
1	15	0.35	2000/6000
2	55/60	0.35	50/200/500
3	-	0.40	30/200

Pavement type 3

Layer	h (cm)	v	E (MPa)
1	26	0.35	2000/4000/8000
2	55/60	0.35	50/200/250/500
3	-	0.40	30/100

Pavement type 4

Layer	h (cm)	v	E (MPa)
1	35	0.35	2000/4000/8000
2	65/60	0.35	50/200/250/500
3	-	0.40	30/100

Figure 3-9 is the results of stress states on the top of the subbase layer of four types of typical Japanese pavement structure, which were calculated with coefficients of interface slip rate of 0.0 and 0.5 calculated by GAMES. In Figure 3-9, the Max. is largest calculated stress on the horizontal plane for each pavement type, while the Ave. is the average stress on the horizontal plane of each pavement type with elastic modulus (E) and the poison's ratio (v). The maximum "Max." value with different slip rates of 0.0 and 0.5 are 49.40 and 67.78 kPa, respectively, while the maximum "Ave." value of each type of pavement structures are 33.39 and 67.56 kPa. Here, the interface slip rate is one parameter in GAMES program. The interface slip rate is defined in terms of shear stresses, which can be represented by using a shear spring model (Maina and Matsui, 2004). The interface slip rate shows the degree of interface slip between the asphalt mixture layer and the subbase course layer on the pavement. Though the interface slip rate ranges from 0.0 to 1.0, the slip rate equal to 0.0 means there is no slip between the layers, and the slip rate equal to 1.0 means no friction between the layers (Maina and Matsui, 2004). Figure 3-9 also shows loading conditions of AASHTO standard method of test for determining the resilient modulus (M_r) of soils and aggregate material (T 307-99, 2003). As shown in Figure 3-9, the calculated confining pressures by GAMES of 33.39 kPa and 67.78 kPa are closed to the confining pressures of 33.4 kPa and 68.9 kPa in the AASHTO standard.

Two kinds of strain rates ($\dot{\varepsilon}_a$), namely 0.05 %/min and 0.5 %/min, were adopted in this study. The strain rate of 0.05 %/min in CD test was selected according to the standard of the Japanese Geotechnical Society (JGS 0527, 2000b), while the strain rate of 0.5 %/min was designed by referring to the axial strain rate of 1.0 %/min in quick shear test of MR test (T 307-99, 2003).

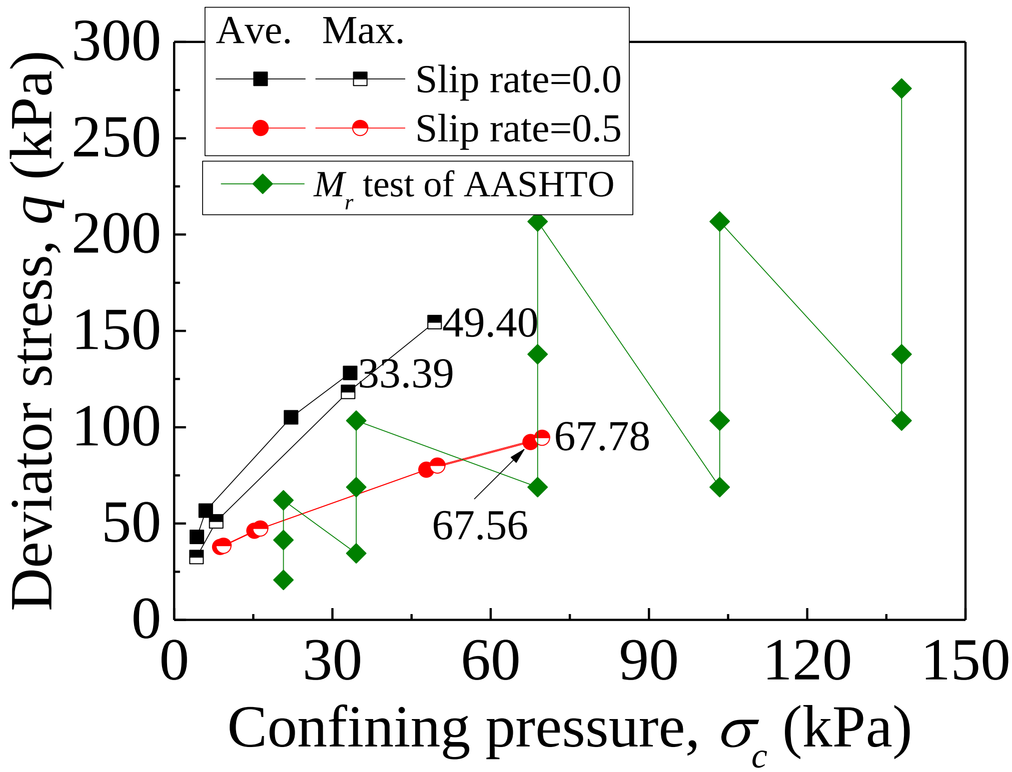

Figure 3-9. Stress state inside typical Japanese pavement structures.

3.2.2 Experimental conditions for resilient modulus test

In order to evaluate the effect of degree of saturation (S_r) on the resilient modulus (M_r) of the granular subbase course material C-40, three different degrees of saturation were selected for resilient modulus tests (MR tests), i.e., air-dried, simulated, and saturated conditions, respectively. The degree of saturation (S_r) for the air-dried specimen was 8.2 %. The degree of saturation (S_r) for the saturated specimen was 100 %, and the *B*-value for the saturated condition was 0.96 or higher. For the simulated condition, the degree of saturation (S_r) was about 36.7 %, which is similar value for degree of saturation in the subbase course layer of the in-situ pavement during the regular seasons.

4 TEST RESULTS OF SOIL-WATER CHARACTERISTIC TEST

4.1 SOIL-WATER CHARACTERISTIC CURVE

The soil-water characteristic curve (SWCC) is the relationship between the degree of saturation (S_r) and the suction for soils. The suction as quantified in terms of the relative humidity is commonly called “total suction”. The total suction contains two components, namely, matric suction and osmotic suction (Fredlund and Rahardjo, 1993). The osmotic suction was considered to be arising from salt solutions in a soil, while the matric suction is the capillary component of free energy and is the major contributor to the total suction. Generally, the matric suction (s) is condemned as the difference between pore air pressure and pore water pressure (i.e., $s=u_a-u_w$). In this study, we considered only the matric suction ($s=u_a-u_w$).

The soil-water characteristic test was performed on C-40 specimen with degree of compaction (D_c) of 95 % based on the test method for water retentivity of soils of the Japanese Geotechnical Society (2009b). The soil-water characteristic curve (SWCC) of C-40 specimen in the drying process is shown in Figure 4-1, which is the desaturation characteristic of C-40 expressed by the relationship between the matric suction ($s=u_a-u_w$) and the degree of saturation (S_r). Note that the matric suction is equal to suction without regard for the osmotic suction in this study. The SWCC curve in Figure 4-1 was J-shaped curve with no clear air entry value (AEV), owing to the rapid drainage concurrent with the application of the matric suction.

The red line in Figure 4-1 is the fitting curve for soil-water characteristic curve (SWCC) by using logistic model-A, called LG-A model (Mori et al., 2009). The LG-A model can be expressed as Equation 4-1. The residual degree of saturation (S_{r0}) of C-40 is 23.94 %, which was estimated by the fitting curve shown in Figure 4-1. Based on Equation 4-1, the matric suction value under the residual degree of saturation is infinite. The various unsaturated specimens can be obtained by applying corresponding matric suctions based on the SWCC curve in Figure 4-1.

$$s_e = \frac{\left(s_r - s_{r0}\right)}{\left(s_{r,max} - s_{r0}\right)} = \frac{1}{\left\{1 + \exp\left(a_{\mathrm{lg}} s + b_{\mathrm{lg}}\right)\right\}^{c_{\mathrm{lg}}}} \tag{4-1}$$

here, s_e and s_r are the effective degree of saturation and the degree of saturation, respectively. s_{r0} and $s_{r,max}$ are the residual degree of saturation and the degree of saturation under saturated condition, respectively. s is the matric suction. a_{lg}, b_{lg} and c_{lg} are fitting parameters for SWCC curve.

Figure 4-2 is the relationship between the degree of saturation (S_{r}) and the matric suction (s) in logarithmic scale for C-40 material. However, the SWCC curve formed in the logarithmic scale shows no clear air entry value (AEV), due to the high permeability of C-40 material concurrently with the application of the matric suction. Therefore, it could be understood that the air entry value (AEV) of C-40 material is located at the matric suction range less than 0.5 kPa.

In addition, the distribution of water content (w) inside the large unsaturated specimen should be evaluated. The SWCC test was performed on Toyora sand using this medium-size triaxial compression apparatus by Ishikawa et al. (2014). The water content of Toyora sand of every layer was examined after SWCC test. For example, the results show w = 4.06 %, 4.22 %, and 5.22 % for layer 0-5 cm, 5-10 cm, and 10-15 cm away from the end of the specimen, respectively. This indicates that the distribution of water content against the height could be almost uniform in the range with 10 cm from both ends where the matric suction is well controlled.

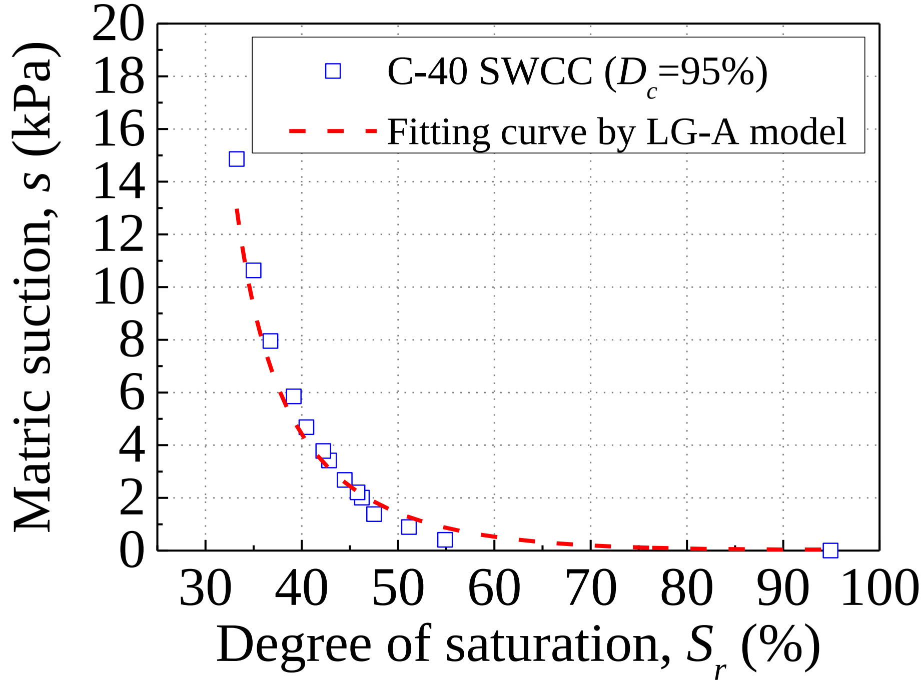

Figure 4-1 Soil-water characteristic curve of the C-40 specimen.

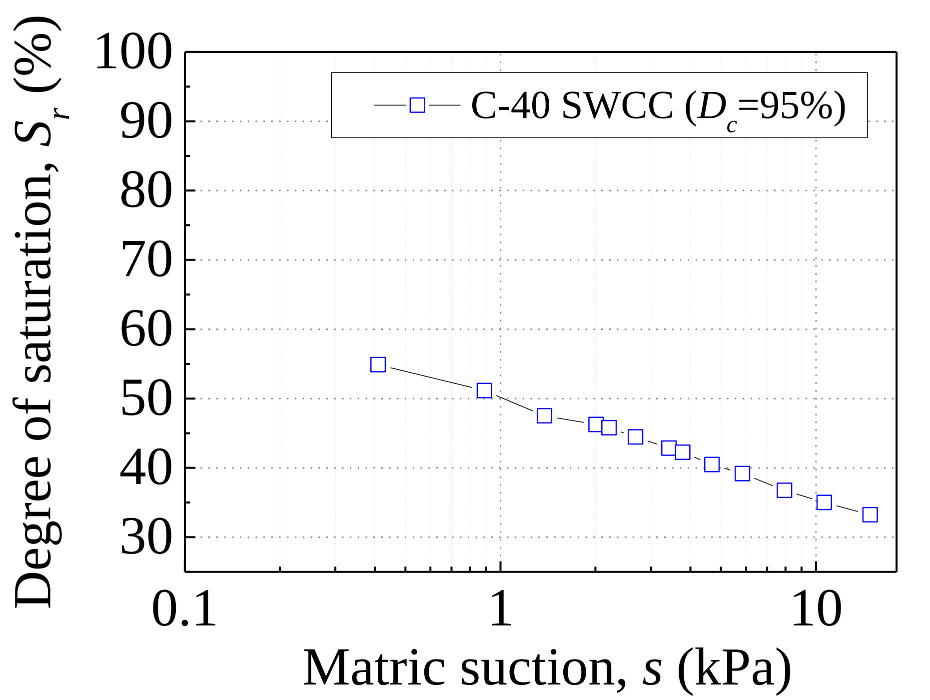

Figure 4-2 SWCC curve of the C-40 specimen drawn in the logarithmic scale.

4.2 WATER-AIR-PARTICLE SYSTEM

Throughout the SWCC curve, the water-air-soil particle system in the specimen varies with the degree of saturation. A number of investigations have been carried out on the water-air-soil particle relationships of unsaturated soils (e.g., Yu and Chen, 1965; Wu et al., 1984; Kohgo et al., 2007a). For example, Yu and Chen (1965) interpreted that three basic water-air-soil particle systems in unsaturated soils, namely, closed-air, bi-opened, and closed-water systems shown in Figure 4-3. The same descriptions of the three partially saturation conditions were postulated by Kohgo et al. (2007a), which were the corresponding insular air saturation, fuzzy saturation and pendular saturation. In the closed-air system (*see* Figure 4-3a) with high degree of saturation, the pore air is closely hemmed in by pore water and exists in the form of air bubble. While in closed-water system as shown in Figure 4-3c, the pore water is discontinuous and separated by pore air and soils. The bi-opened system (*see* Figure 4-3b) is the transition period between closed-air system and closed-water system.

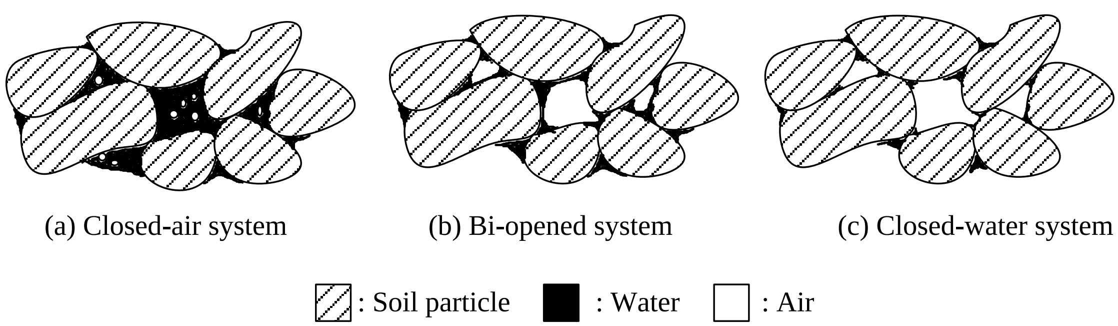

Figure 4-3. Three basic possible saturation conditions in unsaturated soils (Yu and Chen, 1965).

In general, these three different systems in unsaturated soil can be divided by air-entry value (AEV) and residual matric suction value in SWCC curve as shown in Figure 4-4. Kohgo et al. (2007b) proposed that the effects of matric suction on mechanical properties of unsaturated soils are as follows: (1) In the insular air saturation (closed-air system), pore air exits as air bubbles surrounded by water. Therefore, an increase in matric suction increases effective stresses; (2) In the pendular saturation (closed-water system), matric suction can only induce a force named capillary force. Hence, an increase in matric suction enhances yield stresses and affects the resistance to plastic deformations. (3) Both of the two suction effects above-mentioned in (1) and (2) should be considered in the fuzzy saturation (bi-opened system).

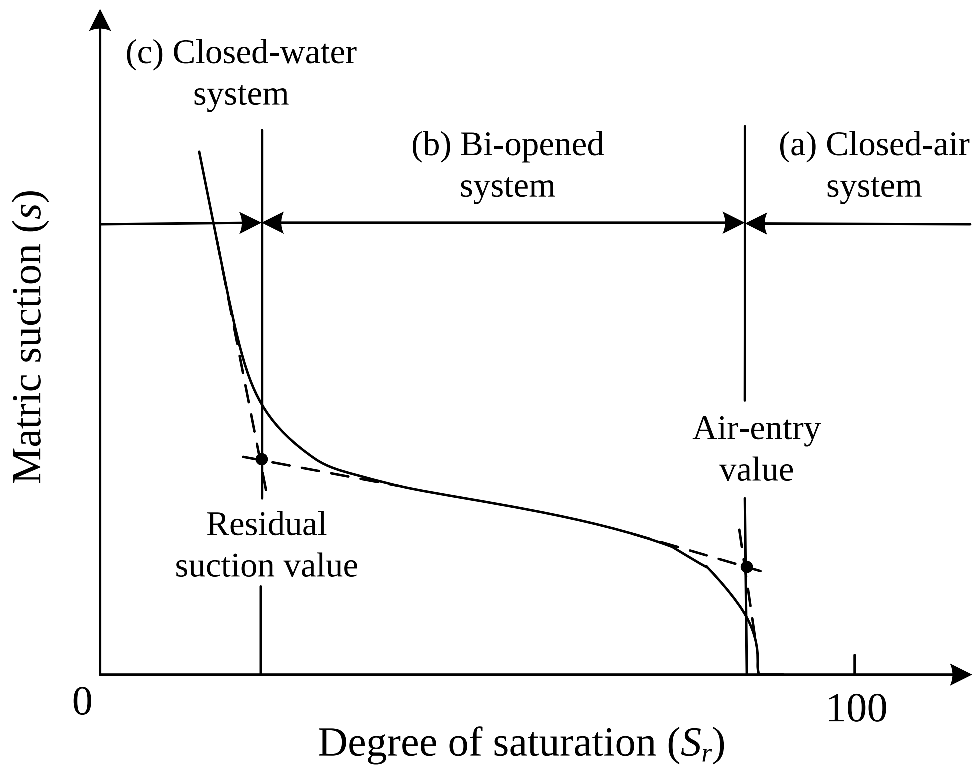

Figure 4-4. Typical SWCC curve showing different systems for unsaturated soils.

5 TEST RESULTS OF MONOTONIC TRIAXIAL COMPRESSION TESTS

5.1 EVALUATION OF MEASUREMENT PRECISION

In this section, the reliabilities of measurement systems in monotonic triaxial compression tests for C-40 specimens are discussed. Firstly, the influence of system compliance (SC) and bedding errors (BE) in the monotonic triaxial compression test on C-40 specimen are presented. Secondly, the applicability of the calculation method for the volumetric strain using gap sensors during shear is exhibited.

5.1.1 System compliance and bedding errors

The system compliance (SC) and bedding errors (BE) have been addressed as problems encountered in accurately measuring the axial displacement with an external displacement transducer, especially in triaxial compression tests for hard geomaterials such as gravel (Tatsuoka and Shibuta, 1992). In order to check the effects of system compliance (SC) and bedding errors (BE), one saturated specimen was sheared at small axial strain ranging from 0 to 2 %, meanwhile, the axial displacement was measured using the external displacement transducer (EXT), the two linear variable differential transformers (LVDTs) installed on the top of the cap inside the triaxial cell and two LVDTs (hereafter referred to as "LLVDTs") attached at the center of the specimen, in parallel with two side lines located at the diagonal position as discussed before.

Figure 5-1 presents the relationships between the deviator stress (q) and various kinds of axial strain (ε_a) obtained from the tests results of the saturated specimen at axial strain ranging from 0 to 2 %. Here, ε_a (LVDT) and ε_a (LLVDT) are the axial strain measured by linear variable differential transformers (LVDTs and LLVDTs, respectively). When comparing axial strain measured at different locations in the range up to 2 %, the axial strain value at the same deviator stress (q) increased in order of ε_a (LLVDT), ε_a (LVDT) and ε_a (EXT). In this case, the difference between ε_a (LVDT) and ε_a (EXT) mainly indicates the effect of SC, while the difference between ε_a (LLVDT) and ε_a (LVDT) mainly explains the effect of BE.

Figure 5-2 shows the relationship between ε_a (LVDT) and ε_a (EXT) at the axial strain range from 0 to 2 %. The value of ε_a (LVDT) is almost 90 % of ε_a (EXT) and the effect is nearly stable regardless of the strain level. Therefore, it can be considered that the measuring error caused by system compliance (SC) is approximately 10 % of ε_a (EXT) in this study.

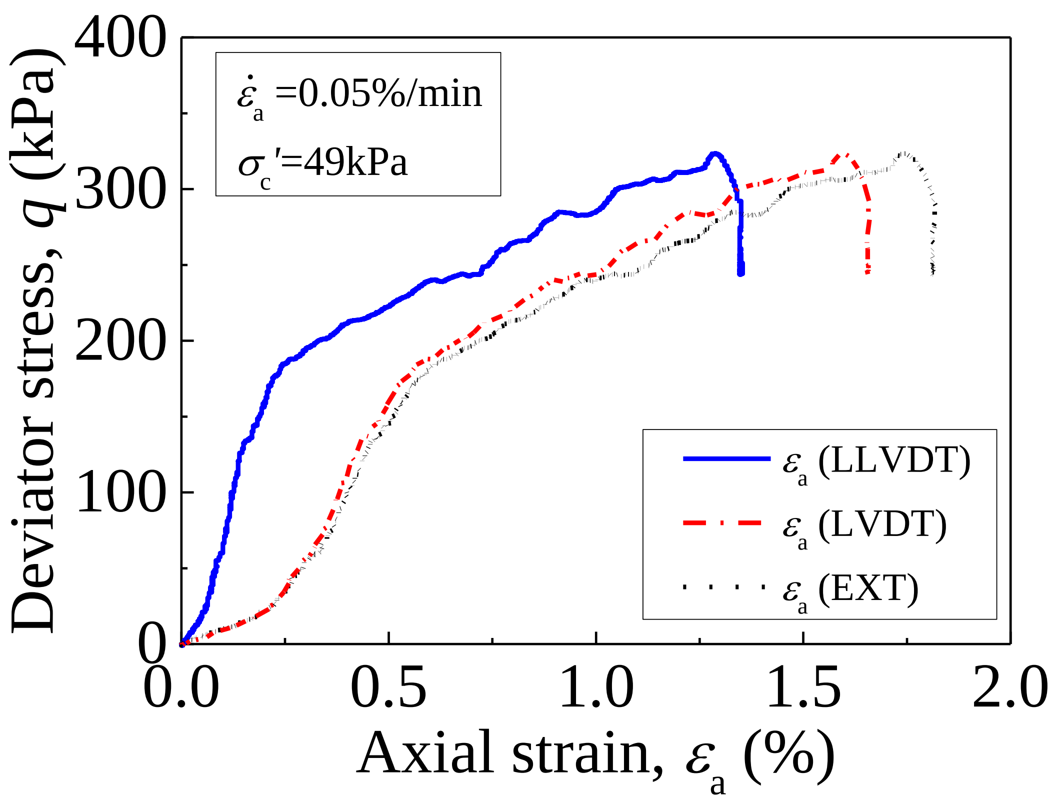

Figure 5-1 Comparison of axial strain obtained from different measuring methods.

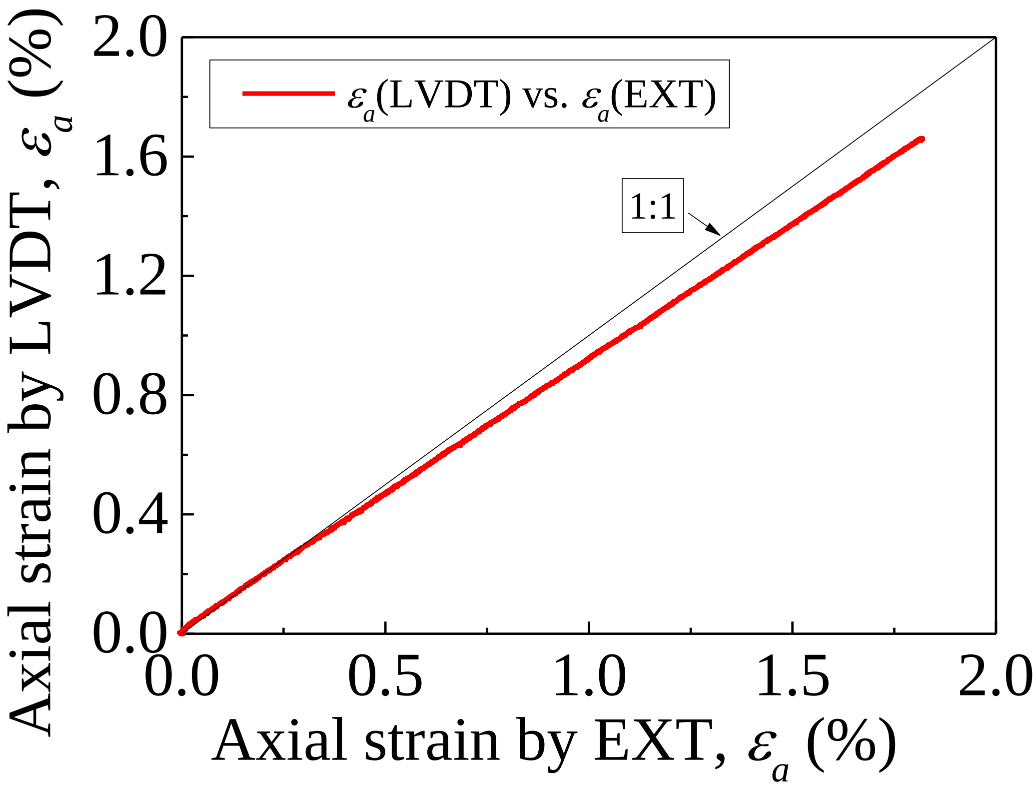

Figure 5-2 Measuring error due to system compliance.

On the other hand, the result of bedding errors (BE) was evaluated by using other two LLVDTs as shown in Figure 5-3a. The result shows that BE appears strongly during the initial loading stage lower than about ε_a (LVDT) = 0.5 %, and then the increasing rate of ε_a (LVDT) is almost equal to that of ε_a (LLVDT) at the axial strain range from 0.5 % to 2 %. Figure 5-3b shows the relationship between axial strains measured by LLVDTs and LVDTs under ε_a (LVDT) of 0.5 %, which could be fitted by polynomial relationship. It should be noted that the axial strains in the range up to 0.5 % for all tests were converted from ε_a (LVDT) data to ε_a (LLVDT) data based on the polynomial fitting relationship shown in Figure 5-3b.

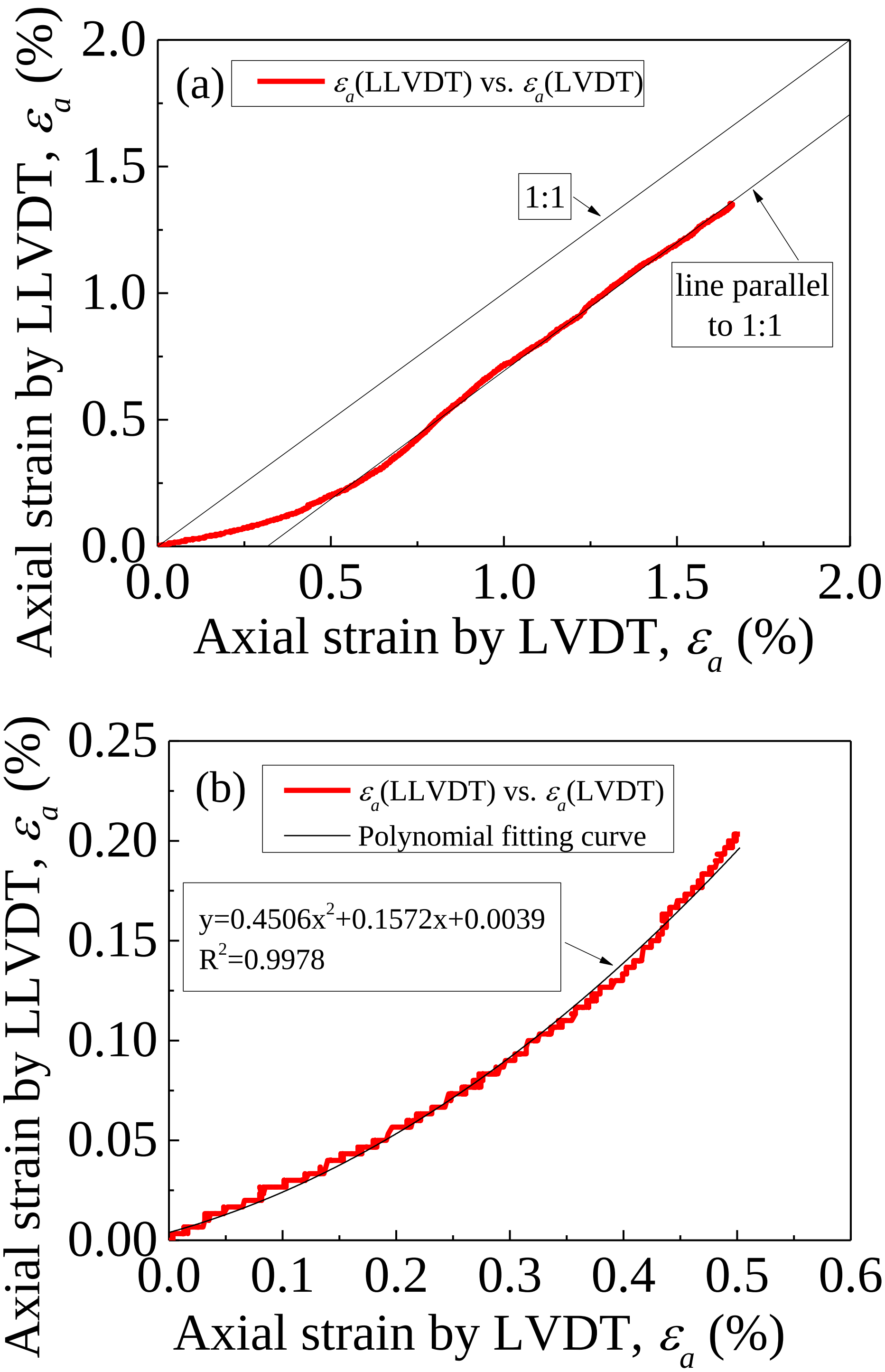

Figure 5-3 (a) Measuring error due to BE and (b) Relationship between axial strains measured by LLVDTs and LVDTs under axial strain (LVDT) up to 0.5%.

5.1.2 Measuring accuracy of volumetric strain

The gap sensors were used to measure the volumetric strain for specimens on monotonic triaxial compression tests. Note that a double tube burette was also used to measure the volumetric strain for saturated specimens. The volumetric strain (ε_v) measured by gap sensors is the average value of volumetric strains (ε_{v1}) and (ε_{v2}) derived from two different calculation methods shown in Figure 5-4. The ε_{v1} was calculated supposing that the specimen after shear has a vertical cross section, like the shape of a beer barrel, whose curved boundary is approximated by a parabola as shown Equation 5-1 (Kato and Kawai, 2000). While the ε_{v2} was calculated supposing the specimen diameter uniformly spreads like a cylinder regardless of the height during compression. In ε_{v1} calculation method, the specimen was separated into two parts, i.e., the upper and lower parts. The volumetric strain of upper part and lower part specimen were determined by two parabola functions from the lateral displacement by gap and height at the position of the gap sensor (e.g., point B in Figure 5-4), and the end of the specimen (e.g., point A in Figure 5-4).

$$y = ax^2 + c \tag{5-1}$$

Here, a and c are variables.

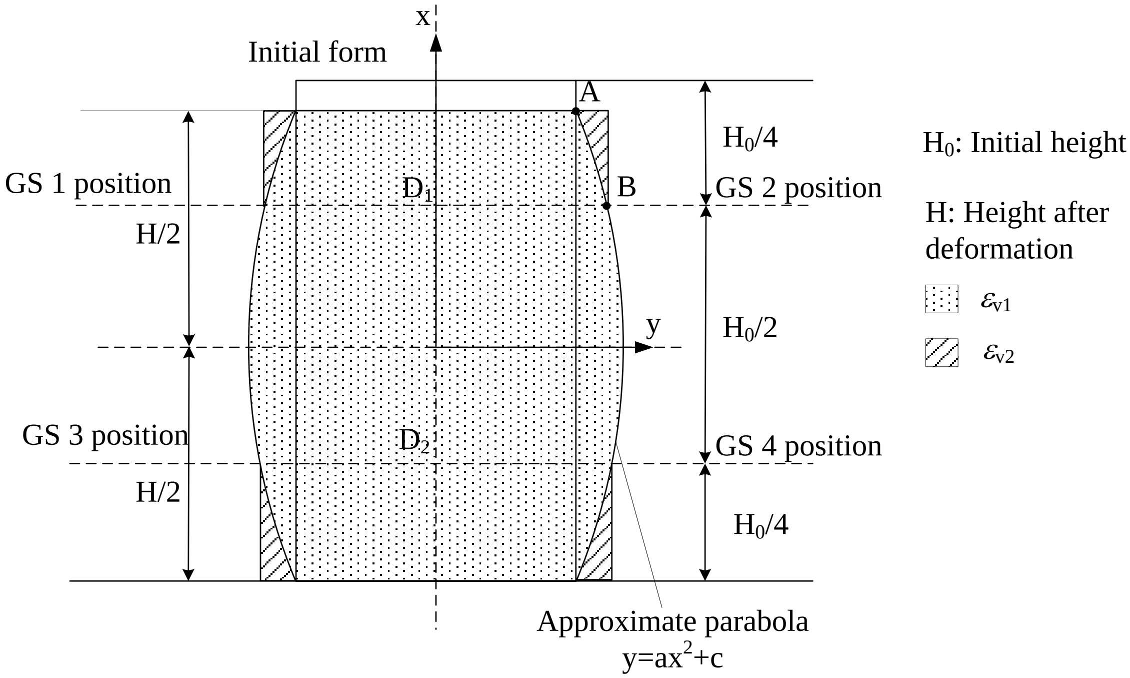

Figure 5-4 Calculation methods for volumetric strain.

In order to evaluate the applicability and the usefulness of gap sensors, Figure 5-5 and Figure 5-6 show the deviator stress (q)-axial strain (ε_a) curves and volumetric strain (ε_v) - axial strain (ε_a) curves for the saturated specimen under effective confining pressure of 49 kPa, respectively. In Figure 5-5, the deviator stress (q) was calculated by the Equation 5-2, which was a function of vertical load (P), initial cross-sectional area of the specimen (A_i), axial strain (ε_a), and volumetric strain (ε_v). Due to different method to calculate ε_v, q (GS) was obtained by the data of ε_v (GS), while q (DTB) was obtained by the data of ε_v (DTB). Note here the ε_v (GS) was volumetric strain measured by gap sensors, while the ε_v (DTB) was volumetric strain measured by a double tube burette.

$$q = \frac{P}{A_c} = \frac{P}{A_i} \times \frac{\left(1-\frac{\varepsilon_a}{100}\right)}{\left(1-\frac{\varepsilon_v}{100}\right)} \times 10 \qquad \text{(kPa)} \qquad (5\text{-}2)$$

where, P is vertical load. A_i is initial cross-sectional area of the specimen, while A_c is cross-sectional area of the specimen subjected to loading. ε_a is axial strain and ε_v is volumetric strain.

Figure 5-6 compares the volumetric strain (ε_v) - axial strain (ε_a) curves of the saturated specimen during shear obtained by gap sensors and a double tube burette. Measurements by the two methods are in reasonable agreement with each other in the change of volumetric strain during shear up to the axial strain of about 5 %, that is, until the deviator stress reaches peak as shown in Figure 5-5. However, the ε_v (GS) - ε_a relation after axial strain of 5 % is extremely different from ε_v (GS) - ε_a relation due to large deformation of the specimen. Accordingly, in this study, we do not adopt the ε_v calculated with the lateral displacements of the specimen measured by gap sensors as an experimental data in the range of ε_a of 6 % or more from the viewpoint of the measurement precision.

It must be pointed out that the axial stresses, i.e., q (GS) and q (DTB) shown in Figure 5-5 do not coincide with each other after peak stress due to the calculated method by gap sensors. However, the coefficient of correlation, R, between q (GS) and q (DTB) in the range of an axial strain up to around 4.5 % is 0.99, which means the q (GS) and q (DTB) agree well with each other in the range of stress up to peak stress. Besides, the stress level for monotonic triaxial compression tests should be dealt with in this research corresponds to the pre-failure behavior of the subbase course material. Therefore, the q (GS) were adopted as deviator stress hereinafter.

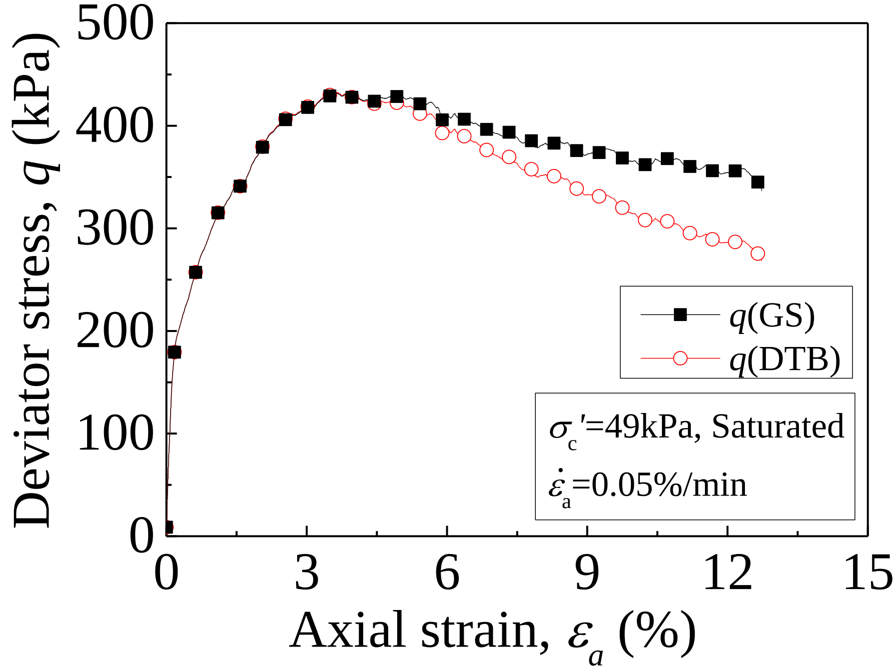

Figure 5-5 Comparison of deviator stress obtained from different measuring methods.

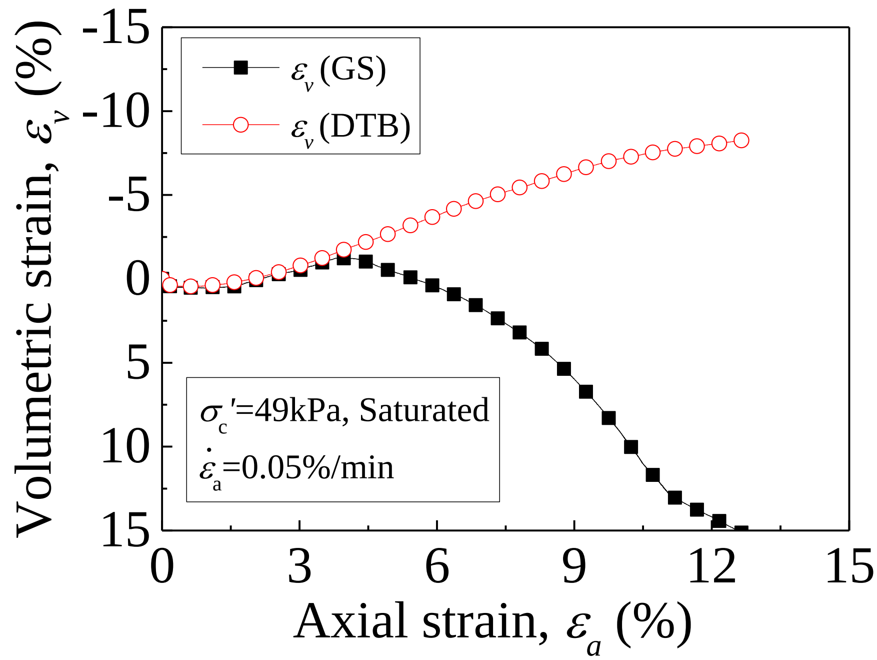

Figure 5-6 Comparison of volumetric strain obtained from different measuring methods.

5.2 EFFECT OF DEGREE OF SATURATION

The effect of degree of saturation on strength characteristics of C-40 material under drainage condition was investigated by air-dried specimens “A-1, A-3, A-5”, simulated specimens “U-1, U-3, U-5”, optimum specimens “O-1, O-3, O-5” and saturated specimens “S-1, S-3, S-5” as indicated in Table 3-2. The CD tests were performed with the strain rate of 0.05 %/min. Each series of tests was conducted on three effective confining pressures (σ_c') as 34.5 kPa, 49 kPa and 68.9 kPa.

Figure 5-7 shows deviator stress (q) versus axial strain (ε_a) relationship and volumetric strain (ε_v) versus axial strain (ε_a) relationships obtained from the monotonic triaxial compression tests under air-dried, simulated, optimum, and saturated conditions. As shown in Figure 5-7, with the increase of the axial strain (ε_a), the deviator stress (q) sharply increases to the peak stress at an axial strain (ε_a) of about 4 % regardless of the degree of saturation (S_r), and then it gradually decreases to the residual strength at ε_a = 12 %. During shear, the degrees of saturation (S_r) of unsaturated specimens have barely changed. Therefore, it can be thought the suction of the specimen during shear was controlled well.

Furthermore, the volume change initially decreases, and then the specimen shows the trend of dilatancy regardless of the degree of saturation. In this case, the positive dilatancy tends to be stronger in the order of saturated, optimum, simulated, and air-dried specimens. This phenomenon is thought to be caused by the capillary force between particles which attempts to maintain the soil skeleton structure of the unsaturated soils, as Karube and Kato (1994) point out. These results indicated that the degree of saturation of the specimen has a considerable influence on the strength characteristics of C-40 material in the monotonic triaxial compression tests.

It is interesting to note that only the specimen sheared under air-dried condition shows brittle failure. Guo and Su (2007) deemed that the shear resistance of cohesionless soils is considered to be the result of interparticle friction and dilation. The interparticle locking could restrain sliding and rotation between particles and the dilation tends to degrade the interparticle locking. Therefore, large shear stress is required to break the interlocking between particles. As shown in Figure 5-7, the volumetric strain under air-dried condition is larger than that of other conditions, which implies that more stress is needed to break the interlocking between air-dried particles.

In contrast, the peak strength for the specimen with higher degree of saturation is smaller than that with lower degree of saturation with exception of the optimum specimen. The tendency of higher peak strength (q_{max}) along with lower degree of saturation has been observed for various soil materials (Ho and Fredlund, 1982; Kohgo et al., 2007b; Nishimura et al., 2008). The q_{max}-S_r relationship is influenced by the matric suction. According to Kohgo et al., (2007b), the resistance of soils to plastic deformation is strongly influenced by shear resistance between grain contact points. The matric suction here is presented in the capillary force (the second effect as mentioned before), which acts perpendicularly on grain contact points and attracts soil particles together. Then this force restrains relative small sliding between soil particles (Kohgo et al., 2007b). Therefore, the peak strength is correspondingly increasing with decrease of the degree of saturation (S_r). However, the peak strength of optimum degree saturation comes near to the peak strength of the simulated condition. Therefore, the matric suction under low ranges (i.e., from 0.5kPa to 10kPa) has not played an important role in the shear strength of C-40 material.

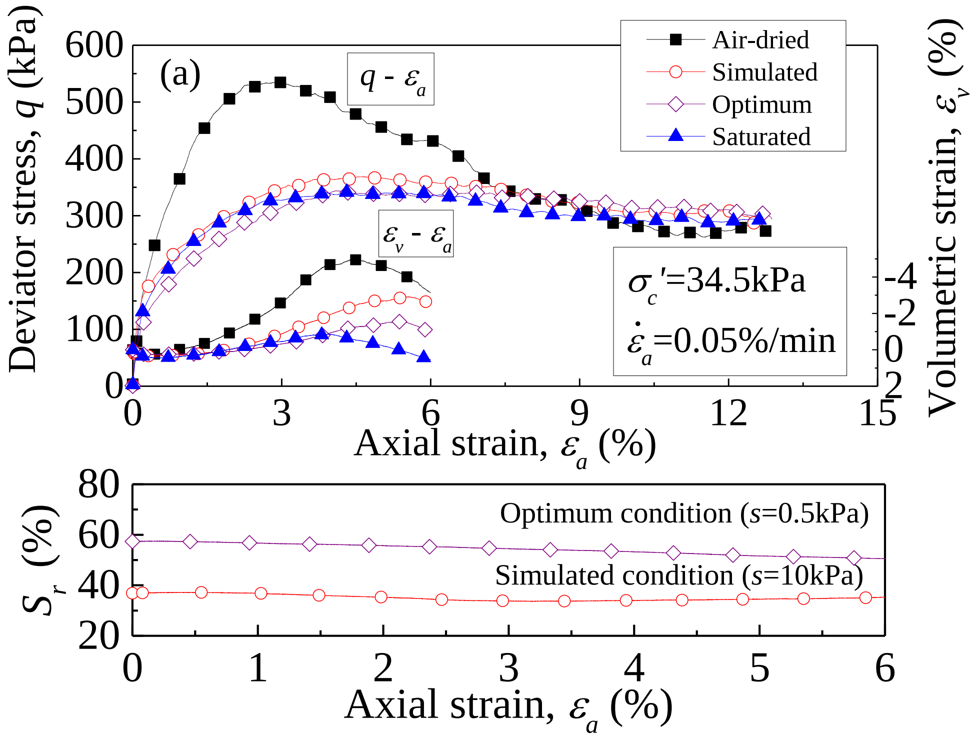

Deviator stress, q (kPa)
Volumetric strain, εv (%)
(a)
q - εa
εv - εa
Air-dried
Simulated
Optimum
Saturated
σc'=34.5kPa
ε̇a=0.05%/min
Axial strain, εa (%)
Sr (%)
Optimum condition (s=0.5kPa)
Simulated condition (s=10kPa)
Axial strain, εa (%)

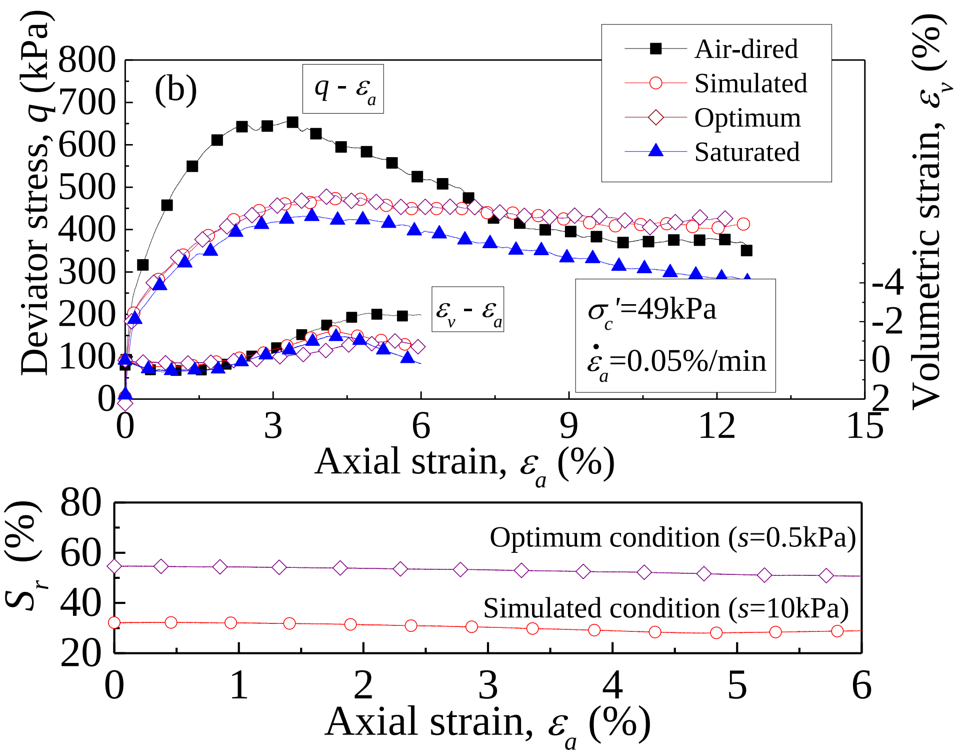

Deviator stress, q (kPa)
Volumetric strain, εv (%)
(b)
q - εa
εv - εa
Air-dired
Simulated
Optimum
Saturated
σc'=49kPa
ε̇a=0.05%/min
Axial strain, εa (%)
Sr (%)
Optimum condition (s=0.5kPa)
Simulated condition (s=10kPa)
Axial strain, εa (%)

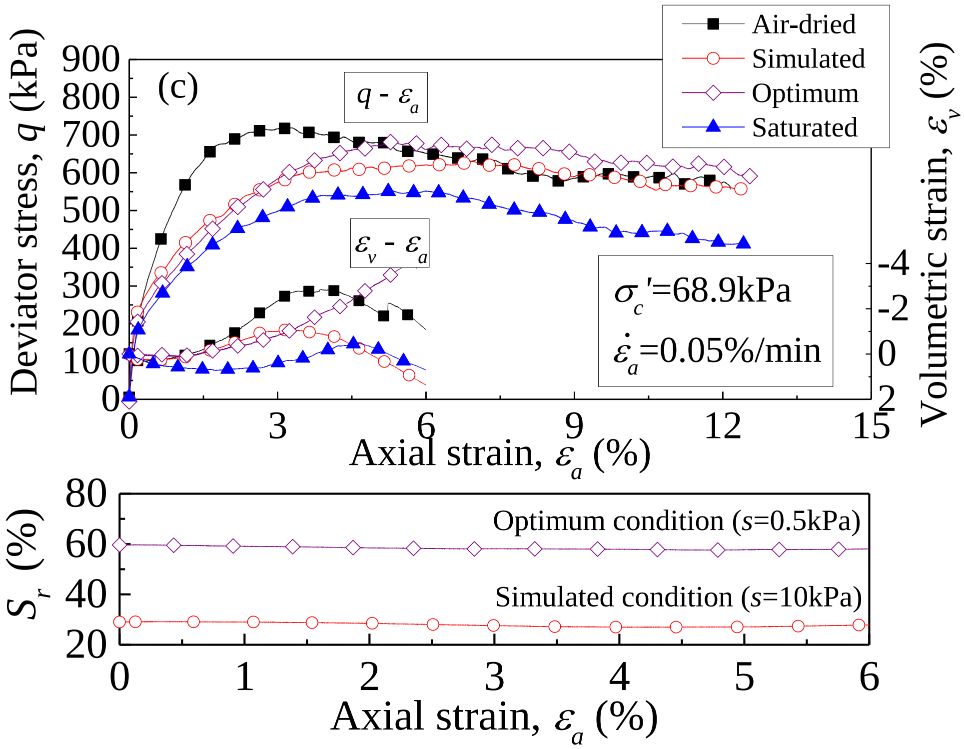

Figure 5-7. Comparison of stress-strain-dilatancy relationships of different degrees of saturation under σ_c' of (a) 34.5 kPa, (b) 49 kPa and (c) 68.9 kPa.

Figure 5-8 shows the relationship between the deviator stress at failure (q_{max}) and the mean effective principal stress at failure (p') for specimens with different degrees of saturation. In the unsaturated condition and the air-dried condition, the mean effective principal stress at failure (p') was expressed by Equation 5-3. Note that pore air pressure (u_a) is equal to zero in air-dried condition. Equation 5-4 was applied to calculate p' in the saturated condition. For plots with the same p', the effective stress ratio at failure ($\eta_{max}= q_{max} / p'$) decreases with increasing S_r, while for plots with the same S_r, $\eta_{\max}$ is thought to be almost constant as the q_{max}-p' relationships seem to be linear.

$$p'=\frac{1}{3}(\sigma_a+2\sigma_c)-u_a \tag{5-3}$$

$$p'=\frac{1}{3}(\sigma_a+2\sigma_c)-u_w \tag{5-4}$$

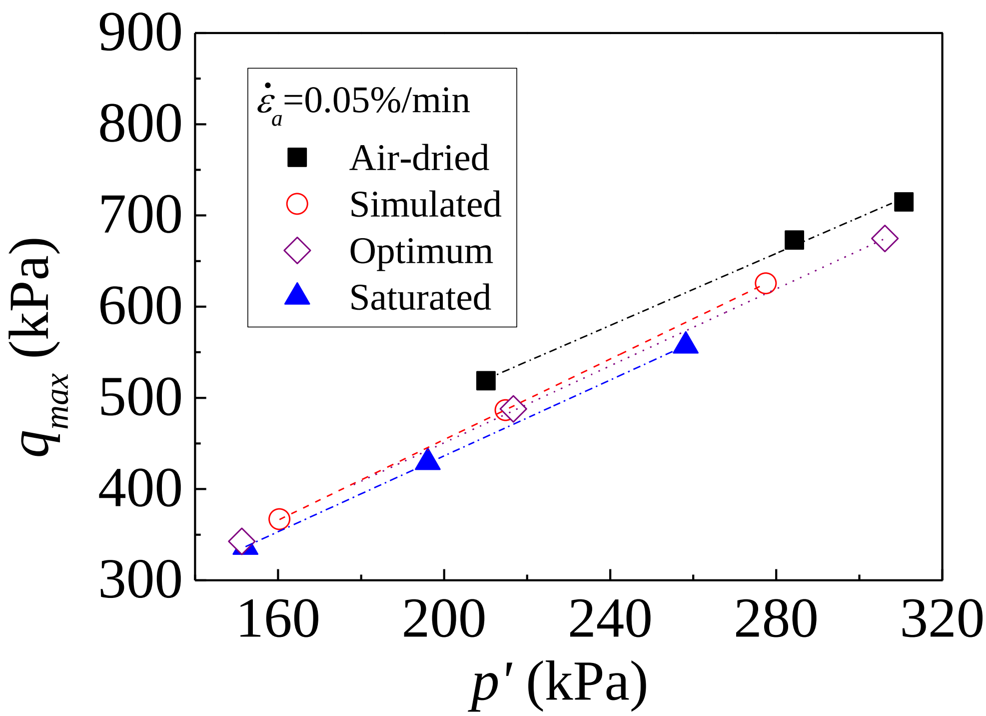

Figure 5-8. Influence of the degree of saturation on the effective stress ratio.

Figure 5-9 shows deviator stress (q) - axial strain (ε_a) curves at small axial strain ranging from 0.05 % to 0.15 %. It should be noted that the axial strain (ε_a) at small range (i.e., 0.05% to 0.15%) was converted from axial strain (LVDTs) data to axial strain (LLVDTs) data based on the polynomial fitting relationship shown in Figure 5-3b. The deviator stress (q) - axial strain (ε_a) curves shown in Figure 5-9 approximate straight lines. Therefore, the tangent deformation modulus (E_{tan}) at axial strain (ε_a) of 0.1 % is the slope of q - ε_a curve.

Figure 5-10 presents the relationship between degree of saturation (S_r) and tangent deformation modulus (E_{tan}) at small axial strain (ε_a) of 0.1 %, which were obtained from the deviator stress - axial strain curves in Figure 5-9. For C-40 specimens, an increase in degree of saturation produces the decrease in tangent deformation modulus (E_{tan}) irrespective of effective confining pressure; however, the reduction in E_{tan} is the greatest at S_r = 57.2 % (i.e., simulated condition), and gets smaller as degree of saturation increases. This result indicates that the degree of saturation has a noted influence on the degradation of the deformation characteristic of C-40 material.

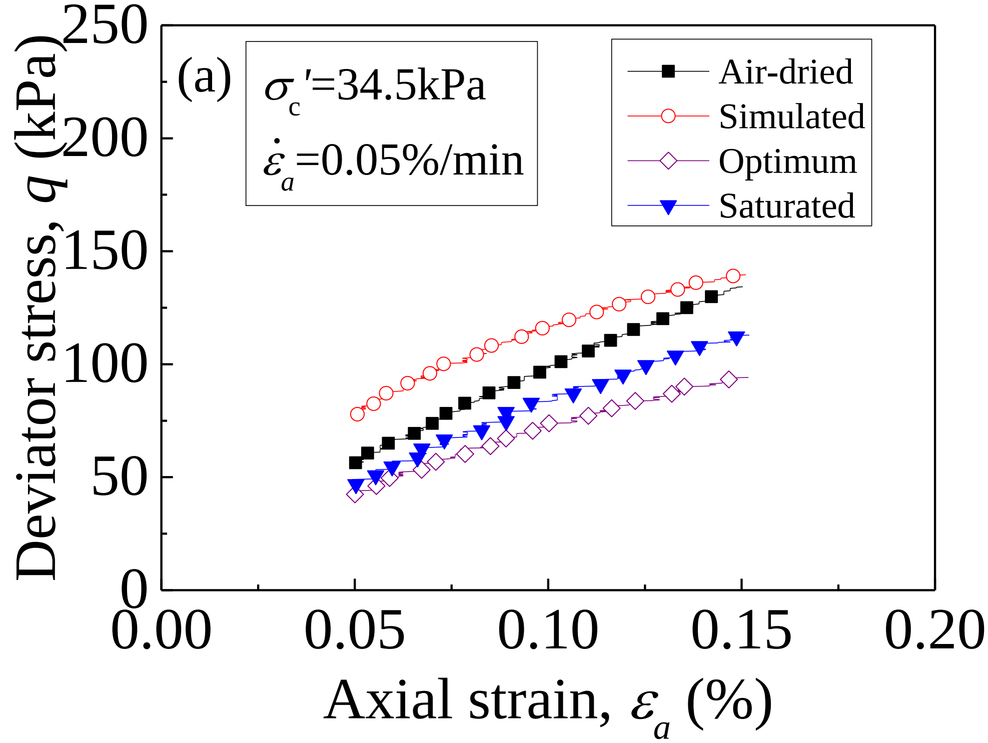
(a)
σc'=34.5kPa
ε̇a=0.05%/min
Air-dried
Simulated
Optimum
Saturated
Deviator stress, q (kPa)
Axial strain, εa (%)
0
50
100
150
200
250
0.00
0.05
0.10
0.15
0.20

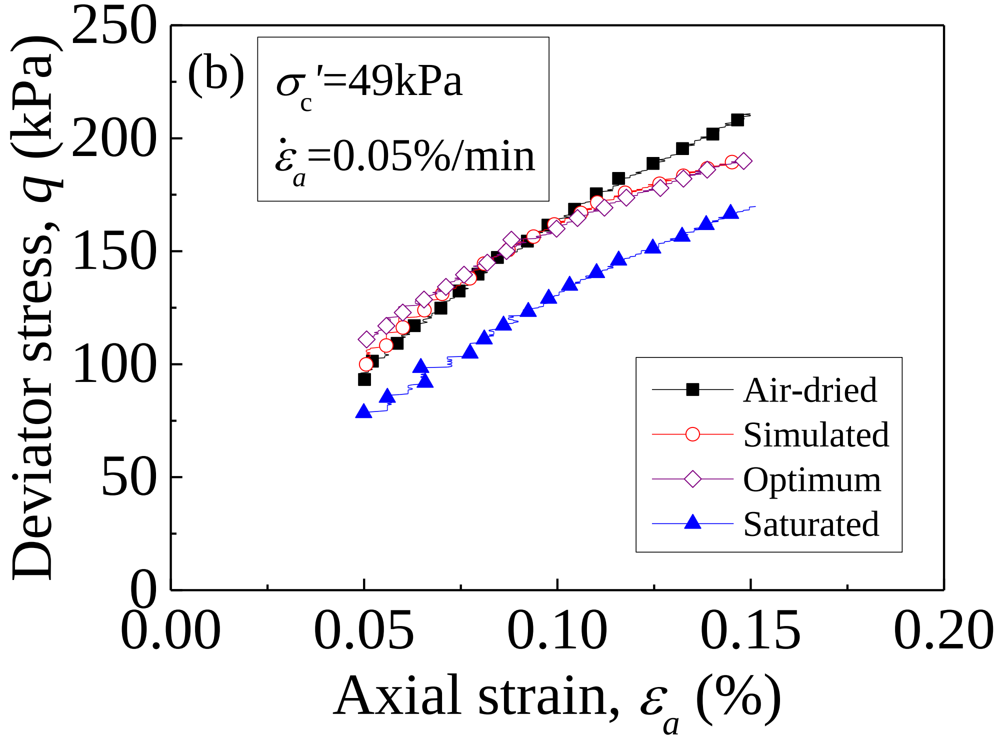
(b)
σc'=49kPa
ε̇a=0.05%/min
Air-dried
Simulated
Optimum
Saturated
Deviator stress, q (kPa)
Axial strain, εa (%)
0
50
100
150
200
250
0.00
0.05
0.10
0.15
0.20

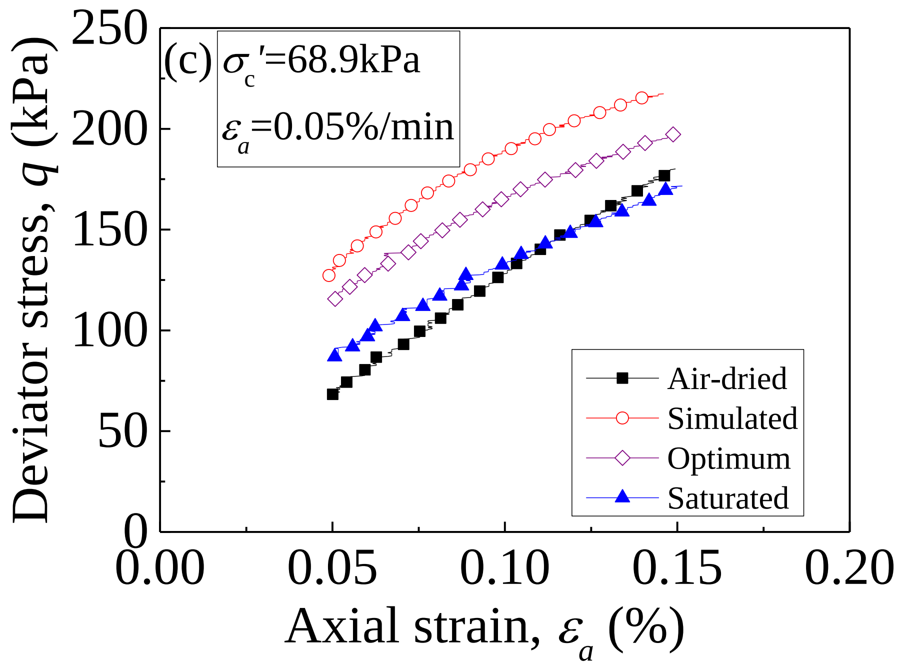

Figure 5-9. Relationship between deviator stress and axial strain in the range 0.05 to 0.15 % under strain rate of 0.05 %/min.

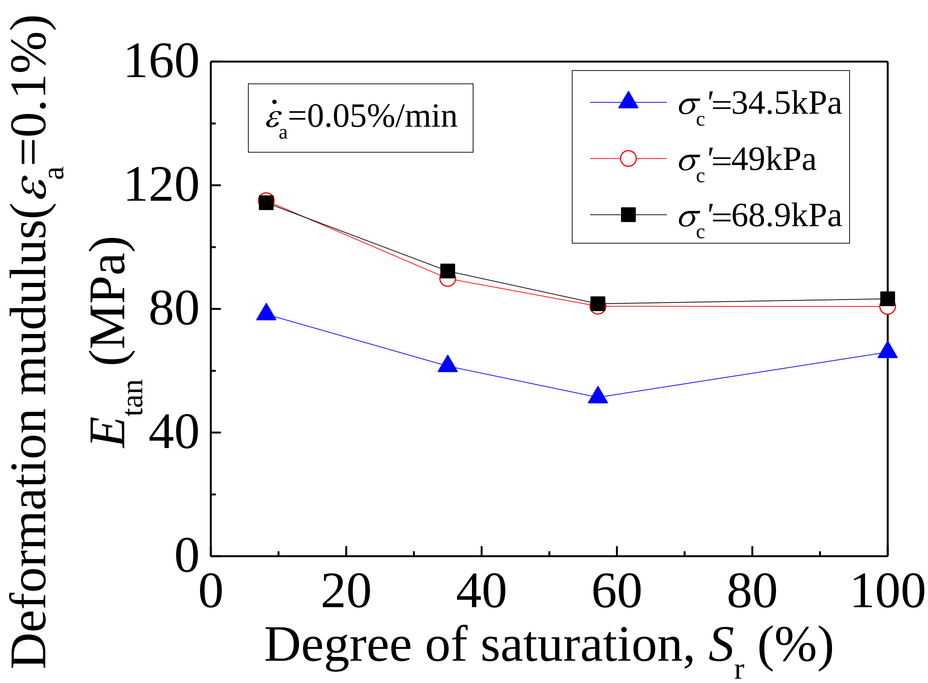

Figure 5-10. Tangent deformation modulus E_{tan} versus degree of saturation.

Figure 5-11 indicates the secant deformation modulus (E_{50}) at half of the maximum deviator stress (q_{max}), which was obtained from the deviator stress-axial strain curves in Figure 5-7, against the degree of saturation (S_r). The secant deformation modulus (E_{50}) tends to decrease when the degree of saturation increases from 8.2 % to 100 % regardless of effective confining pressure as shown in Figure 5-11. However, the reduction in the secant deformation modulus (E_{50}) is the greatest on the optimum condition, and it becomes smaller as the degree of saturation (S_r) increases irrespective of effective confining pressure. These results indicate that the degree of saturation has a considerable influence on the reduction in secant deformation modulus (E_{50}) of C-40 material.

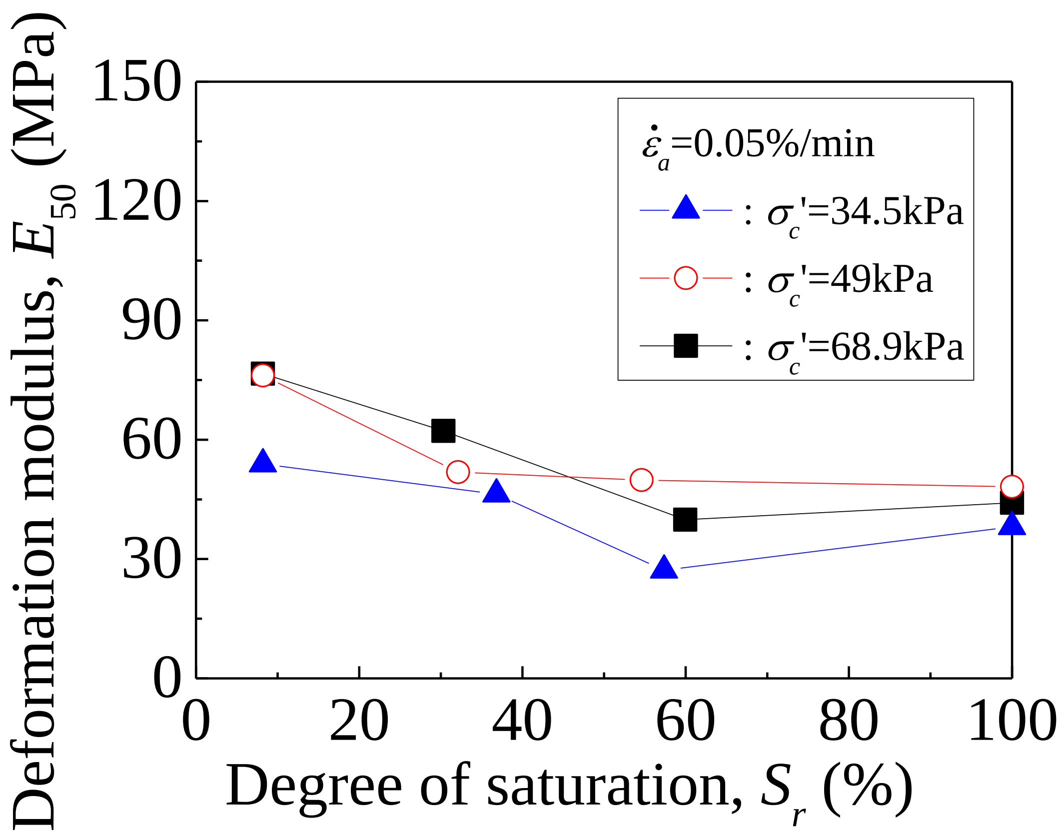

Figure 5-11. Degree of saturation versus the secant deformation modulus E_{50}.

5.3 EFFECT OF STRAIN RATE

The influence of the strain rate on the shearing behavior of the subbase course material C-40 was discussed for all the specimens shown in Table 3-2. The CD tests were performed with the strain rates of 0.05 %/min and 0.5 %/min.

Figure 5-12 shows the relationship of the deviator stress (q) and the axial strain (ε_a) with regard to each degree of saturation and effective confining pressure. Figure 5-12 clearly shows that shearing behavior of C-40 are affected by the strain rate. For all the specimens, with the increase of the axial strain, the deviator stress (q) sharply increases to the peak stress at an axial strain (ε_a) of about 4 % regardless of the degree of saturation (S_r), and then it gradually decreases to the residual strength at $\varepsilon_a = 12$ %. Disregard for the degree of saturation, when the effective confining pressure is fixed, the deviator stress (q)-axial strain (ε_a) curve of the specimen with higher strain rate is located above on the one with lower strain rate. For unsaturated specimens, the degree of saturation keeps constant during shear, which means the suction for the unsaturated specimen was controlled well during shear.

The trends of the peak strength are shown in Figure 5-13. When the degree of saturation and the effective confining pressure are fixed, an increase in strain rate produces the same increase in peak strength. Yamamuro and Lade (1993) suggested that the reason for this phenomenon is related with volume changes caused by the particle crushing and rearranging during shearing. As the fracturing and rearranging of soil grains requires time, the increment in strain rate leads to less time for the fracturing and rearranging for soil grains, thereby decreasing amounts of the particle crushing and rearranging.

The Figure 5-14 shows the volumetric strain at axial strain ranging from 0 to 6 % during shear. For all specimens, the volumetric strain is firstly increasing at the beginning, and then it gradually decreases. Specimens with higher strain rate are prone to dilation instead of compression. It must be pointed that gap sensors can measure accurate data of volumetric strain until the deviator stress reached peak point. In Figure 5-14, the volumetric strain was adopted for each test at axial strain ranging from 0 to 6 % for uniformity. However, after the peak point, decreases of volumetric strain can be observed for some tests at axial strains larger than 3 % or 5 % due to the limitation of gap sensors.

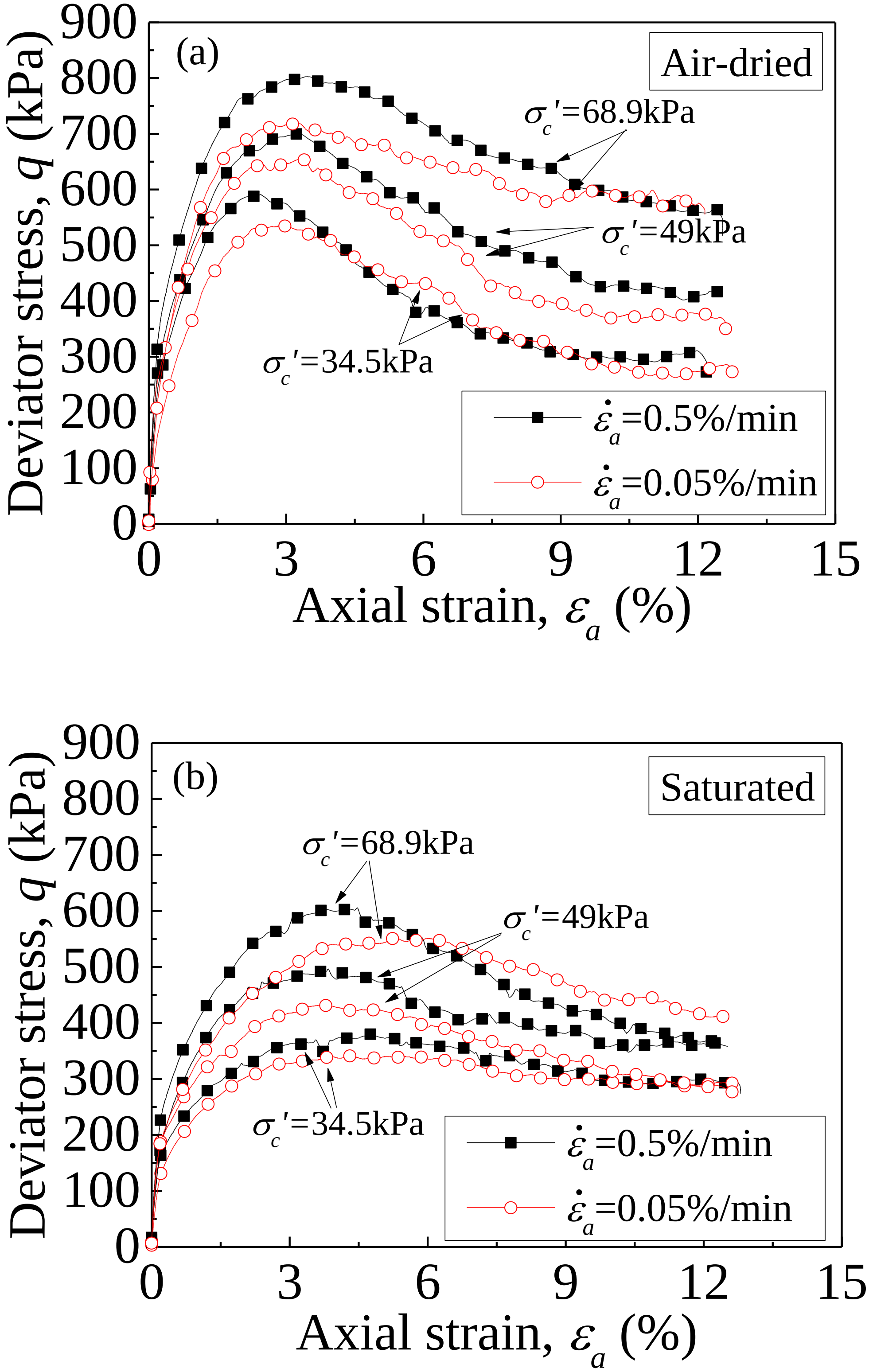
(a)
Air-dried
Deviator stress, q (kPa)
Axial strain, εa (%)
σc'=68.9kPa
σc'=49kPa
σc'=34.5kPa
ε̇a=0.5%/min
ε̇a=0.05%/min
(b)
Saturated
Deviator stress, q (kPa)
Axial strain, εa (%)
σc'=68.9kPa
σc'=49kPa
σc'=34.5kPa
ε̇a=0.5%/min
ε̇a=0.05%/min

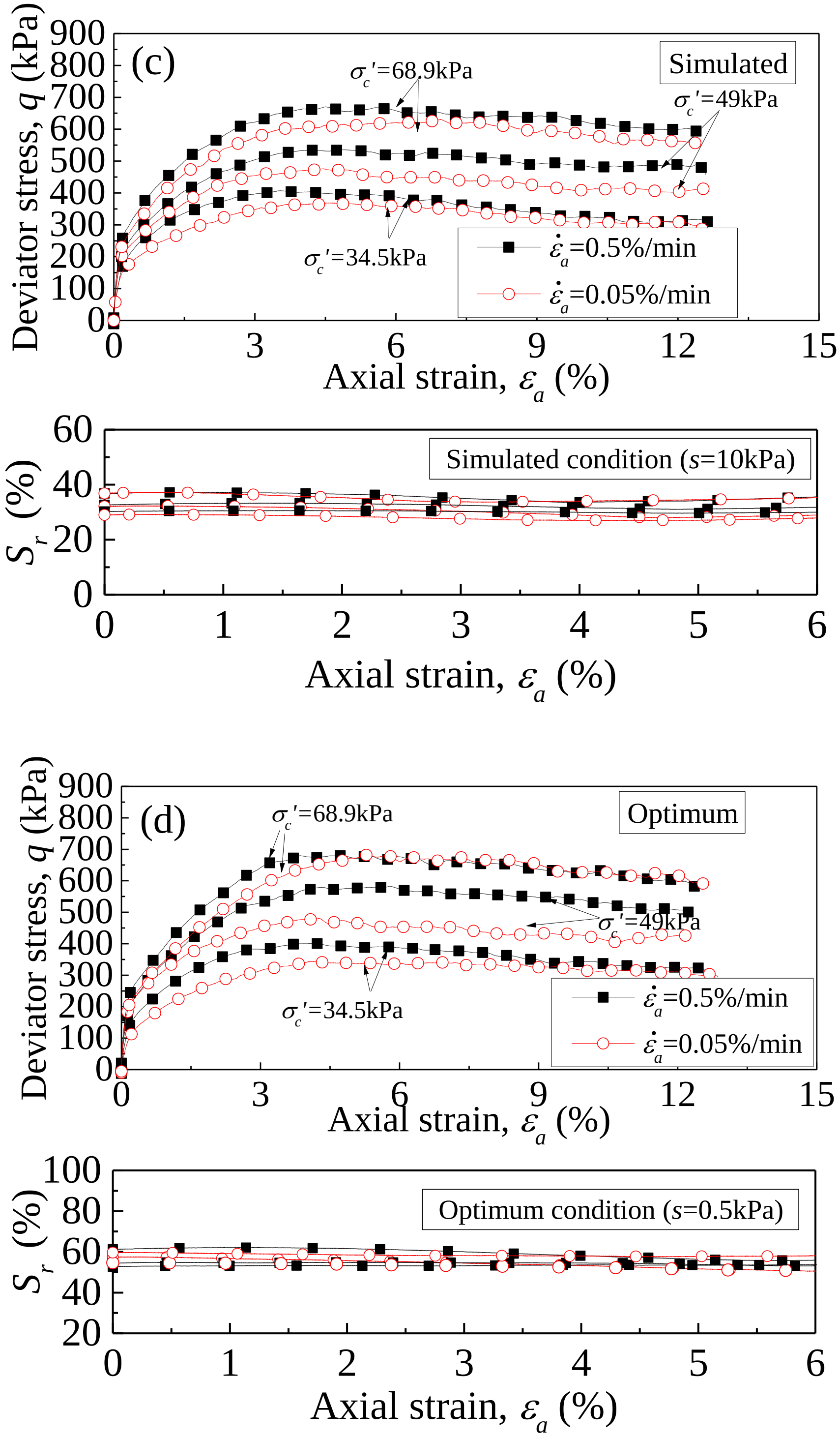

Figure 5-12. Stress-strain relationships of different strain rates under (a) air-dried, (b) saturated, (c) simulated and (d) optimum conditions.

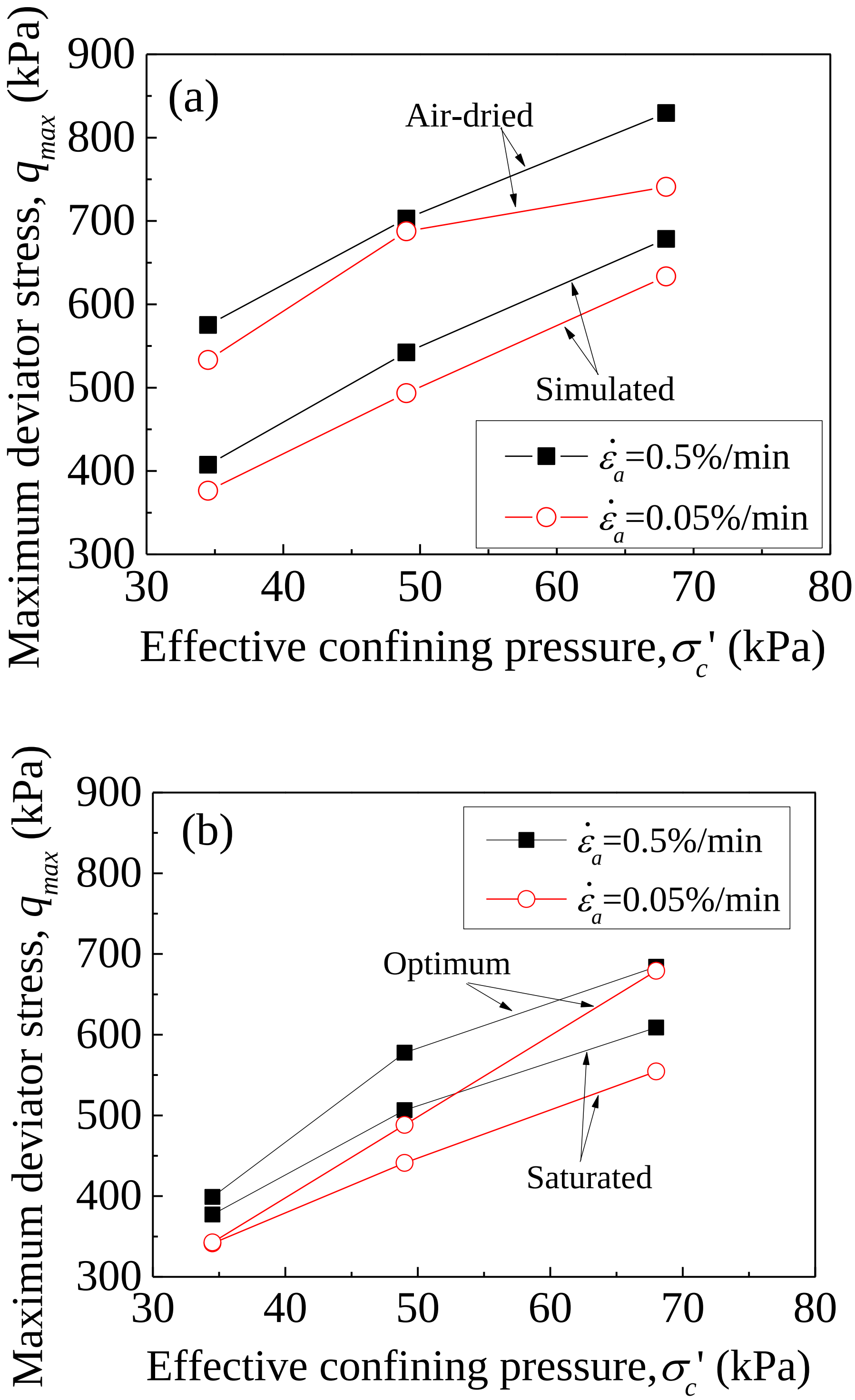

Figure 5-13. Influence of the strain rate on peak strengths for specimens under different degrees of saturation.

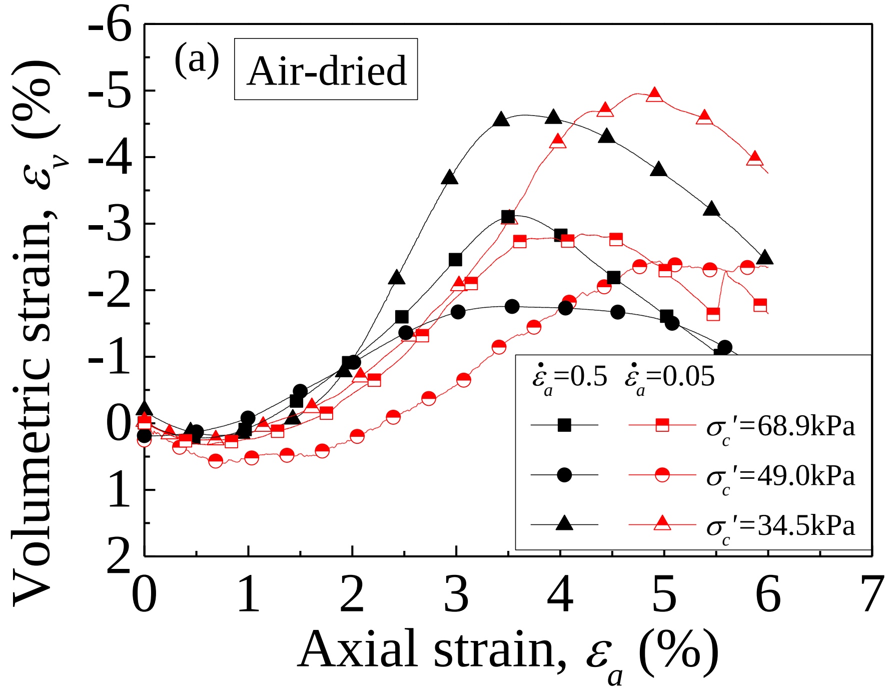

(a)
Air-dried
Volumetric strain, ε_v (%)
Axial strain, ε_a (%)
$\dot{\varepsilon}_a$=0.5 $\dot{\varepsilon}_a$=0.05
σ_c'=68.9kPa
σ_c'=49.0kPa
σ_c'=34.5kPa

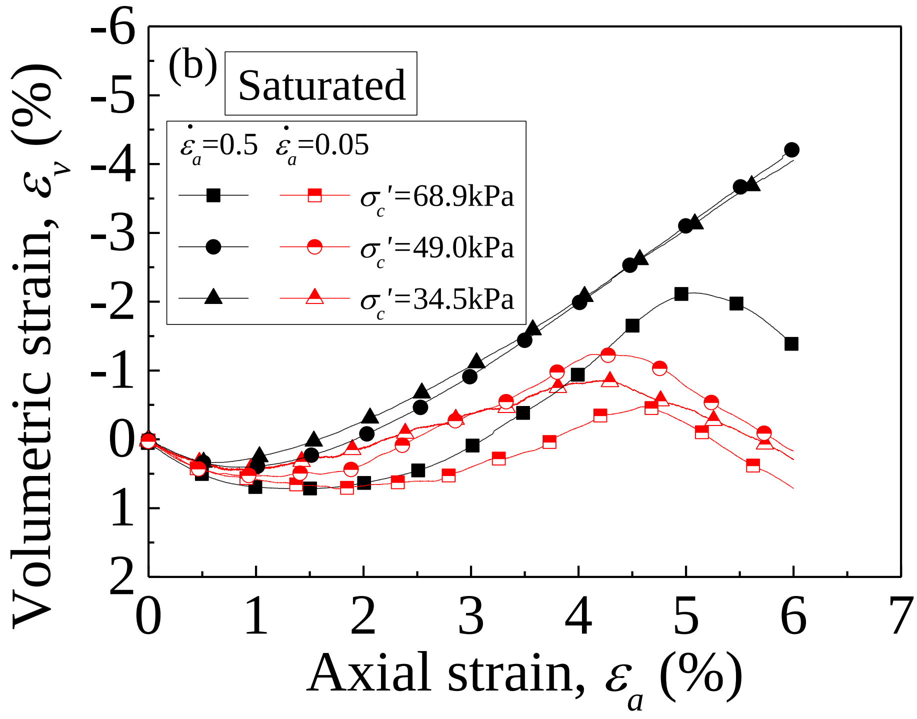

(b)
Saturated
Volumetric strain, ε_v (%)
Axial strain, ε_a (%)
$\dot{\varepsilon}_a$=0.5 $\dot{\varepsilon}_a$=0.05
σ_c'=68.9kPa
σ_c'=49.0kPa
σ_c'=34.5kPa

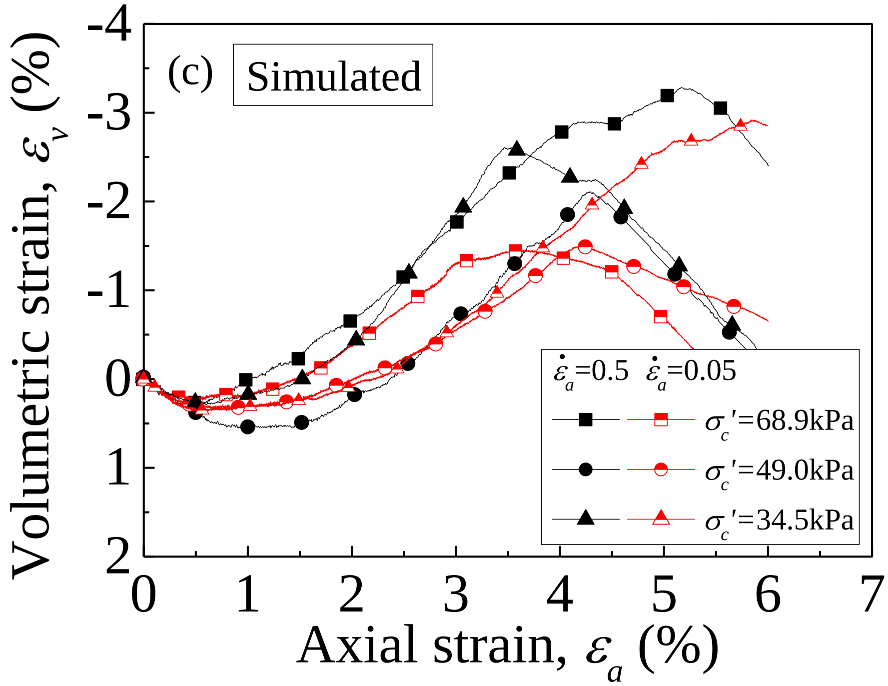

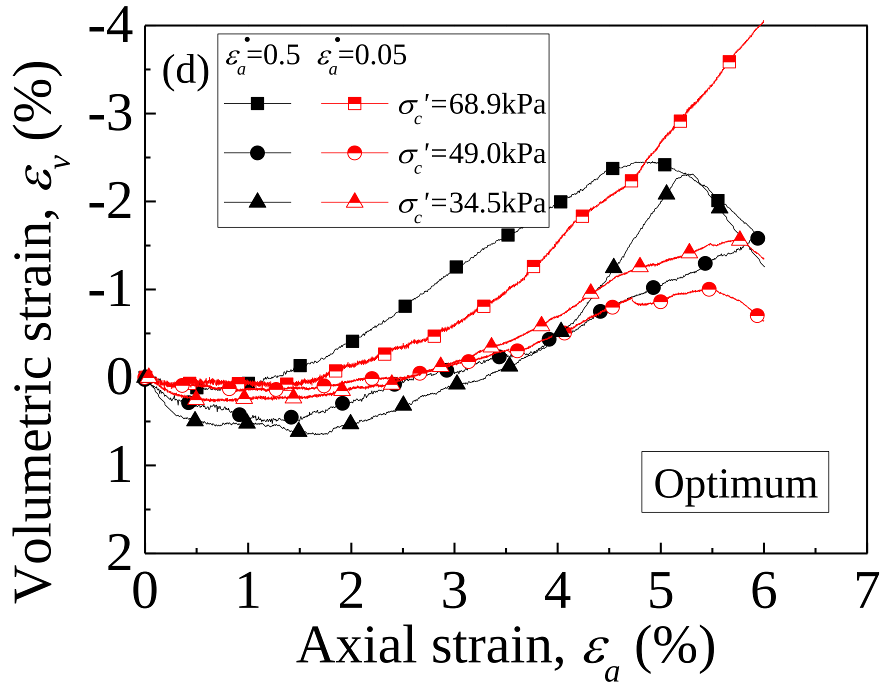

Figure 5-14. Volumetric strain-axial strain relationships of different strain rates under (a) air-dried, (b) saturated, (c) simulated and (d) optimum conditions.

In order to assess the degree of particle breakage that a specimen underwent during testing process, the grain size distributions before and after tests under different strain rates were examined by sieve analysis. The BM value was used to evaluate the degree of particle breakage, given in Equation 5-5 by Marsal (1965), and the concept of BM value is schematically illustrated in Figure 5-15. The increment in percent finer (ΔP_i) in Figure 5-15 is the change in percent finer of a grain size particle (P_i) after and before tests. The degree of particle breakage after and before tests can be assessed by the accumulation of ΔP_i of each particle size in the sieve analysis. It could be deemed that the larger BM value obtained from test means the more particle breakage caused by compaction and shearing processes.

$$\mathrm{BM} = \sum \Delta \mathrm{P}_i \tag{5-5}$$

where, ΔP_i is the increment in percent finer of a grain size particle after and before tests. The i value is the number of each discrete particle size.

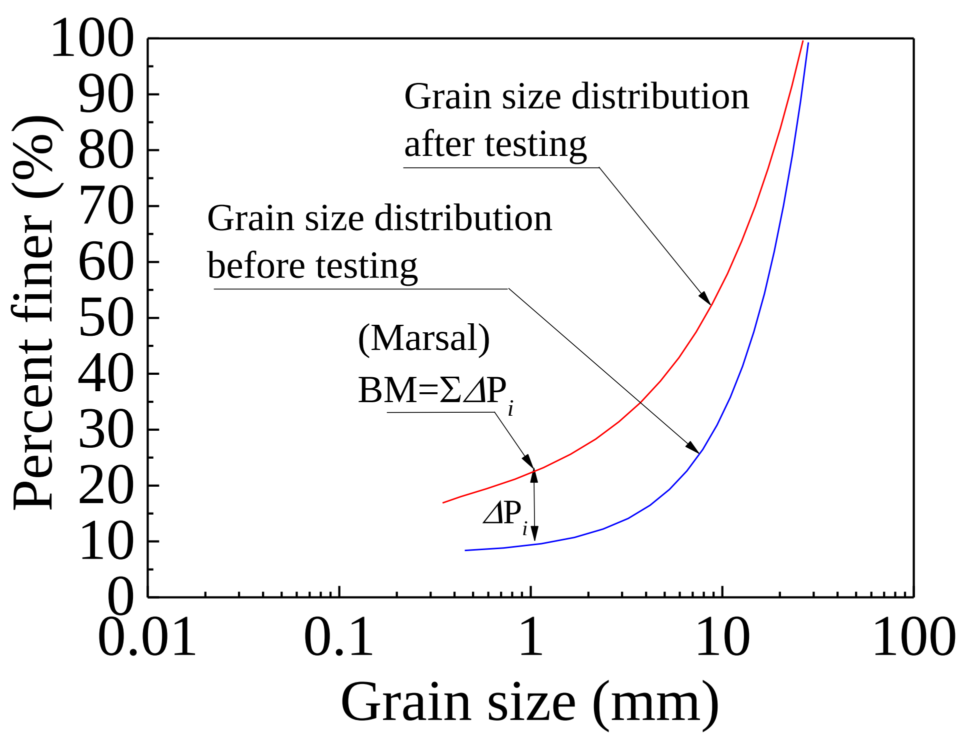

Figure 5-15. The particle breakage parameter of BM value.

Figure 5-16 shows the results of sieve analysis before and after tests under air-dried condition at effective confining pressure (σ_c') of 68.9 kPa with two strain rates (i.e., 0.05 and 0.5 %/min). The calculation results show that the BM value after test under the strain rate of 0.5 %/min equals to 14.56%, while the BM value under the strain rate of 0.05 %/min is 16.38%, which is larger than that under the strain rate of 0.5 %/min. Therefore, it can be seemed that less particle breakage occurred under larger strain rate than that under lower strain rate. That is because the time for the particle breakage and rearranging soil particle reduces under larger strain rate, and amounts of the particle breakage decrease due to shortage of the shearing time. Therefore, the specimen with larger strain rate has higher peak strength.

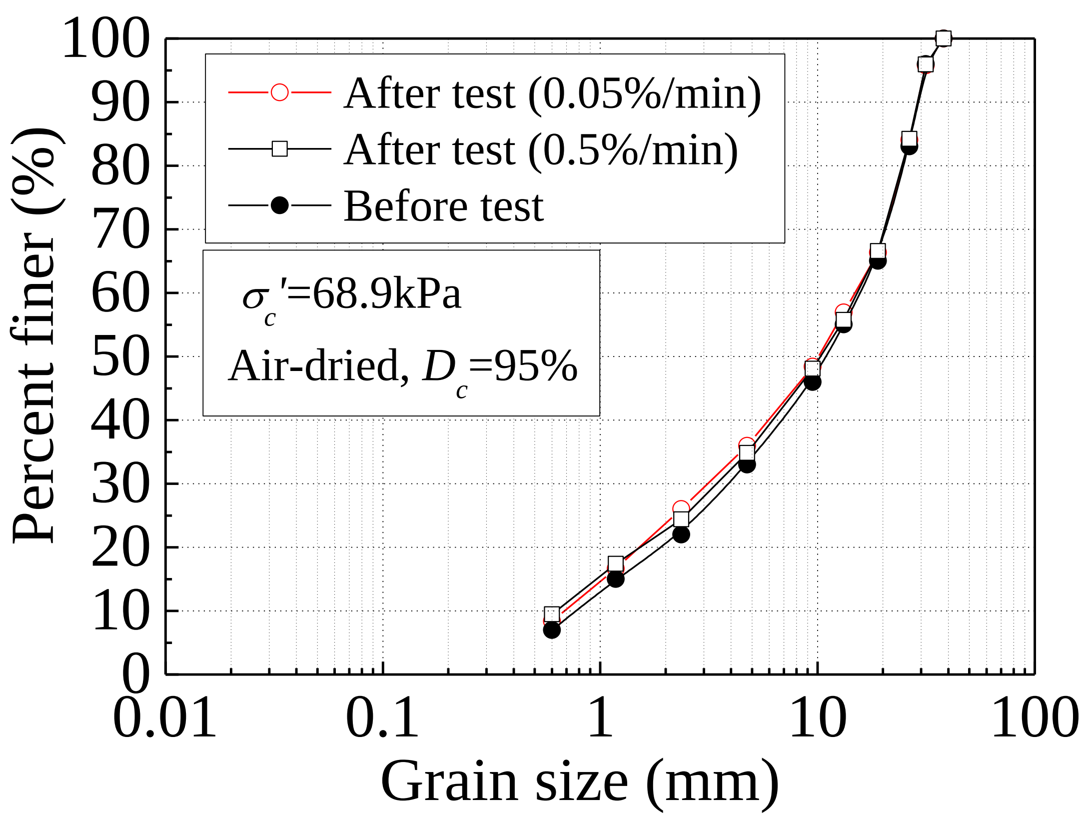

Figure 5-16. Grain size distributions of the air-dried specimen before and after tests

Next, the effect of the strain rate on the strength characteristics of C-40 material is discussed as follows. Figure 5-17 shows the relationship between the deviator stress at failure (q_{max}) and the mean effective principal stress at failure (p') for the strain rate of 0.5 %/min. For plots with the same strain rate and S_r, $\eta_{\max}$ is thought to be almost constant as the q_{max} - p' relationships seem to be linear.

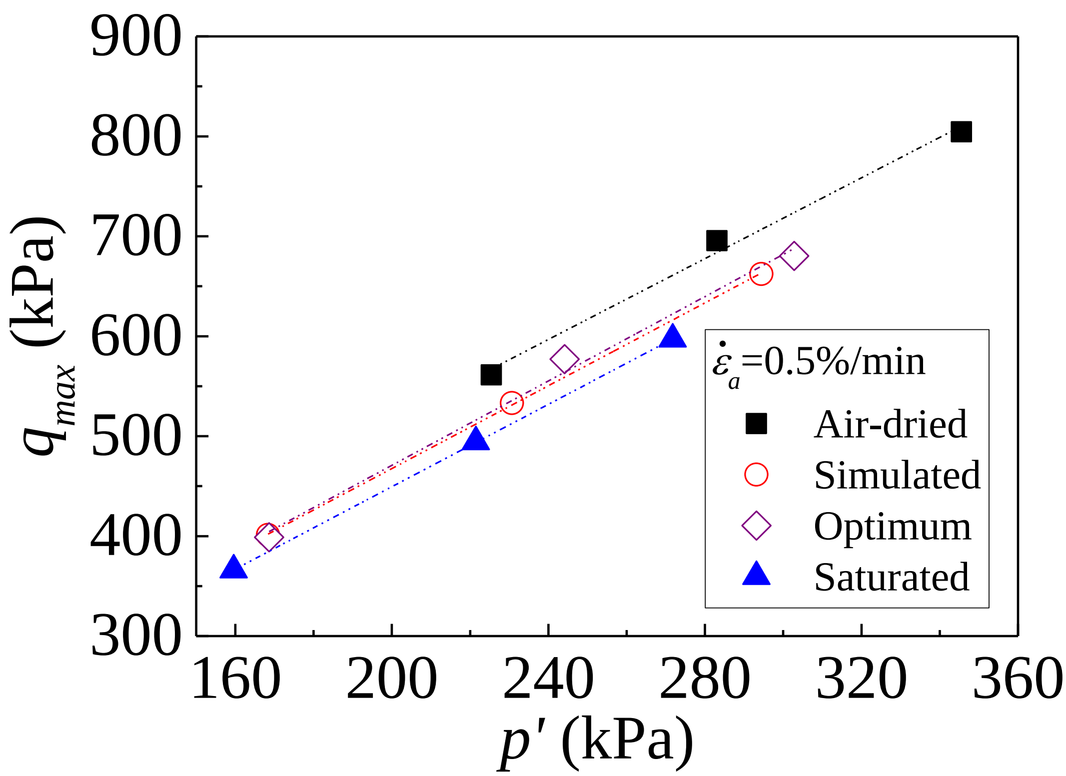

Figure 5-17. Effective stress ratio under strain rate of 0.5 %/min.

The deviator stress (q) and axial strain (ε_a) at small range (i.e., 0.05% to 0.15%) under the strain rate of 0.5 %/min is presented in Figure 5-18, and the tangent deformation modulus (E_{tan}) is the slope of the deviator stress (q) - axial strain (ε_a) curve.

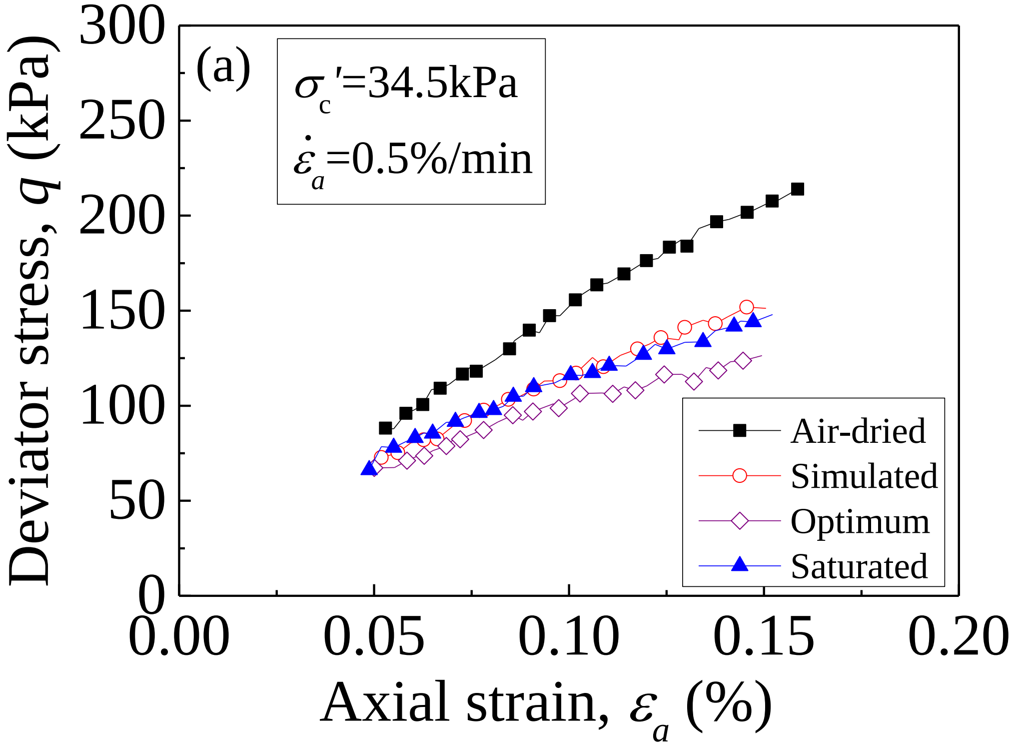
(a)
σc'=34.5kPa
ε̇a=0.5%/min
Air-dried
Simulated
Optimum
Saturated
Deviator stress, q (kPa)
Axial strain, εa (%)
0
50
100
150
200
250
300
0.00
0.05
0.10
0.15
0.20

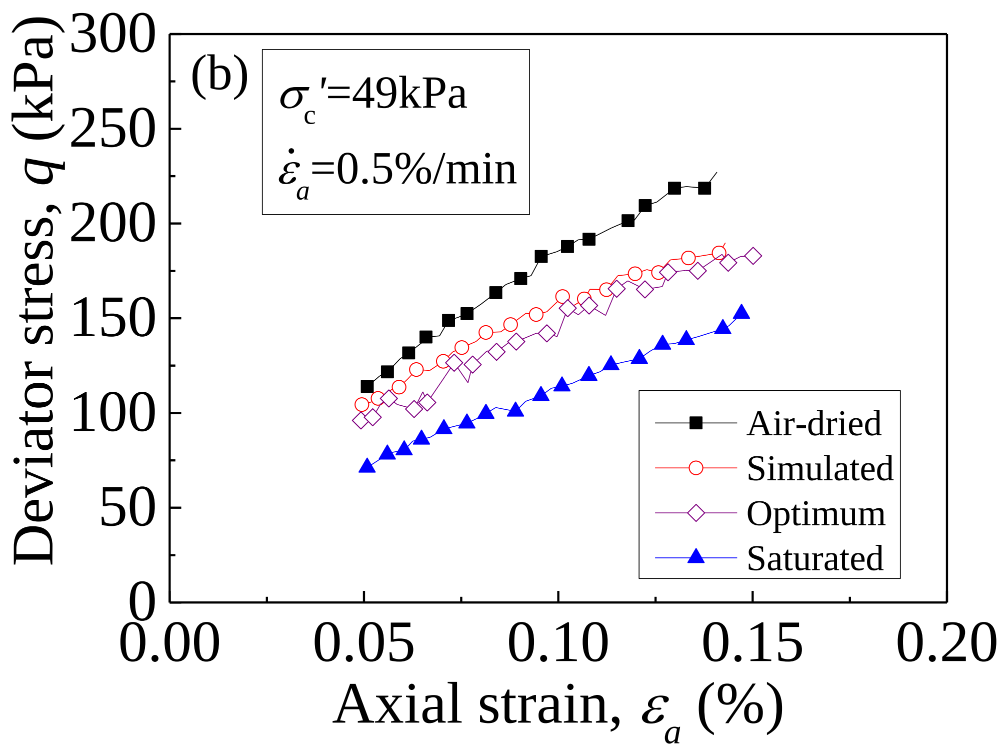
(b)
σc'=49kPa
ε̇a=0.5%/min
Air-dried
Simulated
Optimum
Saturated
Deviator stress, q (kPa)
Axial strain, εa (%)
0
50
100
150
200
250
300
0.00
0.05
0.10
0.15
0.20

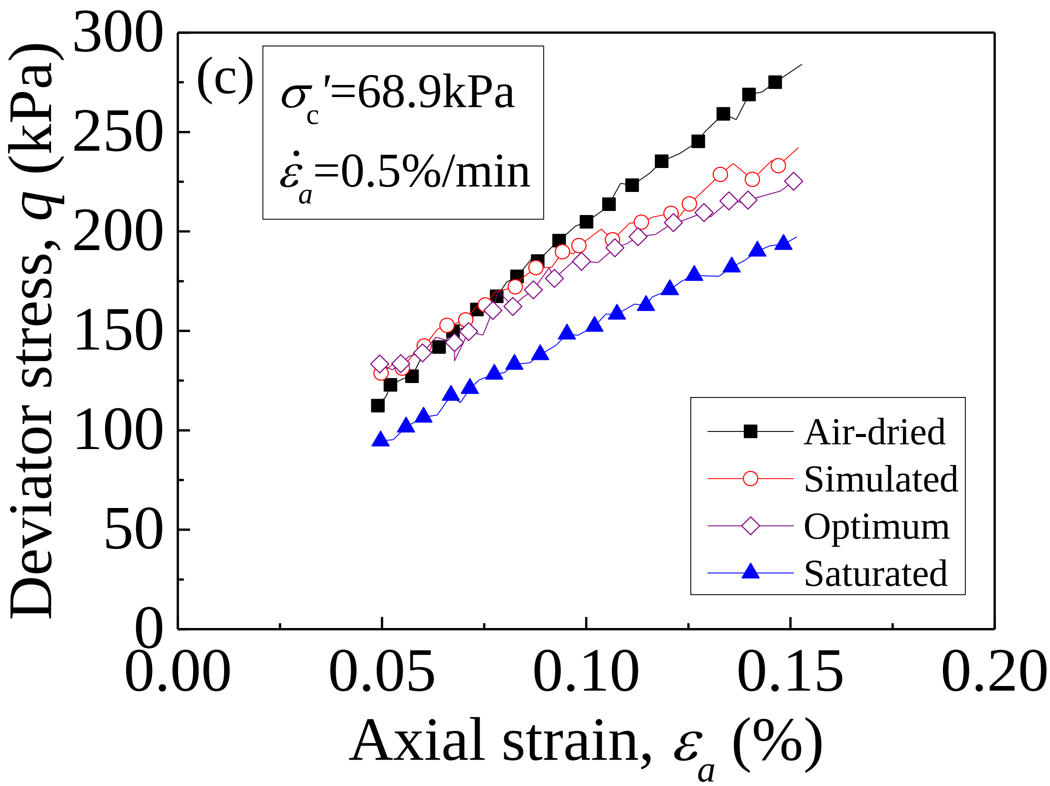

Figure 5-18. Relationship between deviator stress and axial strain in the axial strain range from 0.05 to 0.15 % under strain rate of 0. 5 %/min.

Figure 5-19 compared the tangent deformation modulus (E_{tan}) under different strain rates (i.e., 0.05%/min to 0.5%/min) obtained from Figure 5-18 and Figure 5-9. For plots with the same effective confining pressure (σ_c'), the tangent deformation modulus (E_{tan}) with lager strain rate is located above the one with smaller strain rate. Therefore, it can be considered that the E_{tan} increases with an increase in the strain rate.

On the other hand, Figure 5-20 compares the secant deformation modulus (E_{50}) with different strain rate (i.e., 0.05%/min to 0.5%/min) under effective confining pressure of 34.5 kPa, 49 kPa and 68.9 kPa. As we can see from Figure 5-20, the secant deformation modulus (E_{50}) with higher strain rate is located above the curve with lower strain rate, regardless of the effective confining pressure.

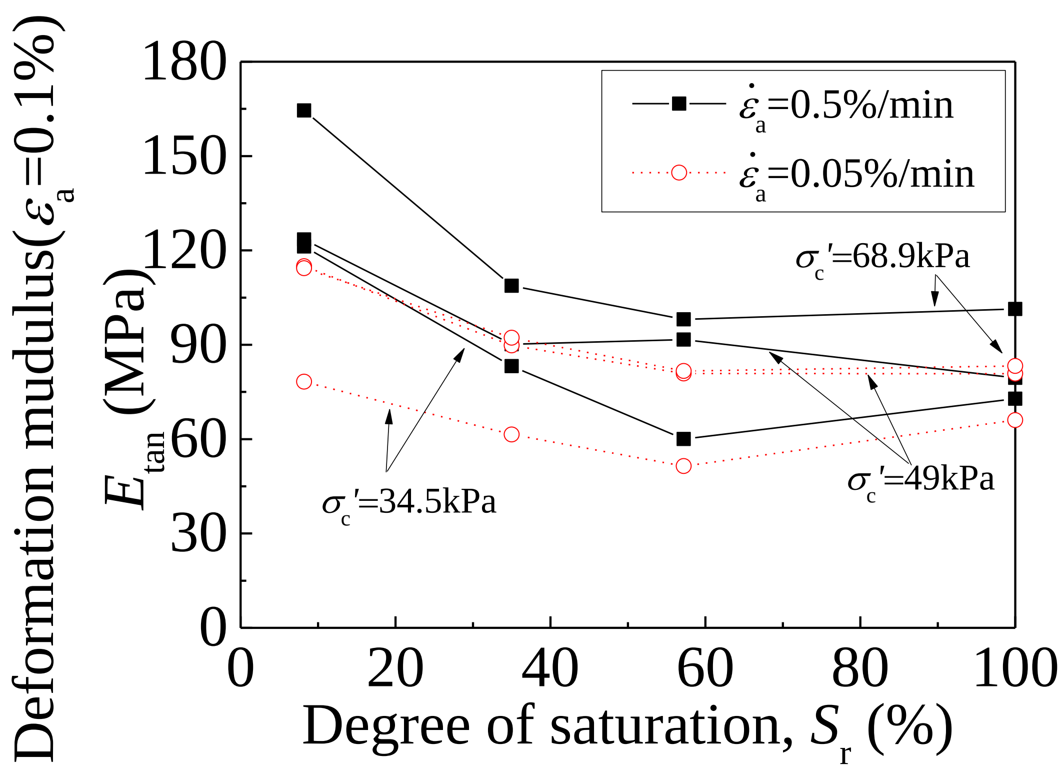

Figure 5-19. Tangent deformation modulus E_{tan} versus degree of saturation under different strain rate.

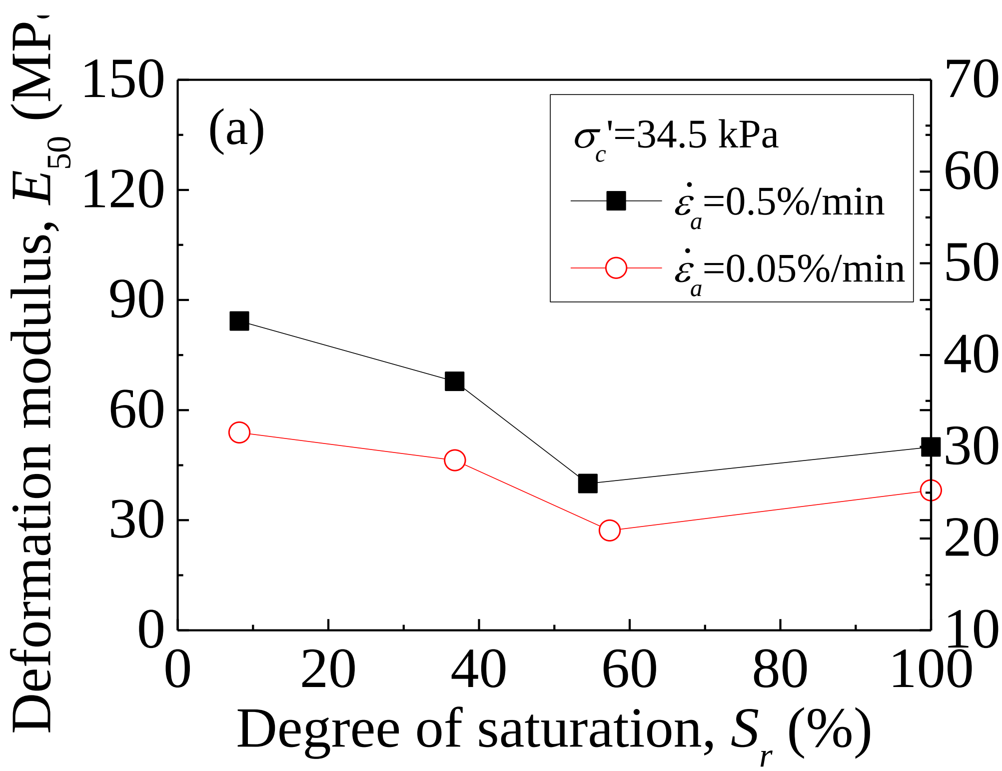

(a)
σ_c'=34.5 kPa
$\dot{\varepsilon}_a$=0.5%/min
$\dot{\varepsilon}_a$=0.05%/min
Deformation modulus, E_{50} (MPa)
Degree of saturation, S_r (%)

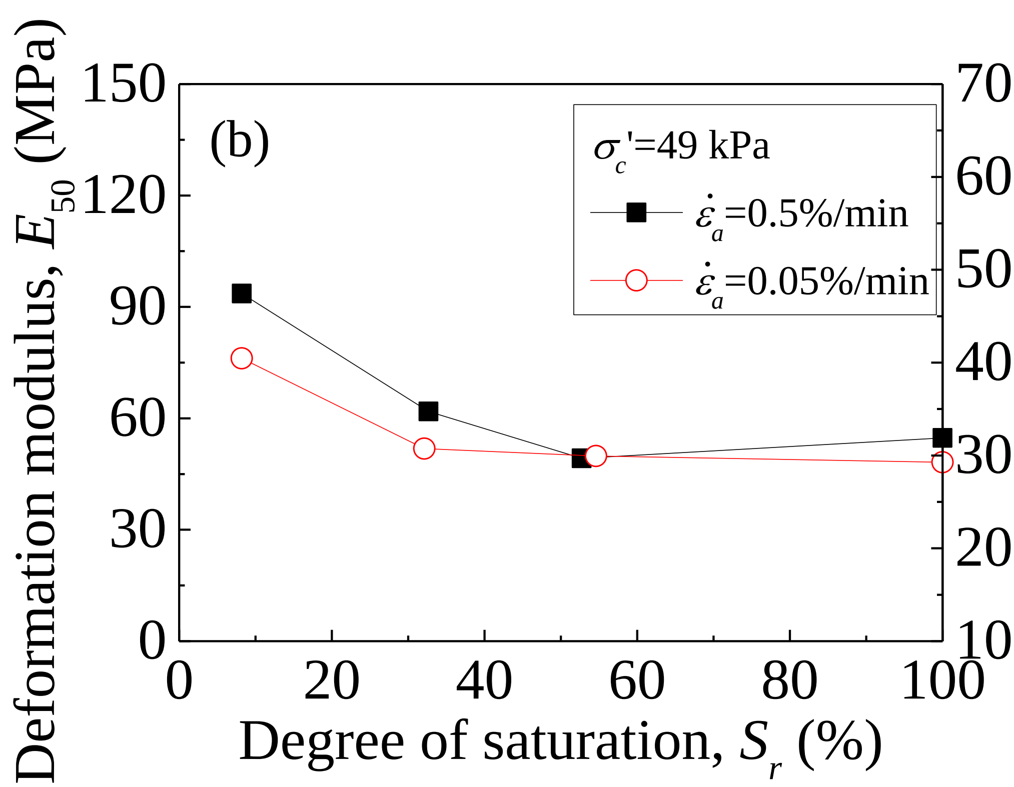

(b)
σ_c'=49 kPa
$\dot{\varepsilon}_a$=0.5%/min
$\dot{\varepsilon}_a$=0.05%/min
Deformation modulus, E_{50} (MPa)
Degree of saturation, S_r (%)

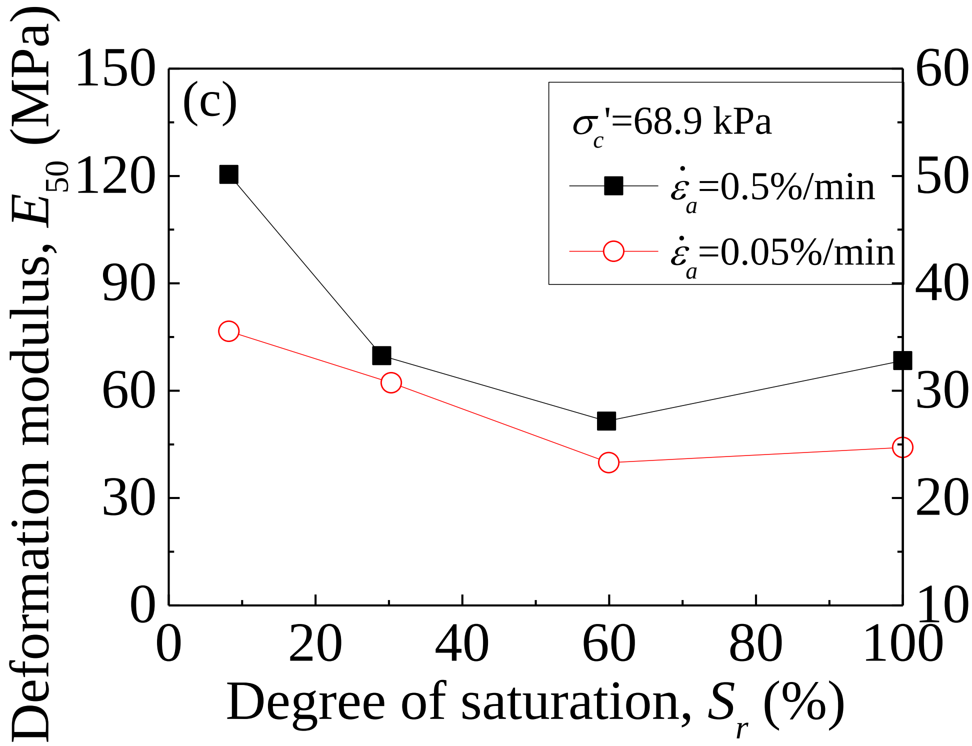

Figure 5-20. Influence of the strain rate on E_{50} under σ_c' of (a) 34.5 kPa, (b) 49 kPa, and (c) 68.9 kPa.

As previously mentioned, the strain rate has an effect on mechanical behaviors of C-40 material, especially under lager strain rate. Therefore, it is necessary to discuss that the strain rate selected in this study is suitable in order to ensure equalization or dissipation of induced pore pressure. Figure 5-21 shows the matric suctions during shear for simulated and optimum specimens under effective confining pressure of 34.5 kPa, respectively. As shown in Figure 5-21, matric suctions under simulated condition is controlled well on 10 kPa, while specimens under optimum condition are also externally controlled at a constant values (i.e. 0.5 kPa) during shear. In other words, there is no excess pore pressure built up during shear. The test results on unsaturated soils under different strain rates are obtained under stationary condition.

More specifically, Figure 5-22 presents the water drainage velocity of unsaturated and saturated specimens during shear under effective confining pressure of 34.5 kPa. Water drainage velocities are nearly constant under the unsaturated condition regardless of strain rates. The maximum water drainage for unsaturated specimens under strain rate of 0.5 %/min is 4.06 ml/min, which is equal to 0.38 ml/min/cm with considering the area of the water plumbing path for the versapor membrane filter. However, the water drainage velocity of 0.38 ml/min/cm is much smaller than the maximum water flow of the versapor membrane filter of 142 ml/min/cm. In addition, the degrees of saturation of unsaturated specimens keep nearly constant during shear (*see*. Figure 5-12(c) and Figure 5-12(d)), which means the water drainage volume for unsaturated specimens during shear were small. Hence, it can be considered that the specimens were sheared under a stationary condition. For the specimen under the saturated condition, the water drainage velocity with the strain rate of 0.05 %/min is also constant; however, the water drainage velocity curve with the strain rate of 0.5 %/min shows slightly fluctuations under saturated condition. That is because the water content for the specimen under saturated conditions is relatively high.

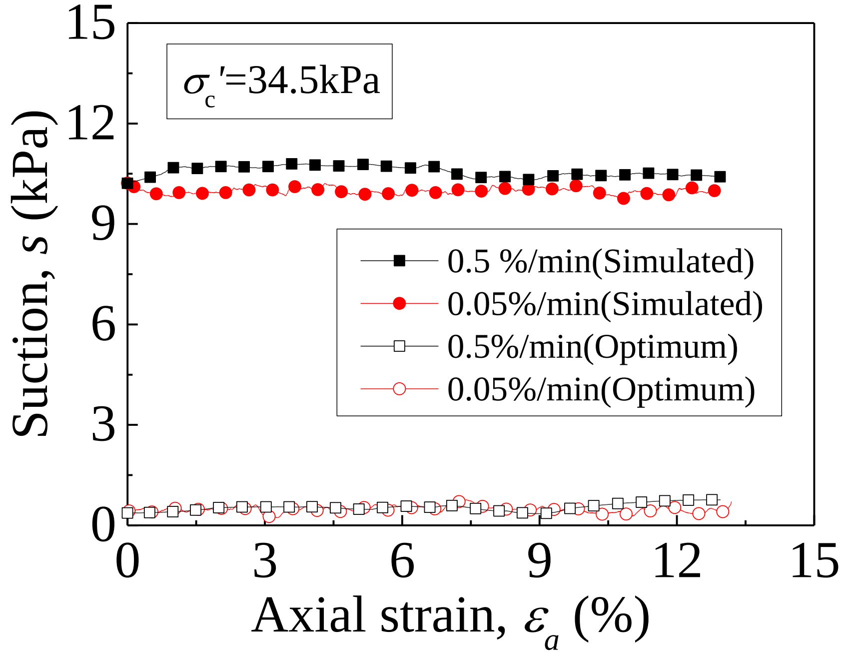

Figure 5-21. Matric suction versus axial strain curve during shear under unsaturated conditions with different strain rates.

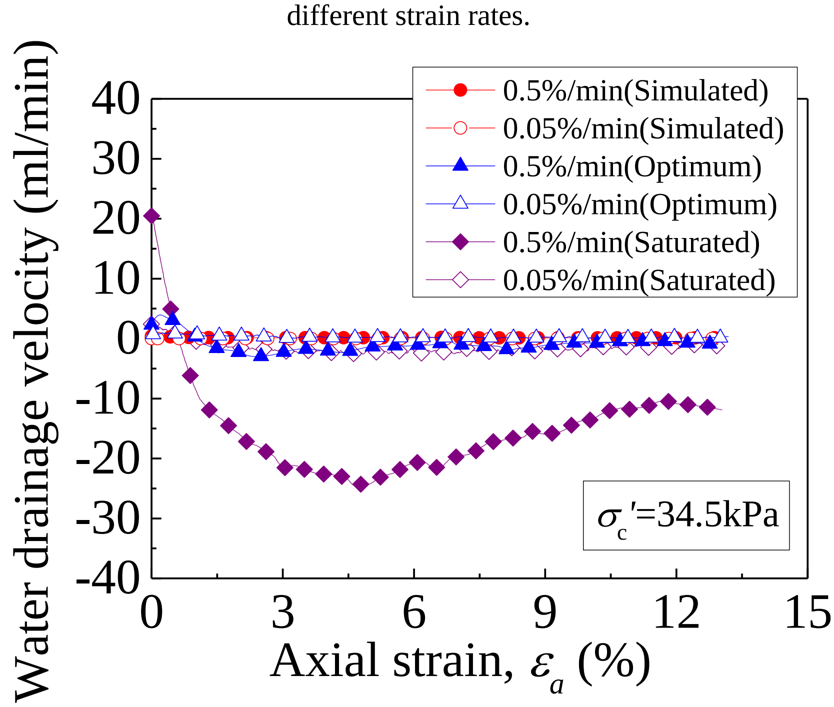

Figure 5-22. Water drainage velocity versus axial strain curve during shear under unsaturated conditions with different strain rates.

5.4 STRENGTH PARAMETERS

5.4.1 The total cohesion and total internal friction angle

Based on Figures 5-8 and 5-17, the failure envelopes are defined using linear lines, and total internal friction angles and total cohesions are expressed as Equations 5-6 and 5-7 based on Nishimura et al. (2008).

$$\frac{q_{\max}}{p'} = \frac{6\sin\phi}{3-\sin\phi} \tag{5-6}$$

$$c = b\frac{3-\sin\phi}{6\cos\phi} \tag{5-7}$$

where, ϕ is the total internal friction angle. Note here that for the saturated specimen, the total internal friction angle is replaced by the effective internal friction angle ϕ'. The c is the total cohesion, and b is the intersection of linear line on the vertical axis.

Figure 5-23 presents the results of the shear strength parameters, ϕ and c for C-40 specimens with various degrees of saturation at different strain rates obtained from Equations 5-6 and 5-7. The values of ϕ are almost constant regardless of the degree of saturation and the strain rate, although there is a slight fluctuation in the simulated condition. In other words, it can be deemed that the ϕ value of C-40 is not affected by the degree of saturation and the strain rate. It is noted here that the average ϕ value under the saturated condition between two strain rates is 50.3°, which will be used in the later text.

In addition, the total cohesion (c) is affected by the degree of saturation and the strain rate. The total cohesion (c) values decreases with increase in degree of saturation in the same manner at different strain rates. The total cohesion (c) values start to decrease significantly from the air-dried condition to the simulated condition, and then the decrease becomes small with the increase of degree of saturation. On the other hand, for specimens with the same degree of saturation, the c values with the strain rate of 0.5 %/min are higher than those with the strain rate of 0.05 %/min. It must be noted here that the cohesion under saturated condition was generated from the Coulomb's failure criteria with the envelope drawn by a linear line.

In general, it is said that cohesion of a densely-compacted and saturated sand or gravel with less finer fraction appears due to interlocking between particles as discussed before. Besides, the total cohesions under the saturated condition with strain rates of 0.05 %/min and 0.5 %/min are different due to the effect of strain rate, which plays a part in particle breakage and rearrangement as mentioned previously.

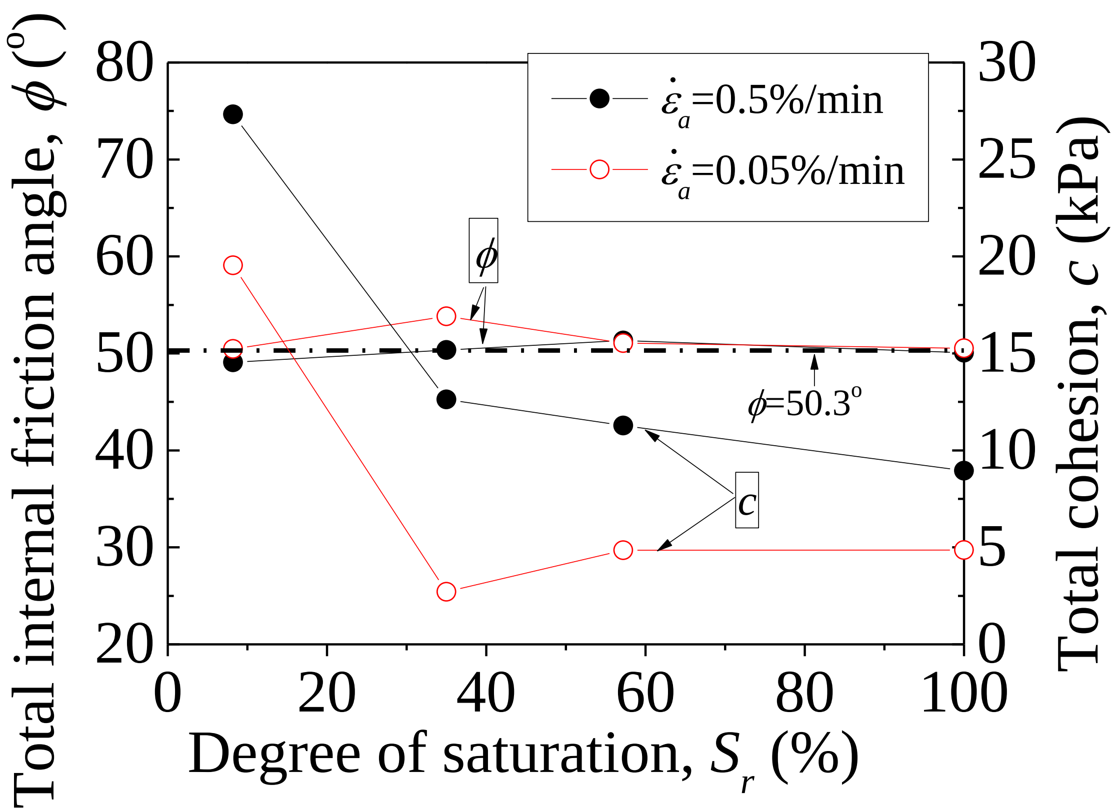

Figure 5-23. Influence of the degree of saturation and the strain rate on the total internal friction angle and the total cohesion.

5.4.2 The shear parameters for unsaturated soils

Fredlund et al. (1978) provided shear strength equations for unsaturated soils as shown in Equations 5-8 and 5-9. Equation 5-8 could be considered an extension of the Mohr-Coulomb equation (Terzaghi, 1936). Equation 5-9 defines that the total cohesion consists of two components; i.e., one is the effective cohesion for the saturated condition, and the other is associated to the matric suction. When an unsaturated soil becomes saturated and the matric suction is equal to zero, the total cohesion approaches to the effective cohesion value.

$$\tau = c' + (\sigma - u_a)\tan\phi' + (u_a - u_w)\tan\phi^b \tag{5-8}$$

$$c = c' + (u_a - u_w)\tan\phi^b \tag{5-9}$$

where, c is the total cohesion for the unsaturated soil, c' is the effective cohesion for the saturated soil, ϕ' represents the effective internal friction angle under the saturated condition, and ϕ^b is the internal friction angle with respect to the matric suction.

Based on unsaturated soil mechanics theory proposed by Fredlund and Rahadjo (1993), Equations 5-8 and 5-9 can be drawn in a three-dimensional manner composed of two stress state variables; the net normal stress (σ_{net}=σ-u_a) and the matric suction (s=u_a-u_w). In other words, the three-dimensional manner is Mohr-Coulomb circles with respect to the matric suction for unsaturated soils. In Figures 5-24a, the failure envelopes for saturated specimens are obtained by drawing the Mohr-Coulomb circles on a two-dimensional plot, as the matric suction is 0 kPa in the saturated condition. In the case of unsaturated condition, the Mohr-Coulomb circles are plotted in the same way as Mohr-Coulomb circles under saturated condition. However, the location of Mohr-Coulomb circle of unsaturated specimen is a function of the matric suction in the three-dimensional manner. Figure 5-24b presents a two-dimensional graph of the failure envelopes onto the shear stress (τ), versus the net normal stress (σ_{net}=σ-u_a) plane. The intersection between the failure envelope and the ordinate is a total cohesion (c), or effective cohesion (c'). The matric suction versus cohesion curves are plotted in the upper left in Figure 5-24b. Then, the effect of the matric suction on the total cohesion can be quantified by the ϕ^b value in the Figure 5-24b, which is equal to an angle indicating the rate of increase in shear strength relative to the matric suction (Fredlund and Rahadjo, 1993). Note, the effective internal friction angle (ϕ') under the saturated condition is assumed to be constant regardless of stress state variables.

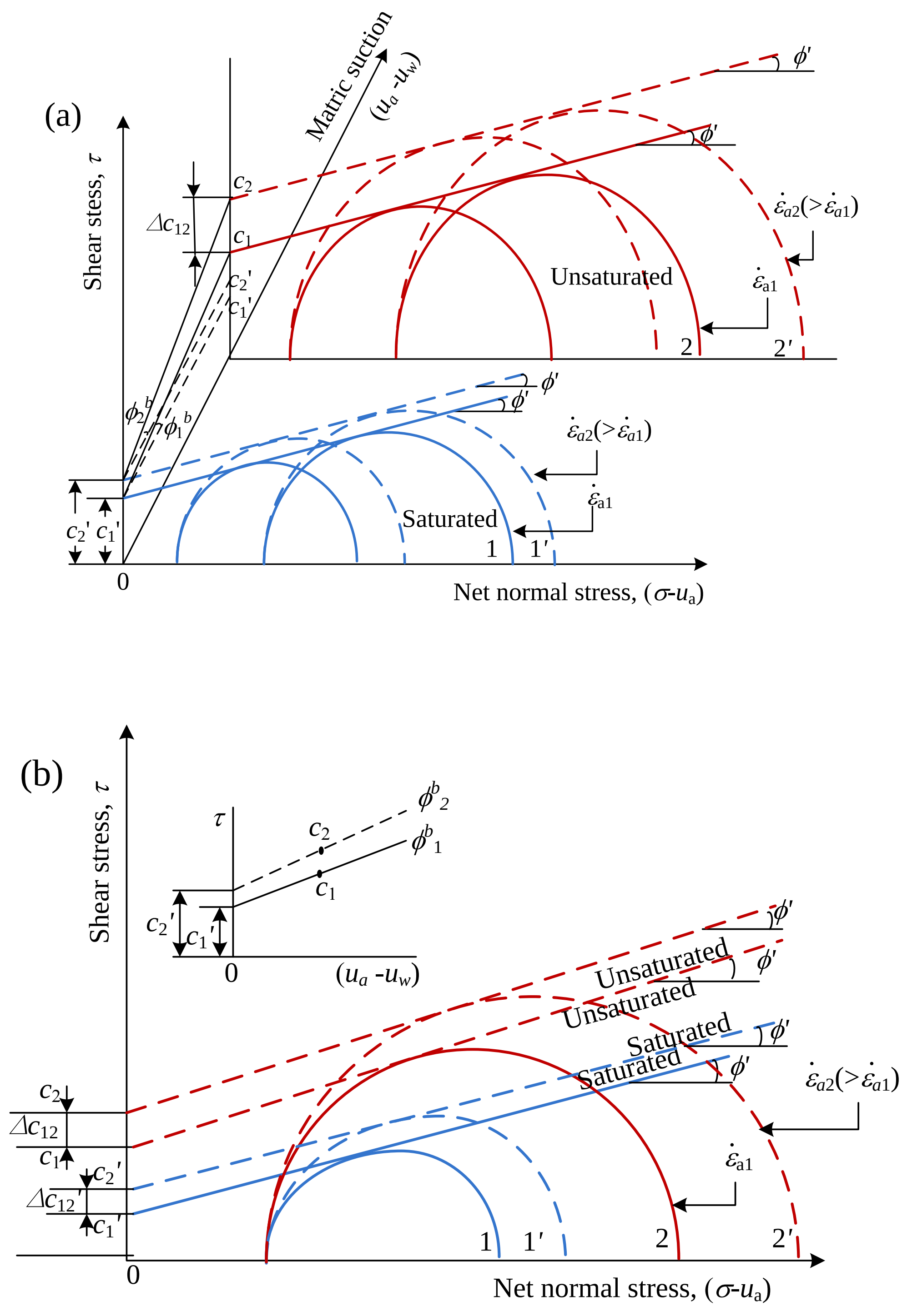

Figure 5-24. Diagrammatic sketches of (a) three-dimensional failure surface and (b) two-dimensional graph for unsaturated soils.

In order to evaluate the effect of the matric suction and the strain rate on the total cohesion, Figures 5-25a and 5-25b indicate Mohr-Coulomb circles and those failure envelopes for unsaturated specimens with regard to different strain rates (i.e. 0.05 and 0.5 %/min) under the simulated and the optimum conditions, respectively. Note that the slopes of failure envelopes for unsaturated specimens commenced at an angle equal to ϕ' under saturation (i.e., 50.3^{o}), because the total internal friction angle ϕ tends to be constant irrespective of degree of saturation, as could be understood in Figure 5-22 and in the previous discussion (Fredlund and Rahadjo, 1993).

Figure 5-26 shows relationships between total cohesions and the matric suction along with the difference of total cohesions (Δc_{12}) under different strain rates, obtained from above-mentioned Mohr-Coulomb circles in Figure 5-25. The total cohesion-matric suction curves are nonlinear, regardless of the strain rate. At the matric suction in the range of 0 to 0.5 kPa, the total cohesion increases with increasing matric suction disregard for the strain rate, then the total cohesion remains constant ranging from the optimum to the simulated condition. In other words, the degree of saturation has significant effect on the total cohesion at the lower suction range in this study. Therefore, the matric suction plays an important role on the total cohesion of the subbase course material C-40. Fredlund et al. (2012) suggest that the total cohesion versus matric suction relationship should not be limited to a linear relationship, and the failure surface could possibly be somewhat curved in the three-dimensional manner, especially at low suction range (equal to the high degree of saturation). The research results in this study were in consonance with the viewpoint proposed by Fredlund et al. (2012). It must be pointed out that that matric suction-total cohesion curve in Figure 5-26 shows peak point under matric suction of 0.5 kPa and the tendency of matric suction-total cohesion curve was obtained under limited experimental conditions (i.e., suction=0.5kPa and suction=10kPa). Therefore, in order to obtain the tendency of matric suction-total cohesion distinctly, more tests under various suction conditions on C-40 will be necessary as a future work.

On the other hand, the total cohesion versus matric suction curves associated with higher strain rate are located above those with lower strain rate as shown in Figure 5-26. Besides, the Δc_{12} increases with decreasing the degree of saturation from the saturated condition to the optimum conditions, and then becomes constant in the range from the optimum condition to the simulated condition. The nonlinearity in Δc_{12} versus matric suction relationship is also observed in Figure 5-26. It must be pointed out that in Figure 5-24, failure states under a higher strain rate ($\dot{\varepsilon}_{a2}$) are illustrated with the dashed lines as well as those under a lower strain rate ($\dot{\varepsilon}_{a1}$) drawn by the solid lines. Therefore, the Δc_{12} can be used to evaluate the influence of the strain rate on the total cohesion. In this study, the influence of the strain rate on the total cohesion is greater under unsaturated conditions as compared with that under the saturated condition. According to the standard of the Japanese Geotechnical Society (JGS 0527, 2000b), in general, the triaxial compression tests on unsaturated soils are performed with a strain rate no greater than 0.05 %/min in consideration of the soil particle size and the degree of saturation. However, the above-discussed experimental results imply the importance of investigation on the shear behaviors of the unsaturated C-40 under different strain rates in case of traffic loads with a high loading rate.

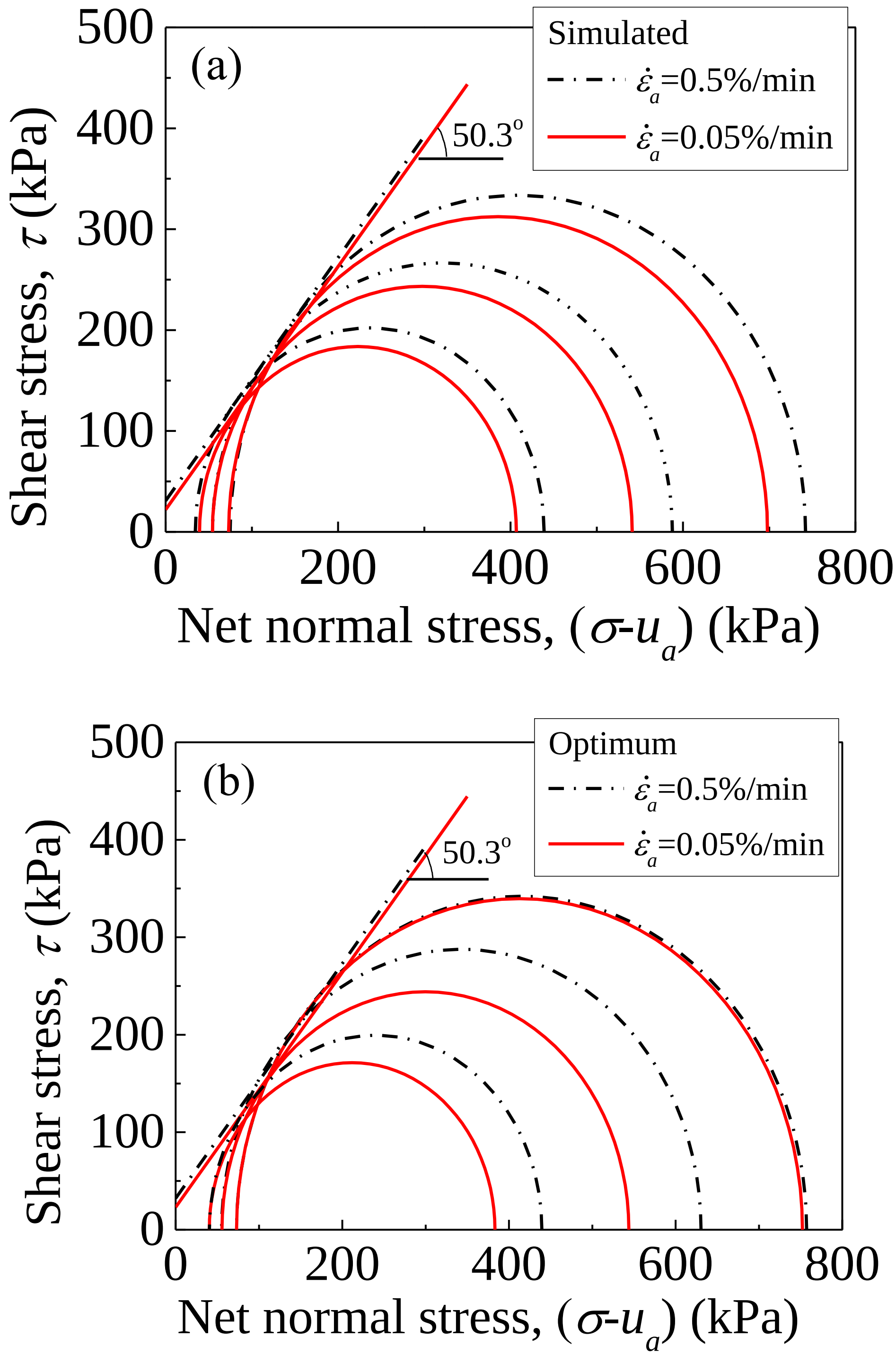

Figure 5-25. Mohr-Coulomb circles with different strain rates under (a) the simulated condition and (b) the optimum condition.

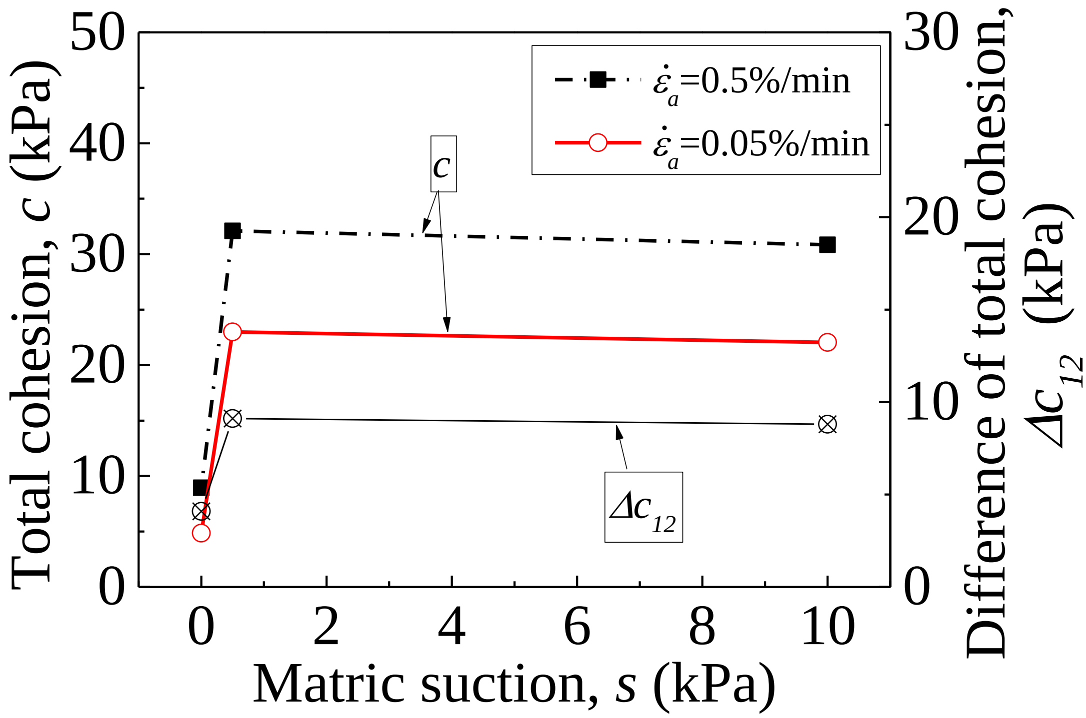

Figure 5-26. Relationship between the total cohesion and the matric suction along with the difference of total cohesion under different strain rates.

6 TEST RESULTS OF RESILIENT MODULUS TESTS

6.1 REPRODUCTION OF LOADING CONDITIONS FOR MR TEST

For the mechanical analysis of pavements, the resilient modulus (M_r) of pavement material is an important material property, which can be used to mechanistically evaluate the pavement structural response to wheel loads and to design pavement structures. The resilient modulus (M_r) is belong to Young's modulus, which is defined as the ratio of cyclic deviator stress and resilient (recoverable) axial strain. Figure 6-1 presents an example of loading waves for air-dried specimens measured in MR-15 shown in Table 3-1. In Figure 6-1, the maximum load for C-40 specimen is about 275.8 kPa, while the contact load is about 27.6 kPa. Therefore, the maximum and contact load agreed well with the standard loading for MR-15 on Table 3-1. The cyclic time for one cycle is nearly 1 second. It is recognized that the intended haversine-shaped load pulses were almost reproduced using the hybrid actuator in this study.

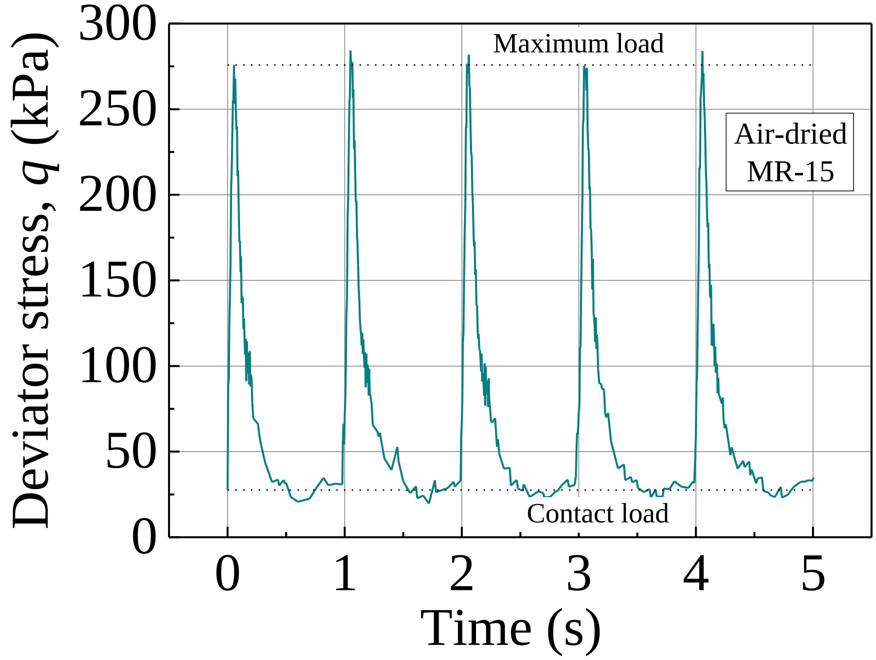

Figure 6-1 Example of cyclic loading waves measured in MR tests.

6.2 INFLUENCES OF DEGREE OF SATUTION ON RESILIENT MODULUS

The granular subbase course materials used in the subbase course layer of pavement structures are usually compacted under optimum water content. However, the degree of saturation of granular subbase course material used in subbase course layer of pavement structures varies due to seasonal change. Especially in cold region, such as Hokkaido, Japan, the degree of saturation rises in the subbase course material (C-40) owing to the infiltration of thaw water and the thawing of ice lenses during the thawing season, resulting in the temporary degradation of the bearing capacity and the stiffness (Ishikawa et al., 2012a). Therefore, it is important to examine the effects of degree of saturation on the resilient deformation characteristics for the granular subbase course material C-40.

To evaluate the resilient deformation characteristics of the granular subbase course material, the resilient modulus tests (MR tests) on C-40 under different degree of saturation were performed using the medium size triaxial apparatus for unsaturated soils pursuant to AASHTO T307-99 (2003). The degrees of saturation for specimens are air-dried, simulated and saturated conditions as discussed before. The loading condition and loading wave for MR test are shown in Table 3-1 and Figure 3-5, respectively.

Figure 6-2 presents typical relationship at the last five cycles in MR-15 between deviator stress (q) and axial strain (ε_a) obtained from the MR tests on C-40 specimen under air-dried, simulated and saturated conditions, respectively. Regardless of degree of saturation, the loading and unloading of deviator stress evidently cause the formation of small clear hysteresis-loops with elasticity showing little residual axial strain, and the deformation behavior of the subbase course material after preliminary cyclic loading seems to exhibit almost constant stiffness at each degree of saturation.

In addition, a virgin loading curve generally exhibits a deviator stress (q) - axial strain (ε_a) relationship with a convex loading curve, while a loading curve after preliminary cyclic loading (*see* Figure 6-2) shows a slightly concave shape, which illustrates the non-linearity of the deformation behavior, i.e., the stiffness increases with an increase in deviator stress (q). The same shape of deviator stress (q) - axial strain (ε_a) for unbound granular base material was obtained by Craciun and Lo (2010) and evidently cleaner loops were obtain with the increase of loading cycles. The difference between them is caused by the fact that the plastic deformation in the deviator stress (q) - axial strain (ε_a) is dominant in the early stages of cyclic loading, whereas the deformation behavior of C-40 material becomes elastic with the increment in loading cycles. Lenart and Koseki (2012) found that the stress - strain relationship for dense gravel material changed from concave shape to convex shape when the cyclic deviator stress increased, exhibiting additional accumulation of plastic strain. Therefore, the loading state has an influence on stress - strain behavior of C-40 material.

Besides, with the decrement of the degree of saturation (S_r), the deformation behavior of the test specimen became stiffer and more elastic. During loading process, when comparing the deviator stress (q) with different degrees of saturation measured in MR-15 cycle, the value under the same axial strain (ε_a) increased in order of deviator stress under air-dried, deviator stress under simulated condition, and deviator stress under saturated condition. These results indicate that the degree of saturation of the specimen has a considerable influence on the resilient deformation characteristics of the subbase course material C-40 in the MR test.

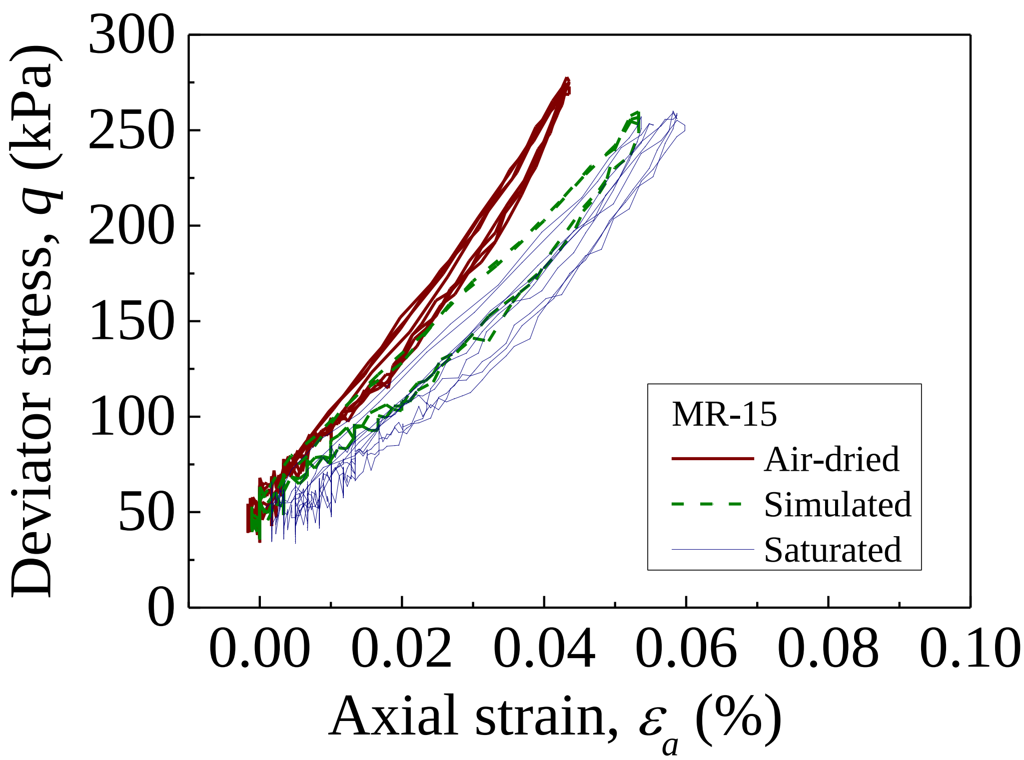

Figure 6-2 Comparison of hysteresis-loops in MR tests under different degrees of saturation.

Next, the influence of stress state on the resilient deformation characteristics of the subbase course material in terms of the resilient modulus (M_r) will be discussed. Figure 6-3 shows the relationship between deviator stress and axial strain for granular materials subjected to repeated loading. Granular materials have a complex (elastoplastic) behavior under cyclic loading, which show some non-recoverable deformation (i.e., accumulated strain) at the first few load application, and then the recoverable deformation (i.e., resilient strain) increases. After the load is repeated for a large number of times, the deformation under each application is nearly completely recoverable, then the behavior of granular materials can be considered elastic. This response is usually characterized by the resilient modulus as shown in Figure 6-4. Here, resilient modulus (M_r) is defined as the ratio of cyclic deviator stress and the resilient (recovered) axial strain, i.e., $q_{\mathrm{cyclic}}/\varepsilon_{\mathrm{r}}$ as discussed before.

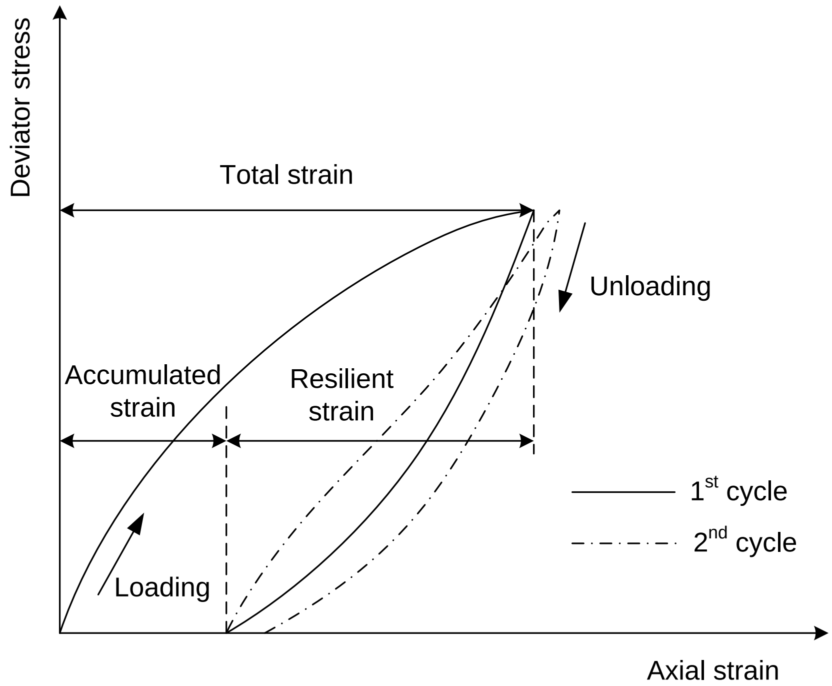

Figure 6-3 Relationship of deviator stress and axial strain subjected to cyclic loading.

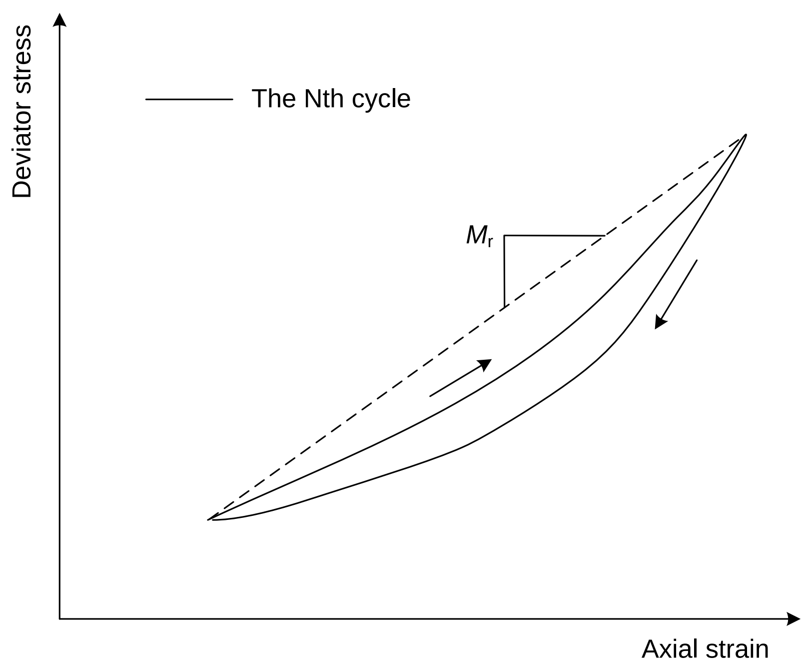

Figure 6-4 Diagrammatic sketch for resilient modulus.

Figure 6-5 presents the relationships between resilient modulus (M_r) and the mean principal net stress (p_{net}) obtained from suction controlled MR tests on C-40 material in an simulated condition (i.e., degree of saturation = 36.7%). Figure 6-6 shows resilient modulus (M_r) - the deviator stress (q) curves under different net normal stress (σ_{net}) obtained MR tests under simulated condition. As shown in Figure 6-5 and Figure 6-6, for plots with the same net normal stress (σ_{net}), the resilient modulus (M_r) decreases with the increment in the mean principal net stress (p_{net}) and deviator stress (q). When under the same mean principal net stress (p_{net}) and deviator stress (q), the resilient modulus (M_r) increases with an increase in the net normal stress (σ_{net}). A dominant effect for the deformation behavior of C-40 specimen is an increase in resilient modulus (M_r) with increasing confining pressure. A similar tendency was observed in MR tests under saturated and air-dried conditions. According, as in past researches like the AASHTO standards pointed out, the resilient modulus (M_r) of the subbase course materials measured in this study exhibits strong stress-dependency.

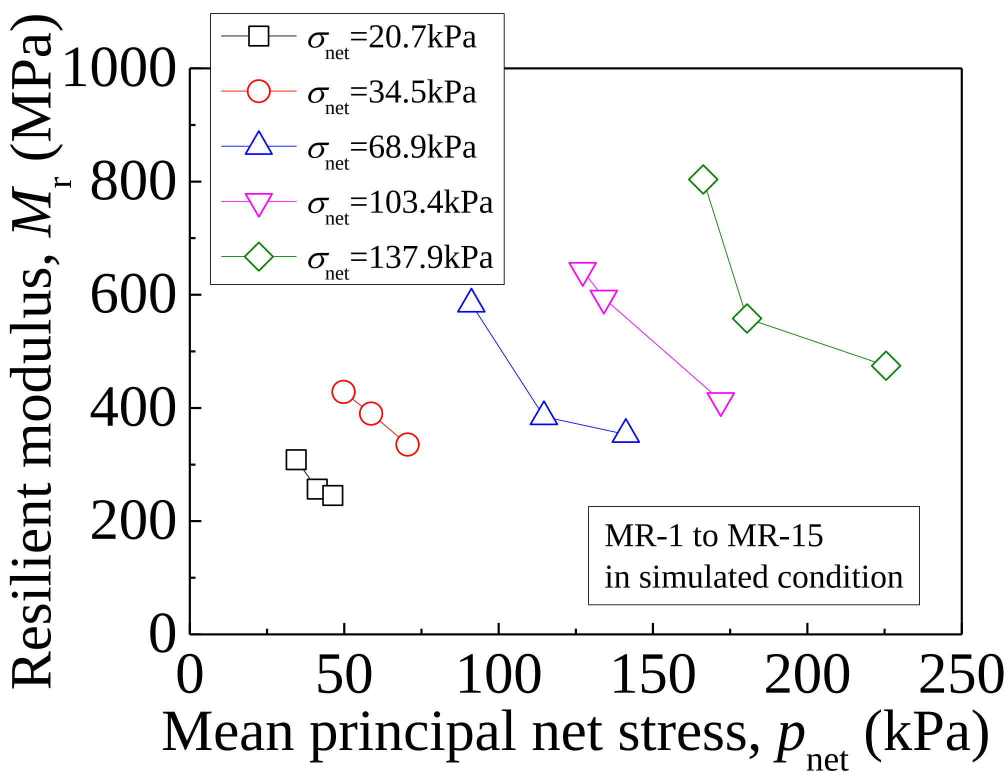

Figure 6-5 Influence of mean principal net stress on M_r in simulated condition.

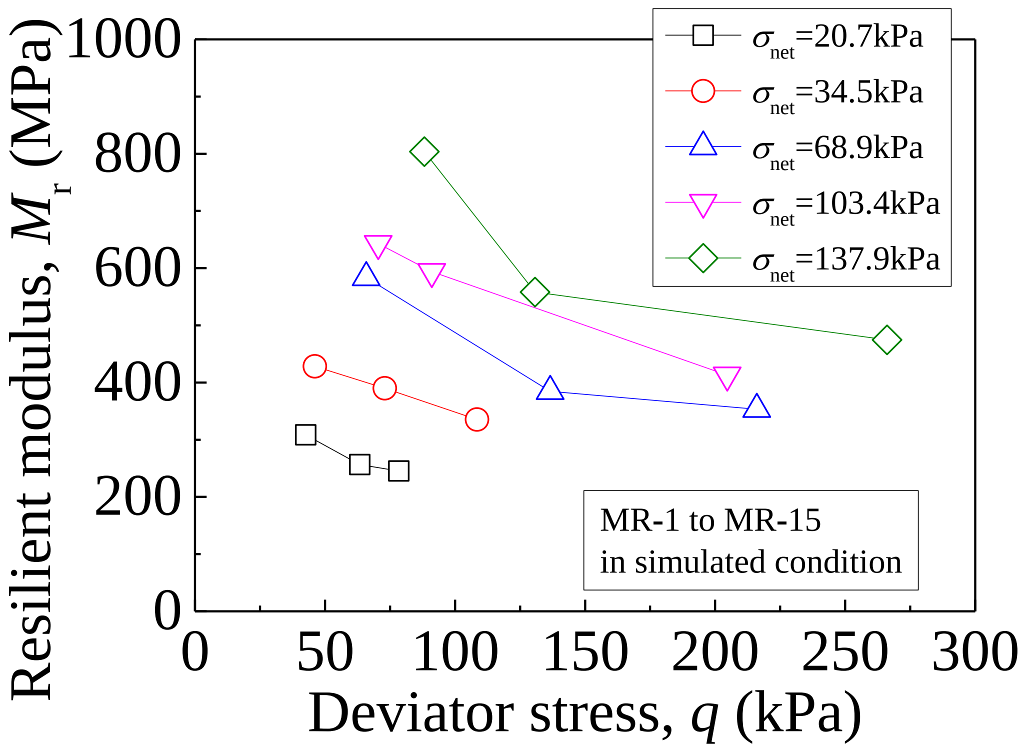

Figure 6-6 Influence of deviator stress on M_r in simulated condition.

The resilient modulus test is performed under various axial stresses and confining pressures to evaluate the nonlinear elastic behavior of the granular subbase course material. So far, various types of mathematical models have been used to estimate resilient modulus for unbound granular base materials in consideration for the stress state at the subbasse course layer (e.g. Uzan, 1985; Yan and Quintus, 2002; Yoshita et al., 2003). The Mechanistic Empirical Pavement Design Guide (MEPDG) (AASHTO, 2008) utilizes a resilient modulus constitutive equation provided in Equation 6-1 (Yan and Quintus, 2002), which can predict the M_r non-linear behavior of granular materials (Doucet, 2006). The model is generally referred to as a "universal model" with the advantage of being able to consider the stress state (i.e., normal and shear stress) of the material during the MR tests. The M_r in Equation 6-1 is a function of the bulk stress (σ_{ii}) and the octahedral shear stress (τ_{oct}). The k_1 parameter should be positive because the M_r can never be negative. The k_2 parameter should be positive, because increasing the σ_{ii} produced hardening of the material, while the k_3 should be negative, because increasing τ_{oct} produces softening of the material (Doucet, 2006).

$$M_r = k_1 p_a \left(\frac{\sigma_{ii}}{p_a}\right)^{k_2} \left(\frac{\tau_{oct}}{p_a} + 1\right)^{k_3} \quad (6\text{-}1)$$

where: k_1, k_2 and k_3 are regression constants, σ_{ii} is the bulk stress ($\sigma_{ii} = \sigma_1 + \sigma_2 + \sigma_3$), p_a is the atmospheric pressure (normalizing stress), and τ_{oct} is the octahedral shear stress (deviator stress under axisymmetric stress condition). Note: the octahedral shear stress becomes (σ_1 - σ_3) for axisymmetric stress condition.

Figure 6-7 and Figure 6-8 show the relationship of between M_r and stress states (i.e., p_{net} and q) under different degree of saturations with the effective confining pressure (σ_c') of 20.7 kPa and 34.5 kPa, respectively. In order to examine the applicability of Equation 6-1 to test results, Figure 6-7 and Figure 6-8 present comparison of the simulation results obtained by Equation 6-1 with the experimental test results. When comparing the plots with the same mean principal net stress (p_{net}) or deviator stress (q) under the same effective confining pressure (σ_c'), the remarkable decreasing tendency of resilient modulus (M_r) followed by the increase in the degree of saturation is recognized irrespective of effective of confining pressure (σ_c'). The stress-dependency of resilient modulus (M_r) derived from the experimental result agrees well with the regression analysis results of Equation 6-1, regardless of the degree of saturation. Accordingly, it seems reasonable to conclude that the suction controlled MR test results for C-40 material in this study qualitatively match those of previous studies. Besides, the coefficients k_1, k_2, and k_3 in Equation 6-1 were calculated by regression analysis using M_r under different degrees of saturation (i.e., air-dried, simulated, and saturated conditions). Influences of stress states and degree of saturation in M_r are accounted when Equation 6-1 is adopted. Thus, it is surmised that Equation 6-1 adopted in the AASHTO standard has high applicability in the estimation of the resilient modulus for the subbase course in Japanese pavement structures.

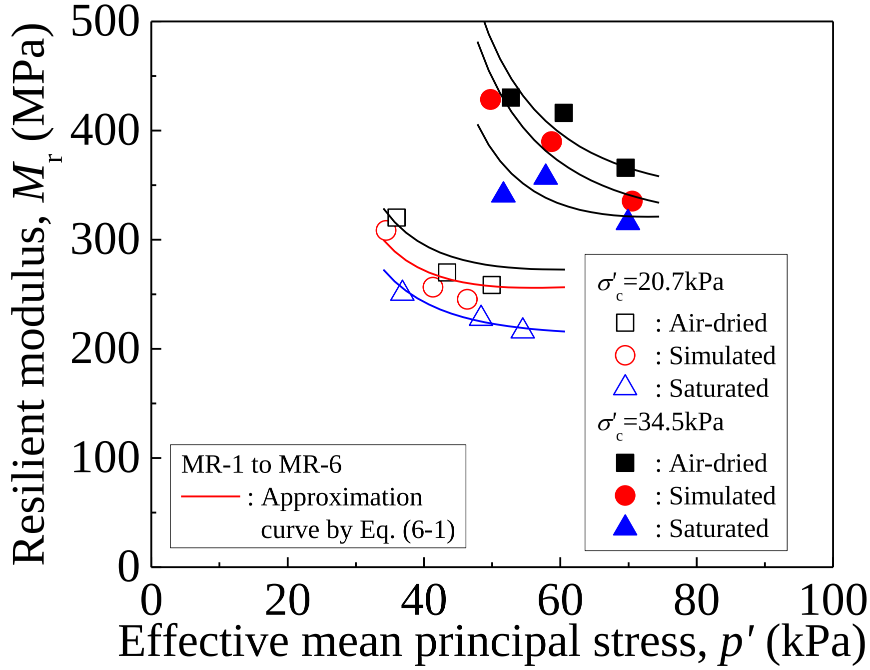

Figure 6-7 Influence of mean principal net stress on M_r under various degrees of saturation.

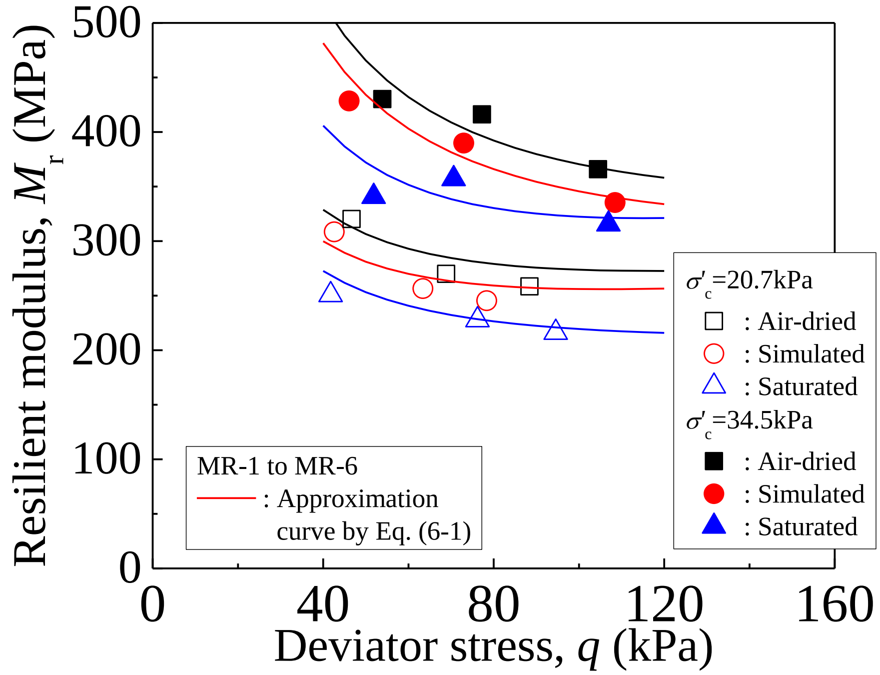

Figure 6-8 Influence of deviator stress on M_r under various degrees of saturation.

7 CONCLUSIONS AND SUGGESTIONS

7.1 CONCLUSIONS

The following findings have been obtained from this study.

(1) The influences of degree of saturation and strain rate on strength characteristics of the subbase course material C-40 under monotonic triaxial compression tests:

- The degree of saturation has an influence on the deviator stress-axial strain curve for the subbase course material under the drained condition. The maximum deviator stress decreases with increment of the degree of saturation besides the optimum condition. The matric suction plays a role in the shear resistance between grain contact points under unsaturated conditions.
- For C-40 specimens with different degree of saturation, the volume change initially decreases and specimens shows the trend of dilatancy. The positive dilatancy tends to be stronger in the order of saturated, optimum, simulated, and air-dried specimens.
- The degree of saturation effects significantly strength characteristics of the subbase course material. The secant deformation modulus at half of maximum deviator stress tends to decrease when the degree of saturation increases. The greatest reduction of the secant deformation modulus is observed at the optimum condition, and then the reduction becomes smaller as the degree of saturation increases.
- The strain rate has effects on the relationships among the deviator stress, the volumetric strain, and the axial strain of the C-40 specimen in CD tests. The specimen with higher strain rate shows larger maximum deviator stress than that with lower strain rate. According to the measurement result of the volumetric strain, the specimen under higher strain rate shows more dilatancy instead of compression than that under lower strain rate.
- The secant deformation modulus at half of maximum deviator stress with higher strain rate is located above the curve with lower strain rate. The time for the particle breakage and rearranging decrease due to shortage of the shearing time for specimen with higher strain rate. Therefore, less particle breakage occurred under larger strain rate than that

under the lower strain rate.

- The subbase course material has a fairly constant value for total internal friction angle, which is unaffected by the degree of saturation and the strain rate. The total cohesion decreases with increase of the degree of saturation, while the effect of strain rate on the total cohesion is predominant for the specimen at lower degree of saturation in comparison of higher degree of saturation.
- The relationship between the total cohesion and the matric suction is nonlinear under the low matric suction range regardless of the strain rate. Therefore, the failure surface for the unsaturated subbase course material is a curved surface in three-dimensional manner. The total cohesions for unsaturated specimens with higher strain rate are located above these with lower strain rate. The difference of the total cohesion under different strain rates increases with the increase of the matric suction, and then becomes constant.

(2) The effect of degree of saturation on resilient deformation characteristics of subbase course material under resilient modulus tests (MR tests):

- The loading and unloading of deviator stresses in MR tests cause the formation of small clear hysteresis-loops, and the deformation behavior of the subbse course material after preliminary cyclic loading seems to exhibit almost constant stiffness at each degree of saturation.
- The deviator stress-axial strain relationship at virgin loading exhibits a convex loading curve, while after preliminary cyclic loading, the loading curve shows a slightly concave shape, which illustrates the non-linearity of the deformation behavior.
- The degree of saturation of the specimen has a considerable influence on the resilient deformation characteristics of the subbase course material C-40 in the MR test. With the decrement of the degree of saturation, the deformation behavior of the test specimen became stiffer and more elastic.
- For the subbase course material C-40, the resilient modulus obtained from resilient modulus tests depend on both mean principal net stress and deviator stress regardless of degree of saturation. A dominant effect for the deformation behavior of C-40 specimen is an increase in resilient modulus with increasing confining pressure.

This study only focused on two factors, i.e., degree of saturation and strain rate on mechanical behaviors of C-40 specimen while other factors were kept the same at each monotonic and cyclic test. The testing results clarified the dependency of mechanical behaviors of the granular subbase course material C-40 on the degree of saturation and the strain rate. Therefore, it can be concluded that a laboratory element test, which takes the influences of above-mentioned two factors into account, should be employed in order to understand the mechanical behaviors of the subbase course layer caused by traffic loads and seasonal variations of degrees of saturation.

7.2 SUGGESTIONS

The research proposed a suction-controlled laboratory element test with the newly developed medium-size triaxial apparatus for unsaturated soils in order to quantitatively evaluate the effects of degree of saturation and strain rate on the deformation strength characteristics of the unsaturated granular subbase course material. Therefore, the forgoing findings provide experimental support to rationalize a design method for pavement structures better suited to the climatic conditions in cold snowy regions and confirm the applicability of suction-controlled method for monotonic and cyclic triaxial compression tests for the granular subbase course material.

However, the above conclusions are obtained on account of limited amount of experimental data. It should be noted that many factors, such as the finer particle, grading of particles, and degree of compaction may be also important for the shear behaviors of C-40 under monotonic and cyclic triaxial compression tests. Therefore, there is room for further investigation understand deformation-strength characteristics of the subbase course material C-40. In the further study, the monotonic and cyclic triaxial compression tests will be performed under different experimental condition to analyze effect of other factors on the mechanical behavior of unsaturated subbase course material, such as undrianed conditions, different grain size distribution, and various degree of compaction.

REFERENCES

[1] Dempsey, B.J. and Elzeftawy, A. (1976): Mathematical model for predicting moisture movement in pavement systems, *Journal of Transportation Research Board*, 612, pp. 48-55.

[2] Ishikawa, T., Kawabata, S., Kameyama, S., Abe, R. and Ono, T. (2012a): Effects of freeze-thawing on mechanical behavior of granular base in cold regions, *The 2nd International Conference on Transportation Geotechnics (ICTG)*, Sapporo, September 2012, pp. 118-124.

[3] Oloo, S.Y., Fredlund, D.G. and Gan, K.M. (1997): Bearing capacity of unpaved roads, *Canadian Geotechnical Engineering Journal*, Vol. 34, No. 3, pp. 398-407.

[4] Yamamuro, J.A. and Lade, P.V. (1993): Effects of strain rate on instability of granular soils, *Geotechnical Testing Journal*, Vol. 16, No. 3, pp. 304-313.

[5] Aqil, U., Tatsuoka, F., Uchimura, T., Lohani, T.N., Tomita, Y., and Matsushima, K. (2005): Strength and deformation characteristics of recycled concrete aggregate as a backfill material, *Soils and Foundations*, Vol. 45, No. 5, pp. 53-72.

[6] Tatsuoka, F., Benedetto, H.D., Enomoto, T., Kawabe. S. and Kongkitkul. W. (2008): Various viscosity types of geomaterials in shear and their mathematical expression, *Soil and Foundations*, Vol. 48, No. 1, pp. 41-60.

[7] AASHTO. (2003): Standard method of test for determining the resilient modulus of soils and aggregate materials, AASHTO Designation (T 307-99), *Standard specifications for transportation materials and methods of sampling and testing*, pp. T 307-1-T307-42.

[8] Nishimura, T., Koseki, J., Fredlund, D.G. and Rahardjo, H. (2012): Microporous membrane technology for measurement of soil-water characteristic curve, *Geotechnical Testing Journal*, Vol. 35, No. 1, pp. 61-77.

[9] Ishikawa, T., Tokoro, T., Ito, K. and Miura, S. (2010): Testing methods for hydro-mechanical characteristics of unsaturated soils subjected to one-dimensional freeze-thaw action, *Soils and Foundations*, Vol. 50, No. 3, pp. 431-440.

[10] Ishikawa, T., Zhang Y., Tokoro, T. and Miura, S. (2014): Medium-size triaxial

apparatus for unsaturated granular subbase course materials, *Soils and Foundations*, Vol. 54, No. 1, pp. 67-80.

[11] Fredlund, D.G., Rahardjo, H. and Fredlund M.D. (2012): Unsaturated soil mechanics in engineering practices, *A Wiley-Interscience Publication*, *JOHN WILEY & SONS, INC*, pp. 535.

[12] Bishop, A.W. and Donald, I.B. (1961): The experimental study of partly saturated soil in the triaxial apparatus, *Proc. of the 5th International Conference on Soil Mechanics and Foundation Engineering*, Paris, Vol. 1, pp. 13-21.

[13] Fredlund, D.G., Morgenstern, N.R. and Widger, A. (1978): Shear strength of unsaturated soils, *Canadian Geotechnical Journal*, Vol. 15, No. 3, pp. 313-321.

[14] Rahardjo, H., Heng, O.B. and Choon, L.E. (2004): Shear strength of a compacted residual soil from consolidated drained and constant water content triaxial tests, *Canadian Geotechnical Journal*, Vol. 41, No. 3, pp. 421-436.

[15] Zhan, T.L.T. and Ng, C.W.W. (2006): Shear strength characteristics of an unsaturated expansive clay, *Canadian Geotechnical Journal*, Vol. 43, pp. 751-763.

[16] Vanapalli, S.K. and Lacasse, F. (2010): Comparison between the measured and predicted shear strength behavior of four unsaturated sands, *In Buzzi, O., Fityus, S. & Sheng, D. eds, Unsaturated Soils, Taylor & Francis Group*, London, pp. 121-127.

[17] Oka, F., Kodaka, T. and Suzuki, H. (2010): Experimental study on the behavior of unsaturated compacted silt under triaxial compression, *Soil and Foundations*, Vol. 50, No. 1, pp. 27-44.

[18] Ng, C.W.W., Zhou, C., Yuan, Q. and Xu, J. (2013): Resilient modulus of unsaturated subgrade soil: experimental and theoretical investigations, *Canadian Geotechnical Journal*, Vol. 50, pp. 223-232.

[19] Ekblad, J. and Isacsson, U. (2008): Water in coarse granular materials: Resilient and retentive properties. In: Ellis, Yu, McDowell, Dawson, Thom (Eds.), *Proceedings of the International Conference on Advances in Transportation Geotechnics, Nottigham,* 25-27 August 2008, PP. 117-123.

[20] Fredlund, D.G. (2006): Unsaturated soil mechanics in engineering practice, *Journal of Geotechnical and Geoenvironmental Engineering*, Vol. 132, No. 3, pp. 286-321.

[21] Kolisoja, P., Saarenketo, T., Peltoniemi, H. and Vuorimies, N. (2002): Laboratory testing of suction and deformation properties of base course aggregates, *Transportation Research Record* 1787, pp. 83-89.

[22] Coronado, O., Fleureau. J., Correia, A. and Caicedo, B. (2005): Influence of suction on the properties of two granular road materials, In: I. Horvli (Ed.), *Proceedings of the 7th International Conference on the Bearing Capacity of Roads, Railways and Air-fields,* Trondheim, 27-29 June 2005 [1/1(CD-ROM)260].

[23] Zhang, L.M., Li, X. and Fredlund, D.G. (2009): SWCCs and permeability functions for coarse-grained soils, *In: Buzzi, Fityus, Sheng (Eds.), Proceeding of the International 4th Asia-Pacific Conference on Unsaturated Soils*, Newcastle, Australia, 23-25 November 2009, pp. 251-256.

[24] Yano, T., Nishimura, S., Nakashima, S., Moriishi, K. and Ohnishi, Y. (2011): Saturated-unsaturated hydraulic properties of subbase course material and subgrade soil, *Journal of Japan Society of Civil Engineering Division*, E1 67, No. 2, pp. 120-130 (in Japanese).

[25] Craciun, O. and Lo, S.-C.R. (2010): Matric sution measurement in stress path cyclic triaxial testing of unbound granular base materials, *Geotechnical Testing Journal*, Vol. 33, No. 1, pp. 33-44.

[26] Ishigaki, T. and Nemoto, S. (2005): A study on water retention and permeability characteristics of granular base course materials, *In: Proceedings of the 60th Annual Conference of the Japan Society of Civil Engineer*, Vol. 5, pp. 117-118 (in Japanese).

[27] Japanese Road Association (2007): Method of test for resilient modulus of unbound granular base material and subgrade soils, *Manual for pavement investigation and test method*, Vol. 4, pp. 55-57 (in Japanese).

[28] Japanese Industrial Standards (2009): Test method for soil compaction using a rammer (JIS A 1210-2009), pp. 373-383 (in Japanese).

[29] Japanese Geotechnical Society (2009a): Test method for minimum and maximum densities of gravels (JGS 0162-2009), *Standards of Japanese Geotechnical Society for Laboratory Soil Testing Methods,* pp. 198-201 (in Japanese).

[30] Ishikawa, T., Zhang, Y., Segawa, H., Miura, S. and Tokoro, T. (2012b): Development of medium-size triaxial apparatus for unsaturated granular base course materials, *The*

2nd International Conference on Transportation Geotechnics (ICTG), Sapporo, September 2012, pp. 534-540.

[31] AASHTO. (1986): Standard method of test for resilient modulus of subgrade soils, AASHTO Designation T 274-82. In: Standard Specifications for Transportation Materials and Methods of Sampling and Testing, pp. 1198-1218.

[32] Japanese Geotechnical Society (2009b): Test method for water retentivity of soils (JGS 0151-2009), *Standards of Japanese Geotechnical Society for Laboratory Soil Testing Methods*, pp. 162-169 (in Japanese).

[33] Japanese Geotechnical Society (2000a): Method for consolidated-drained triaxial compression test on soils (JGS 0524-2000), *Standards of Japanese Geotechnical Society for Laboratory Shear Test*, pp. 23-27.

[34] Japanese Geotechnical Society (2000b): Method for triaxial compression test on unsaturated soils (JGS 0527-2000), *Standards of Japanese Geotechnical Society for Laboratory Shear Test*, pp. 40-46.

[35] Ampadu, S. K. and Tatsuoka, F. (1993): Effect of setting method on the behavior of clays in trixial compression from saturation to undrained shear, *Soils and Foundations*, Vol. 33, No. 2, pp. 14-34.

[36] Maina, J.W. and Matsui, K. (2004): Developing software for elastic analysis of pavement structure responses to vertical and horizontal surface loading, *Transportation Research Record*, No. 1896, pp. 107-118.

[37] Japan Road Association (Eds.). (2006): *Pavement Design Manual*, Tokyo. (in Japanese).

[38] Fredlund, D.G. and Rahardjo, H. (1993): Soil Mechanics for Unsaturated Soil, *A Wiley-Interscience Publication*, *JOHN WILEY & SONS, INC*, pp. 217-258.

[39] Mori, T., Kamiya, K., Chiba, T., Uzuoka, R. and Kazama, M. (2009): The functional model of the soil-water characteristic curve used the logistic function during cyclic shearing, *Proc. of the 44th Japan National Conference Geotechnical Engineering*, pp. 1519-1520 (in Japanese).

[40] Yu, P.J. and Chen, Y.I. (1965): The pore air-water configuration and their effects on the mechanical properties of partially saturated soils, *Journal of Hydraulic Engineering*, 1st issue, pp. 16-24 (in Chinese).

[41] Wu, S., Gray, D. and Richart, F.E. (1984): Capillary effects on dynamic modulus of sands and silts, *Journal of Geotechnical Engineering*, Vol. 110, No. 9, pp.1188-1203.

[42] Kohgo, Y., Asano, I. and Hayashida, Y. (2007a): An elastoplastic model for unsaturated rockfills and its simulations of laboratory tests, *Soils and Foundations*, Vol. 47, No. 5, pp. 919-929.

[43] Kohgo, Y., Asano, I. and Hayashida. Y. (2007b): Mechanical properties of unsaturated low quality rockfills, *Soils and Foundations*, Vol. 47, No. 5, pp. 947-959.

[44] Tatsuoka, F., Shibuya, S. (1992): Deformation characteristics of soils and rocks from field and laboratory tests. In: D. Too (Ed.), *Proc. of the International 9th Asian Regional Conference on Soil Mechanics and Geotechnical Engineering*, 9-13 December 1991, vol. 2, pp. 101-170.

[45] Kato, S. and Kawai, K. (2000): Deformation characteristics of a compacted clay in collapse under isotropic and triaxial stress state, *Soils and Foundations*, Vol. 40, No. 5, pp. 75-90.

[46] Karube, D., Kato, S. (1994): An ideal unsaturated soil and the Bishop's soil. *Proceeding of the 13 International Conference on Soil Mechanics and Foundation Engineering*, New Delhi, India, 5-10 January, Taylor & Francis, New York, Vol. 1, pp. 43-46.

[47] Guo, P.J. and Su, X.B. (2007): Shear strength, interparticle locking, and dilatancy of granular material, *Canadian Geotechnical Journal*, Vol. 44, No. 5, pp. 579-591.

[48] Ho, D.Y.F. and Fredlund, D.G. (1982): Increase in strength due to suction for Hong Kong soils, Proc. *ASCE Geotechnical Conference on Engineering and Construction in Tropical and Residual Soils*, Honolulu, Hawaii, 1982, pp. 263-295.

[49] Nishimura, T., Toyota, H. and Waguri, M. (2008): Influence of high soil on angle of internal friction and cohesion for a statically compacted non plastic silty soil, *Japanese Geotechnical Journal*, Vol. 3, No. 4, pp. 321-329 (in Japanese).

[50] Marsal, R.J. (1965): Soil properties-shear strength and consolidation, *Proc. Of the 6th International Conference soil mechanics and foundation engineering (SMFE)*, Vol. III, pp. 310-316.

[51] Terzaghi, K. (1936): The shearing resistance of saturated soils, *Proc. of the 1st International Conference on Soil Mechanics and Foundation Engineering*, Cambridge,

MA, Vol. 1, pp. 54-56.

[52] Lenart, S., Koseki, J., Sato, T. and Miyashita, Y. (2012): Large-scale triaxial tests of dense gravel material at low confining pressure, *The 2nd International Conference on Transportation Geotechnics (ICTG)*, Sapporo, September 2012, pp. 587-592.

[53] Uzan, J. (1985): Characterization of granular pavement materials, In: *Transportation Research Record* 1022, TBR, National Research Council, Washington D.C., 1985, pp 25-59.

[54] Yoshida, N., Sugisako, Y., Nakamura, H. and Hirotsu, E. (2003): Resilient modulus of hydraulic mechanically stabilized slag base-course material, *Deformation Characteristics of Geomaterials, Proc. International Conference,* Lyon, 22-24 September 2003, pp. 293-298.

[55] Yan, A., and Quintus, H.L.V. (2002): Study of LTPP laboratory resilient modulus test data and response characteristics: *Final report, Publication No. FHWA-RD-02-051, U.S. Department of transportation*, *Federal Highway Administration*, Mclean, VA: 1-161.

[56] AASHTO. (2008): Mechanistic-Empirical Pavement Design Guide: A Manual of Practice, Washington.

[57] Doucet, F. (2006): Resilient modulus characterization of granular materials at MTQ and LCPC, *Proc. of the 10th International Conference on asphalt pavement*, 12-17 August, Quebec city, Canada, 2006, vol. 1, pp. 439-448.

NOTATIONS

The following symbols were used in this dissertation.

ρ_{dmax}: Maximum dry density

S_{r}: Degree of saturation

w_{opt}: Optimum water content

PI: Plasticity index

ρ_{dmin}: Minimum dry density

ρ_{d}: Dry density

e: Void ratio

H: Height of specimen

D: Diameter of specimen

A_i: Initial cross-sectional area of specimen

A_c: cross-sectional area of specimen subject to loading

P: Vertical load

σ_a: Axial stress

ε_v: Volumetric strain

q_{max}: Peak strength (or deviator stress at failure)

ε_a: Axial strain

D_c: Degree of compaction

w: Water content

σ_{net}: Net normal stress

σ_{c}: Confining pressure

u_a: Pore air pressure

u_w: Pore water pressure

s: Matric suction

σ_c': Effective confining pressure

q: Deviator stress

$\dot{\varepsilon}_a$: Axial strain rate

AEV: Air entry value

M_r: Resilient modulus

q_{cont}: Vertical stress placed on the specimen to maintain a positive contact between the specimen cap and the specimen

$q_{\max}$: Total deviator stress applied to the specimen for MR test

q_{cyclic}: Difference between the total deviator and vertical stress

ε_r: Resilient (recovered) axial strain due to cyclic deviator stress

N_c: Loading cycles

E: Elastic modulus

v: Poison's ratio

h: Height of asphalt mixture, subbase course, and subgrade layers

s_e: Effective degree of saturation

s_{r0}: Residual degree of saturation

$s_{r,max}$: Degree of saturation under saturated condition

a_{lg}, b_{lg} and c_{lg}: Fitting parameters of SWCC curve

H_0: Initial height

p': Mean effective principal stress at failure

η_{max}: Effective stress ratio at failure

E_{tan}: Tangent deformation modulus

E_{50}: Secant deformation modulus at half of the maximum deviator stress

P_i: Percent finer of a grain size particle

ΔP_i: Increment in percent finer

ϕ: Total internal friction angle

c: Total cohesion

b: Intersection of linear line on the vertical axis

c': Effective cohesion for the saturated soil

ϕ': Effective internal friction angle under the saturated condition

ϕ^b: Internal friction angle with respect to the matric suction

τ: Shear stress

Δc_{12}: Difference of total cohesions under different strain rates

p_{net}: Mean principal net stress

k_1, k_2 and k_3: Regression constants

σ_{ii}: Bulk stress, $\sigma_{ii} = \sigma_1 + \sigma_2 + \sigma_3$

p_a: Atmospheric pressure

τ_{oct}: Octahedral shear stress